BOOSTED SEARCHES FOR NEW PHYSICS AT THE LHC

Dissertation with the aim of achieving a doctoral degree at the Faculty of
Mathematics, Informatics and Natural Sciences
Department of Physics of the University of Hamburg

Submitted by

Matthias J. Schlaffer

from Horb am Neckar, Germany

Hamburg
2015

Day of oral defense:
June 22, 2015

Head of the examination commission:
Prof. Dr. Jan Louis

Evaluators of the dissertation, both recommend its admission:
Prof. Dr. Andreas Weiler
Jun.-Prof. Dr. Christian Sander

Additional members of the examination commission:
Prof. Dr. Caren Hagner
Dr. Jürgen Reuter

Abstract

During the first run of the LHC, no apparent signs of new physics beyond the Standard Model were discovered, but rather the Standard Model-like properties of the Higgs particle confirmed. Therefore, new and powerful methods are needed to disclose the traces of new physics, which is expected to be at the TeV scale in order to solve the hierarchy problem.

In this thesis, we propose two complementary strategies for the quest for new physics at the LHC. First, we show how a very boosted Higgs in association with a hard jet can be used to determine the important top Yukawa coupling in gluon fusion. In the inclusive gluon fusion process this is not feasible since possible deviations from its Standard Model value are combined and can even cancel with the effective Higgs-gluon interaction mediated by new top partners. This cancellation is motivated within minimal composite Higgs models but also in certain regions of the MSSM parameter space and can lead to a Standard Model-like inclusive cross section that allows no conclusions on the mass spectrum of the new physics. We work out in detail how this degeneracy can be broken in the boosted Higgs channel and find that even in the worst case scenario with a Standard Model-like inclusive cross section, the top Yukawa coupling can be constrained to 0.8–1.3 times its Standard Model value at 95% CL with an integrated luminosity of $3\,000\,\mathrm{fb}^{-1}$.

The second strategy is targeted at direct stop and sbottom searches in the fully hadronic top decay channel. Since the stop, sbottom and neutralino masses are unknown, very different event shapes are imaginable, ranging from unboosted top quarks and low missing energy to highly boosted top quarks and large missing energy in the final state. In order to cover a wide range of possible event shapes and consequently stop, sbottom, and neutralino masses, we combine several top taggers based on jet substructure techniques to obtain a scale invariant search strategy. The performance of this approach is shown in a collider study where we find that stops with masses up to about $1\,100\,\mathrm{GeV}$ can be excluded at 95% CL with an integrated luminosity of $100\,\mathrm{fb}^{-1}$.

Zusammenfassung

Geboostete Suchen nach neuer Physik am LHC

Während des ersten Laufs des LHC wurden keine offensichtlichen Hinweise auf neue Physik jenseits des Standardmodells entdeckt, sondern vielmehr die Standardmodell-artigen Eigenschaften des Higgs Teilchens bestätigt. Dementsprechend werden neue und leistungsstarke Methoden benötigt, um Spuren neuer Physik zu entdecken, die an der TeV Skala erwartet werden, sofern sie das Hierarchie Problem lösen.

In dieser Arbeit schlagen wir zwei komplementäre Strategien für diese Suche nach neuer Physik am LHC vor. Zunächst zeigen wir, wie ein sehr hochenergetisches Higgs zusammen mit einem harten Jet genutzt werden kann, um die wichtige Top Yukawa-Kopplung mit Hilfe von Gluon-Fusion zu bestimmen. Im inklusiven Gluon-Fusionsprozess ist das nicht machbar, da eine mögliche Abweichung vom Standardmodell-Wert mit der direkten Higgs-Gluon Wechselwirkung kombiniert wird. Letztere wird durch neue Partner des Top-Quarks vermittelt. In minimalen Modellen für ein zusammengesetztes Higgs sowie in gewissen Bereichen des MSSM Parameterraums können sich beide Effekte sogar aufheben und zu einem Standardmodell-artigen Wirkungsquerschnitt führen, der keinerlei Rückschlüsse auf das Massenspektrum der Theorie zulässt. Wir arbeiten detailliert heraus, wie diese Entartung im hochenergetischen Higgs-Kanal gebrochen werden kann, und stellen fest, dass die Top Yukawa-Kopplung auf dem 95% Konfidenzniveau mit einer integrierten Luminosität von $3\,000\,\text{fb}^{-1}$ auf 0,8–1,3 mal den Standardmodell Wert beschränkt werden kann.

Die zweite Strategie widmet sich Stop und Sbottom Suchen im vollhadronischen Top Zerfallskanal. Da die Stop-, Sbottom- und Neutralinomassen unbekannt sind, sind sehr unterschiedliche Ausprägungen von Ereignissen denkbar, von niederenergetischen Top Quarks und wenig fehlender Energie bis hin zu sehr hochenergetischen Top Quarks und viel fehlender Energie im Endzustand. Um eine große Anzahl an möglichen Ereignisprofilen und folglich einen großen Bereich von Squark und Neutralino Massen abzudecken, kombinieren wir mehrere Top-Suchalgorithmen, die auf der Unterstruktur von Jets beruhen, zu einer skaleninvarianten Suchstrategie. Die Möglichkeiten dieses Ansatzes demonstrieren wir anhand einer Studie, in der wir zeigen, dass mit einer integrierten Luminosität von $100\,\text{fb}^{-1}$ Stops mit Massen bis zu 1 100 GeV auf dem 95% Konfidenzniveau ausgeschlossen werden können.

Declaration on oath,
Eidesstattliche Versicherung

I hereby declare, on oath, that I have written the present dissertation by my own and have not used other than the acknowledged resources and aids.

Hiermit erkläre ich an Eides statt, dass ich die vorliegende Dissertationsschrift selbst verfasst und keine anderen als die angegebenen Quellen und Hilfsmittel benutzt habe.

Hamburg, September 7, 2015

Matthias J. Schlaffer

List of publications

This thesis is based on the following publications:

[1] C. Grojean, E. Salvioni, M. Schlaffer, and A. Weiler, *"Very boosted Higgs in gluon fusion"*, *JHEP* **1405** (2014) 022, arXiv:1312.3317 [hep-ph].

[2] M. Schlaffer, M. Spannowsky, M. Takeuchi, A. Weiler, and C. Wymant, *"Boosted Higgs Shapes"*, *Eur.Phys.J.* **C74** no. 10, (2014) 3120, arXiv:1405.4295 [hep-ph].

[3] R. Mahbubani, M. Schlaffer, M. Spannowsky, and A. Weiler, "*Scale invariant SUSY searches.*" In preparation.

The Chapters 2, 3, and 4 collect the basics and the notation for the phenomenological models, which are needed in the following analyses. Besides on lecture notes and the references given in the text, Chapter 2 is based on Refs. [4] and [5], Chapter 3 on Refs. [6] and [7], and Chapter 4 mainly on Refs. [8] and [9] but also on Ref. [10].

The basis for the other chapters are the papers I contributed to during my PhD. I performed all the calculations leading to the main results of Ref. [1], in particular the ones given in Table 5.2 and Figure 5.8. Ennio Salvioni and I cross checked them together. The effects of boosting the Higgs in the MSSM are based on my calculations. Figures 5.2 and 5.3 were made by Ennio Salvioni, but I was involved in the discussions leading to them. I wrote substantial parts of the paper and provided the formulas for the helicity amplitudes for Higgs + jet production in the presence of CP-violating couplings, which are given in Appendix A. This appendix already appeared in this form in Ref. [1].

In the follow-up project [2] I was involved in the preparation of the signal events, participated in discussions, and wrote those parts of the paper that deal with the models for new physics. The analysis in all its details was, however, implemented by others. I therefore focus on the main ideas of the analysis and present the results, but refer to the paper for all the details of the implemented cuts. The plots in Figs. 5.10, 5.11, and 5.12 were made by Michael Spannowsky, and a figure similar to Fig. 5.9 appeared already in Ref. [2].

The actual implementations, executions, calculations and plots for Ref. [3] were done by myself, including the detailed design of the analysis. The other authors contributed by providing the initial idea, giving important technical and strategical advice, and participating in the discussions. Large parts of Section 6 will be the basis for Ref. [3].

Appendix B is based on Refs. [11, 12], and [13].

Contents

1. Introduction

High energy physics is currently standing at a very special point in its history. In the past decades, the Standard Model of particle physics (SM) has proven to be a very economic and good description of nature at energies up to a few hundred GeV. Many of its predictions were tested with high precision and confirmed by collider experiments. All the experimental and theoretical efforts eventually culminated in the announcement of the discovery of a Higgs boson at the LHC in July 2012 [14, 15]. This discovery marks a very unique point: With the Higgs as the last missing piece, the SM is now seemingly completed. In particular the fact that the discovered boson has the properties predicted by the SM underlines the success of this framework.

Yet, at the same time it is known that there has to be new physics beyond the SM (BSM). On the one hand there are experimental observations that are not explained within the SM and on the other hand there are also theoretical considerations that motivate BSM physics. In particular the hierarchy problem points to new physics at the TeV scale. This problem addresses the question why the Higgs mass can be $m_h \approx 125\,\text{GeV}$ when its loop correction from the top quark loop is quadratically sensitive to the scale of new physics. If one wants to avoid extreme fine tuning and rather follow the principle of naturalness [16], one comes to the conclusion that there has to be new physics not too far above the electroweak scale that protects the Higgs mass.

Whatever this new physics is, if it solves the hierarchy problem, it needs to change the Higgs properties. Either by modifying its couplings to the SM particles, by introducing new particles which cancel the quadratic divergence of the top quark loop, or by a combination of both. Consequently, two of the best motivated strategies to pin down possible extensions of the SM are to look for modified Higgs couplings and for top partners. The LHC, currently starting at an unprecedented center of mass energy of 13 TeV, offers a unique environment to accomplish this task. Thanks to the higher available energy, more Higgs bosons are produced and, in addition, the production cross section for so far unknown heavy particles increases due to the greater available phase space.

Two of the most discussed and elaborated models for BSM physics at the LHC are supersymmetic and composite Higgs models. They will serve us in their minimal realizations as benchmark models for the analyses presented in this thesis. Both models solve the hierarchy

problem if some of their predicted particles are at the TeV scale. Moreover, they come along with modified Higgs couplings.

In this thesis we pursue a twofold approach and point out two complementary methods to search for new physics at the LHC. On the one hand, we present a study based on very boosted Higgs production in association with a high transverse momentum jet to trace down new physics in the gluon fusion process. In both supersymmetric but especially in composite Higgs models, the effects of top partners and of a modified top Yukawa interaction can balance each other and lead to a SM-like cross section for gluon fusion that contains no information on the mass spectrum of the theory. We show that this degeneracy can be broken by measuring the cross section of very boosted Higgs production. This opens an alternative way to the difficult $t\bar{t}h$ channel to determine the important top Yukawa interaction. In addition, knowing the effective Higgs-gluon interaction that is generated by loops of the top partners, allows to draw conclusions on their mass spectrum.

In the second part of this thesis, we present a direct search strategy for light scalar partners of the third generation quarks, called stops and sbottoms, which are predicted by supersymmetry. In order to solve the hierarchy problem without too much fine tuning, these squarks need to be close to the TeV scale or even below and should therefore be accessible at the LHC. However, the event shape of decaying stops depends strongly on the mass difference between the initial squark and the particles it decays into, mostly higgsinos and top or bottom quarks. This makes it difficult to design an analysis that is capable of detecting squarks over a large range of masses. In this thesis we propose to look for squark pair production where both squarks decay into top quarks which then decay hadronically. Depending strongly on the mentioned mass difference, the typical transverse momentum of the top quarks and thus the distribution of its decay products can range from very collimated for boosted to well separated for unboosted top quarks. We suggest to use different jet substructure techniques to tag the top quarks over a large range of possible transverse momenta and we describe a collider analysis based on this scale invariant approach.

The remainder of the thesis is structured as follows. After setting the notation and briefly reviewing the electroweak symmetry breaking (EWSB) in the SM in Chapter 2, we introduce the main ideas of supersymmetric and composite Higgs models in Chapters 3 and 4, respectively. In these chapters we focus in particular on how the specific model in its minimal realization breaks the electroweak symmetry and solves the hierarchy problem. Thereafter we present the Higgs coupling measurement based on very boosted Higgs production in Chapter 5. Here, we first motivate this measurement in the context of composite Higgs and supersymmetric models in Section 5.1 before we make the actual calculation of the boosted cross section and estimate the resolution power in Sections 5.2 and 5.3, respectively. Finally, in Chapter 5.4 we outline a realistic collider study designed for this measurement.

In Section 6 we describe the strategy for a scale invariant stop and sbottom search. After specifying the event generation in Section 6.1, we give a detailed description of the top quark reconstruction and the analysis cuts in Section 6.2 before summarizing the results in Section 6.3. We conclude in Chapter 7.

2. The Standard Model of particle physics

The Standard Model of Particle Physics (SM), as it was formulated in the 1970s, describes the properties of all known elementary particles and their interactions via the electromagnetic, weak and strong forces. It does not include gravity, firstly because gravity does not play any role at the energy scales relevant at present colliders since its coupling is by many orders of magnitude weaker than that of the other forces. Secondly because there is no known phenomenologically consistent and renormalizable description within the framework of quantum field theory (QFT).

2.1. Electroweak symmetry breaking in the SM

Symmetries play a very profound role in physics since they are linked to conserved quantities via the Noether Theorem [17]. The importance and fundamental role of gauge symmetries[1] in particle physics was established by the overwhelming agreement of the experimental results with the predictions derived from the QED Lagrangian ($U(1)$-symmetry) [18–20]. Gauge symmetries therefore seemed to be a fundamental building block of nature and it was consequently natural to try to describe the weak force by a gauge symmetry as well. However, the gauge bosons of the weak force, $W^{\pm}$ and Z, are massive while their mass terms are forbidden in the Lagrangian by gauge symmetry. This apparent contradiction can be resolved by demanding a spontaneous breaking of the symmetry, meaning that the Lagrangian is symmetric under the given gauge symmetries but the ground state is not.

When a global continuous symmetry is broken spontaneously, a mass- and spinless particle, a so-called Goldstone boson, emerges for each generator which does not leave the vacuum invariant [21–25]. This alone would not solve the problem but rather make it worse as the only known massless particles are the photon and the gluons. However, if the broken symmetry is a gauge symmetry, the Goldstone bosons do not appear in the particle spectrum, but their degrees of freedom are used to give mass to the gauge bosons. This mechanism of gauge bosons becoming massive by "eating" the Goldstone bosons was first discovered by Anderson in the context of condensed matter physics [26], applied to quantum field theory by Higgs and others [27–31] and is now known as the Higgs mechanism. Later, t'Hooft

[1] Strictly speaking, the gauge symmetries are not symmetries but rather redundancies of our description.

showed that renormalizability is not spoiled by the spontaneous breaking [32].

The electroweak sector of the SM describes both the weak and the electromagnetic force communicated by the three massive bosons $W^{\pm}$ and Z and the massless photon, respectively. In order to include all four gauge bosons in the description, the symmetry group G_{EW} of the electroweak theory needs to have four generators out of which three are broken spontaneously, giving mass to the weak gauge bosons. The group $G_{EW} = SU(2)_L \times U(1)_Y$ (weak isospin $\times$ hypercharge) broken down to the electromagnetic $U(1)_{em}$ of QED yields the necessary properties. For the spontaneous breaking the Higgs field, a complex scalar doublet under $SU(2)_L$ with hypercharge 1/2, is introduced with its potential

$$V(\phi) = -\mu^2 \phi^\dagger \phi + \lambda \left(\phi^\dagger \phi\right)^2 \tag{2.1.1}$$

and covariant derivative

$$D_\mu \phi = \left(\partial_\mu - i g A_\mu^a \tau^a - i \frac{1}{2} g' B_\mu\right) \phi \,, \tag{2.1.2}$$

with $\tau^a = \frac{1}{2}\sigma^a$ being the generators of $SU(2)$, g and g' the $SU(2)_L$ and $U(1)_Y$ coupling constants, and A_μ^a and B_μ the respective gauge bosons.

Although the potential is symmetric by construction, the ground state is not when $\mu^2 > 0$. In that case the symmetry breaking minimum is obtained for $|\phi| = \frac{1}{\sqrt{2}}\sqrt{\frac{\mu^2}{\lambda}} \equiv \frac{v}{\sqrt{2}}$. By gauge invariance one can choose the vacuum expectation value (vev) of the Higgs field to point in the direction of the neutral component

$$\langle \phi \rangle_0 = \frac{1}{\sqrt{2}} \begin{pmatrix} 0 \\ v \end{pmatrix} \tag{2.1.3}$$

and expand the Higgs field around it. Omitting the terms which contain the physical Higgs field, the kinetic term of the scalar field becomes

$$(D_\mu \phi)^\dagger \, (D^\mu \phi) \to \frac{1}{2} \frac{v^2}{4} \left(g^2 A_\mu^a A^{a\,\mu} - 2\, g g' A_\mu^3 B^\mu + g'^2 B_\mu B^\mu\right) \tag{2.1.4}$$

$$= \frac{1}{2} \frac{v^2}{4} \begin{pmatrix} A^1, & A^2, & A^3, & B \end{pmatrix}_\mu \begin{pmatrix} g^2 & 0 & 0 & 0 \\ 0 & g^2 & 0 & 0 \\ 0 & 0 & g^2 & g g' \\ 0 & 0 & g g' & g^2 \end{pmatrix} \begin{pmatrix} A^1 \\ A^2 \\ A^3 \\ B \end{pmatrix}^\mu \,. \tag{2.1.5}$$

Diagonalizing the 2×2 sub-matrix yields

$$\frac{1}{2} \frac{v^2}{4} \begin{pmatrix} \frac{g A^3 - g' B}{\sqrt{g^2 + g'^2}} & \frac{g B + g' A^3}{\sqrt{g^2 + g'^2}} \end{pmatrix}_\mu \begin{pmatrix} g^2 + g'^2 & 0 \\ 0 & 0 \end{pmatrix} \begin{pmatrix} \frac{g A^3 - g' B}{\sqrt{g^2 + g'^2}} \\ \frac{g B + g' A^3}{\sqrt{g^2 + g'^2}} \end{pmatrix}^\mu \,, \tag{2.1.6}$$

which suggests the identification of the massless boson with the photon and the massive one with the Z:

$$A_\mu = \frac{gB_\mu + g' A^3_\mu}{\sqrt{g^2 + g'^2}} \qquad Z_\mu = \frac{gA^3_\mu - g' B_\mu}{\sqrt{g^2 + g'^2}}\,. \tag{2.1.7}$$

The rotation matrix used for the diagonalization is given by

$$\begin{pmatrix} \cos\theta_W & \sin\theta_W \\ -\sin\theta_W & \cos\theta_W \end{pmatrix} = \frac{1}{\sqrt{g^2 + g'^2}} \begin{pmatrix} g & g' \\ -g' & g \end{pmatrix} \tag{2.1.8}$$

and defines the weak mixing angle θ_W. From now on we will use the short hand notation s_W and c_W for $\sin\theta_W$ and $\cos\theta_W$, respectively.

Replacing A^3_μ and B_μ in the covariant derivative by the physical bosons A_μ and Z_μ leads to

$$D_\mu\phi = \left(\partial_\mu - \sum_{a=1}^{2} igA^a_\mu \tau^a - iA_\mu \frac{gg'}{\sqrt{g^2 + g'^2}} \left(\tau^3 + Y\right) - iZ_\mu \frac{1}{\sqrt{g^2 + g'^2}} \left(g^2\tau^3 - g'^2 Y\right)\right)\phi\,. \tag{2.1.9}$$

Since the photon is the gauge boson that transmits the electromagnetic force and couples with the electric charge, the charge operator and the unit electric charge are given by

$$Q = \tau^3 + Y \qquad \text{and} \qquad e = \frac{gg'}{\sqrt{g^2 + g'^2}}, \tag{2.1.10}$$

respectively. After combining Eqs. (2.1.8) and (2.1.10), the couplings g and g' can be expressed in terms of e and θ_W as

$$g = \frac{e}{s_W} \qquad \text{and} \qquad g' = \frac{e}{c_W}\,. \tag{2.1.11}$$

The electric charge of the combination $\left(g^2\tau^3 - g'^2 Y\right)$ is given by

$$Q(Z) = \left[Q, \left(g^2\tau^3 - g'^2 Y\right)\right] = 0 \tag{2.1.12}$$

and justifies post-hoc the identification of this combination with the electrically neutral Z-boson. The combinations $\tau^\pm = \tau^1 \pm i\tau^2$ are charge eigenstates with charge ± 1

$$\left[Q, \tau^\pm\right] = \pm\tau^\pm \tag{2.1.13}$$

and make it possible to write the covariant derivative as a combination of charge and mass eigenstates $W^\pm_\mu = \frac{1}{\sqrt{2}}\left(A^1_\mu \mp iA^2_\mu\right)$

$$D_\mu\phi = \left(\partial_\mu - i\frac{g}{\sqrt{2}}\left(W^+_\mu\tau^+ + W^-_\mu\tau^-\right) - ieA_\mu Q - i\frac{g}{c_W} Z_\mu(\tau^3 - s^2_W Q)\right)\phi\,. \tag{2.1.14}$$

From Eqs. (2.1.5) and (2.1.6) together with Eq. (2.1.11) the masses of the gauge bosons can be read off as

$$m_A = 0, \qquad m_Z = \frac{v}{2}\frac{e}{s_W\, c_W}, \qquad \text{and} \qquad m_W = \frac{v}{2}\frac{e}{s_W} \tag{2.1.15}$$

showing the tree-level relation of the gauge boson masses

$$\rho \equiv \frac{m_W^2}{m_Z^2\, c_W^2} = 1\,. \tag{2.1.16}$$

2.2. Particle content

To include the fermions in the SM one needs to specify their transformation properties under the SM gauge groups and build gauge singlets out of the fields. Table 2.1 lists these properties and the electric charge of the fermions and the Higgs doublet. The fermions of the SM come in right- and left-handed chiralities and only the latter transform non-trivially under $SU(2)_L$. The difference between quarks and leptons is that the former live in the fundamental representation of $SU(3)_C$ while the latter transform trivially under the color group.

	$SU(3)_C \times SU(2)_L \times U(1)_Y$	$Q = \tau^3 + Y$
$Q_L = \begin{pmatrix} u_L \\ d_L \end{pmatrix}$	$(\mathbf{3}, \mathbf{2}, 1/6)$	$\begin{pmatrix} 2/3 \\ -1/3 \end{pmatrix}$
u_R	$(\mathbf{3}, \mathbf{1}, 2/3)$	$2/3$
d_R	$(\mathbf{3}, \mathbf{1}, -1/3)$	$-1/3$
$l_L = \begin{pmatrix} \nu_L^e \\ e_L \end{pmatrix}$	$(\mathbf{1}, \mathbf{2}, -1/2)$	$\begin{pmatrix} 0 \\ -1 \end{pmatrix}$
e_R	$(\mathbf{1}, \mathbf{1}, -1)$	-1
$\phi = \begin{pmatrix} \phi^+ \\ \phi^0 \end{pmatrix}$	$(\mathbf{1}, \mathbf{2}, 1/2)$	$\begin{pmatrix} 1 \\ 0 \end{pmatrix}$

Table 2.1.: Transformation properties and electric charges of the SM fermions and the Higgs doublet under the gauge symmetries of the SM. For each fermion there are three more copies with exactly the same quantum numbers, corresponding to the three generations. u and d denote the up- and down-type quarks, ν, e the neutrinos and charged leptons, and ϕ the Higgs doublet. Right-handed fields appear as singlets, left-handed fields and the Higgs as doublets under $SU(2)_L$.

A mass term for the fermions necessarily combines right- and left-handed fields because the combination of two fermions with the same chiralities vanishes, $\bar{\psi}_{L,R}\psi_{L,R} = 0$ but

$\bar{\psi}_{L,R}\psi_{R,L} \neq 0$. This is also the reason why the neutrinos are massless in the SM: since there is no right-handed neutrino, no mass term of dimension 4 or less can be constructed.

Since the left-handed fermions are doublets under $SU(2)_L$ while the right-handed are singlets, the Higgs doublet is needed to form gauge invariant operators. The mass is then generated only after electroweak symmetry breaking via the Yukawa interactions

$$\mathcal{L}_Y = -y_l \bar{l}_L \phi e_R - y_u \bar{Q}_L \tilde{\phi} u_R - y_d Q_L \phi d_R + h.c. \tag{2.2.1}$$

$$\rightarrow \left[-m_e \bar{e}e - m_u \bar{u}u - m_d \bar{d}d\right] \left(1 + \frac{h}{v}\right), \tag{2.2.2}$$

where $\tilde{\phi}_i = \epsilon_{ij}(\phi^j)^*$ with $\epsilon_{12} = +1$ being the anti symmetric tensor. h is the physical Higgs field, l, q_L, e_R, u_R, and d_R are the fermion fields introduced in Table 2.1, and $m_\psi = y_\psi v/\sqrt{2}$ is the mass of the respective fermion which appears in the combination $\bar{\psi}\psi = \bar{\psi}_L\psi_R + \bar{\psi}_R\psi_L$, where ψ stands for one of the fermions of the Lagrangian. From Eq. (2.2.2) it becomes clear that the coupling between the fermions and the Higgs is proportional to the mass of the fermions. Therefore, the Higgs production via valence quarks at the LHC is negligible and gluon fusion via top loops is the most important Higgs production channel despite being loop suppressed.

2.3. Reasons for physics beyond the SM

Despite the enormous success of the SM it is clear that there has to be new physics beyond it to describe the observations that it does not explain, e.g. dark matter and dark energy, neutrino oscillations or the matter-antimatter asymmetry. At the latest at the Planck scale $\Lambda_{Pl} \sim 10^{19}\,\text{GeV}$ when gravity is no longer negligible, some new theory is needed to describe nature. Nowadays the SM is therefore considered to be an effective low energy theory and only valid up to the scale Λ_{NP} where the new physics sets in. This new physics is not only expected to describe at least some of the above observations but also to answer theoretical problems of the SM, e.g. the strong CP-problem (why is the neutron electric dipole moment so small?) [33], the flavor puzzle (why have the Yukawa interactions the structure we observe and where does their hierarchy come from?), or the hierarchy problem [34–37].

The latter is the question why the Higgs is so light. At tree level its mass is obtained from the potential in Eq. (2.1.1) and is given by $m_h^2 = \lambda v^2$. Since λ is expected to be of $\mathcal{O}(1)$ by naturalness arguments, it is expected to have the tree-level Higgs mass at the electroweak scale. However, when calculating loop corrections to the Higgs mass in the SM, one finds a quadratic sensitivity to the UV scale $\delta m_h^2 \sim \mathcal{O}(1)\Lambda_{NP}^2$ from the top loop. Unless unnatural fine tuning is at work, one would therefore expect a Higgs mass of the order Λ_{NP}. Since no new physics beyond the SM has been discovered at the LHC so far,

Λ_{NP} has to be well above the electroweak scale $\Lambda_{EW} \sim 100\,\text{GeV} \ll \Lambda_{NP}$. This leaves us with two possibilities: Either nature is fine tuned and a seemingly "unnatural" cancellation happens in nature[2] or there is new physics to protect the Higgs mass and keep it at the electroweak scale. Supersymmetric models and composite Higgs models, discussed in the next two sections, are two intensively investigated models for such new physics and offer solutions to the hierarchy problem. Having no clear sign that the previously mentioned observations are related to physics at the TeV scale, the hierarchy problem is actually one of the best motivations to look for new physics at the LHC.

[2] One example for fine tuning in nature is the apparent radius of the moon and the sun. Despite having very different sizes, their respective distance to earth is such that they cover nearly the same area in the sky. This corresponds to a tuning of about 1/100. Although the presence of the moon might be explained from an anthropic point of view, this does not explain the observed diameters.

3. Supersymmetry

Supersymmetric extensions of the SM [38–41] are among the most studied models for new physics at the LHC. They provide elegant solutions to several of the aforementioned problems of the SM:

- Supersymmetry (SUSY) reliefs the hierarchy problem. It comes along with scalar partners to the SM fermions which have the same mass as their fermion partner if SUSY is unbroken. Furthermore, their couplings are related by the symmetry requirement such that in the unbroken phase the quadratic sensitivity to the UV scale arising from the top loop is canceled exactly by a loop of the scalar top partner. Even if SUSY is broken[1], which is obviously the case in nature because no supersymmetric particles were discovered so far, the sensitivity is only logarithmically and not quadratically as in the SM.

- R-parity [41], a discrete $\mathbb{Z}_2$ symmetry under which all SUSY particles are odd and all SM and Higgs particles are even, is usually introduced to prevent rapid proton decay. If it is conserved, supersymmetric particles can be only produced in even numbers. Moreover, a decaying SUSY particle has to decay into an odd number of SUSY particles and an arbitrary number of SM particles. Consequently the lightest SUSY particle (LSP) is stable, necessarily neutral, since it has not been discovered yet, and provides therefore an appealing candidate for dark matter.

- The gauge couplings of the SM gauge group do not unify in the UV. While this is not a problem phenomenologically, it contradicts the idea of a grand unified theory at some high scale. SUSY modifies the beta-functions and can lead to gauge coupling unification if the SUSY masses lie between 10^2 GeV and 10^5 GeV [42–44].

- SUSY is not only well motivated from the phenomenological but also from the mathematical point of view. Coleman and Mandula [45] showed in a no-go theorem that there is no non-trivial combination of the Poincaré Group and internal symmetries. Later however, Haag, Łopuszański, and Sohnius [46] showed that there is a loophole

[1] Actually, SUSY has to be broken softly, as we will discuss below. Otherwise it will introduce new UV sensitivities.

in the argument if anti-commuting generators are allowed. Then there is one possible non-trivial combination, the so-called graded or super algebra that establishes a link between the gauge symmetries and gravity and that is the basis of SUSY. Moreover, it looks as if SUSY is an important building block of realistic string models.

The key concept of SUSY is the connection of bosons and fermions through the SUSY generator which transforms one into the other. The details of the SUSY algebra can be looked up in detail for example in Ref. [7] or Ref. [6] and will not be discussed here. In the following we will rather focus on the phenomenological implications and in particular on the electroweak symmetry breaking mechanism in the minimal supersymmetric extension of the SM (MSSM) [47]. The MSSM is an example for $\mathcal{N} = 1$ supersymmetry, i.e. it has only one SUSY generator and its conjugate. Further, the MSSM assumes only the minimal particle content needed to cover all the known particles of the SM and to allow a consistent phenomenology. Non-minimal extensions, which contain additional particles or gauge groups and theories with more SUSY generators are studied in the literature [48–50]. While the former can help to circumvent the restrictions obtained from the LHC or other experiments, the latter are mainly interesting from a theoretical or mathematical point of view.

In the MSSM, the particles are combined in supermultiplets which are irreducible representations of the SUSY algebra. The two simplest supermultiplets are the chiral and gauge supermultiplets. The former consist of a complex scalar and a two component Weyl fermion while the latter consist of a massless spin 1 boson and a two component Weyl fermion as well.

All SM fermions form chiral multiplets together with their respective scalar partner. They are shown together with their transformation properties under the SM gauge group in the first two blocks of Table 3.1. The R, L subscript of the scalars refers to the helicity of their partner fermion. Right handed fermions appear for conventional reasons as their conjugates such that only left-handed Weyl spinors appear in the multiplets.

Unlike the SM, the MSSM needs two complex Higgs doublets: The fermionic superpartner of one of the Higgs bosons contributes to the gauge anomaly and this contribution is canceled by the fermionic superpartners of the other Higgs multiplet which caries opposite $U(1)_Y$ charge. Another reason is that the requirement of SUSY invariance demands a holomorphic superpotential (the part of the Lagrangian that contains the so-called F-terms, which include the Yukawa interactions) and thus forbids any occurrence of the conjugate of the Higgs field. Therefore a Higgs can couple either to the up-type quarks or to the down-type quarks and charged leptons. So, two Higgs doublets are needed to construct Yukawa interactions for each of the two types. The Higgs bosons and their fermionic superpartners are combined in chiral supermultiplets as well, which are shown in the last block of Table 3.1. Finally, the gauge bosons are embedded in the gauge multiplets. Each of the bosons is accompanied by

symbol	Complex scalars	Weyl fermions	$SU(3)_C \times SU(2)_L \times U(1)_Y$
Q	$\left(\tilde{u}_L, \tilde{d}_L\right)$	(u_L, d_L)	$(\mathbf{3}, \mathbf{2}, 1/6)$
$\bar{u}$	$\tilde{u}_R^*$	$u_R^\dagger$	$(\bar{\mathbf{3}}, \mathbf{1}, -2/3)$
$\bar{d}$	$\tilde{d}_R^*$	$d_R^\dagger$	$(\bar{\mathbf{3}}, \mathbf{1}, 1/3)$
L	$(\tilde{\nu}_L, \tilde{e}_L)$	(ν_L, e_L)	$(\mathbf{1}, \mathbf{2}, -1/2)$
$\bar{e}$	$\tilde{e}_R^*$	$e_R^\dagger$	$(\bar{\mathbf{1}}, \mathbf{1}, 1)$
H_u	$\left(H_u^+, H_u^0\right)$	$\left(\widetilde{H}_u^+, \widetilde{H}_u^0\right)$	$(\mathbf{1}, \mathbf{2}, +1/2)$
H_d	$\left(H_d^0, H_d^-\right)$	$\left(\widetilde{H}_d^0, \widetilde{H}_d^-\right)$	$(\mathbf{1}, \mathbf{2}, -1/2)$

Table 3.1.: The chiral supermultiplets of the MSSM. Each multiplet consists of a complex scalar and a left-handed two component Weyl fermion. As in the SM where left-handed fermions come in $SU(2)_L$ doublets, the chiral multiplets containing the left-handed fields are combined in doublets. The first block lists the quark multiplets, the second the lepton multiplets and finally the last block the Higgs doublets with their higgsino superpartners. Like in the SM, there are two more copies for each matter multiplet corresponding to the three generations. This table is taken from [6].

Names	Vector bosons	Weyl fermions	$SU(3)_C \times SU(2)_L \times U(1)_Y$
gluon, gluino	g	$\tilde{g}$	$(\mathbf{8}, \mathbf{1}, 0)$
W bosons, winos	$W^\pm\ W^0$	$\widetilde{W}^\pm\ \widetilde{W}^0$	$(\mathbf{1}, \mathbf{3}, 0)$
B boson, bino	B^0	$\widetilde{B}^0$	$(\mathbf{1}, \mathbf{1}, 0)$

Table 3.2.: The gauge multiplets of the MSSM. Each multiplet consists of a gauge boson with spin-1, corresponding to the gauge bosons of the SM, and a left-handed two component Weyl fermion, the gaugino. This table is taken from [6].

its fermionic superpartner as is shown in Table 3.2.

The nomenclature is as follows: Scalar superpartners are denoted by prepending a "s" to their SM partner, i.e. "stop" for scalar top partner. Scalar quarks and leptons are denoted collectively as "squarks" and "sleptons". Fermionic superpartners are named by appending "-ino" to their SM partners, i.e. "gluino" or "bino". Depending on whether they are the partners of the Higgs bosons or the gauge bosons they are called collectively "higgsinos" or "gauginos", respectively.

3.1. The MSSM Lagrangian

In the following, the MSSM Lagrangian is constructed step by step but without proving its invariance under SUSY. Besides the notation used here, one could employ the superspace and superfield notation in terms of fermionic grassmann variables. This has the advantage that

the obtained Lagrangian is manifestly supersymmetric. As a down-side it is less obvious from the phenomenological point of view which is why it is not used here. The final Lagrangian is of course the same.

For the start only the chiral superfields are considered. A free chiral multiplet with a complex scalar ϕ and a two component Weyl fermion ψ is described by the non-interacting massless Wess-Zumino model [51]

$$\mathcal{L}_{\text{free}} = -\partial^\mu \phi^* \, \partial_\mu \phi + i\psi^\dagger \bar{\sigma}^\mu \partial_\mu \psi + F^* F \,, \tag{3.1.1}$$

where $\bar{\sigma}^0 = \sigma^0$ and $\bar{\sigma}^i = -\sigma^i$ for $i = 1, 2, 3$ and σ^μ are the usual Pauli matrices. The first two terms in Eq. (3.1.1) are just the usual kinetic terms for a scalar and a Weyl fermion, respectively. In the last term a so-called auxiliary field F, a complex scalar with mass dimension 2, is introduced. It is needed to close the superalgebra off-shell where the fermion has two more degrees of freedom than the scalar, but it vanishes on-shell due to its equation of motion $F = F^* = 0$. It is therefore no physical particle and does not appear in the spectrum.

The above Lagrangian is invariant under SUSY transformations, but to be interesting for phenomenology, it needs to include interactions. They are introduced by writing the most general renormalizable and SUSY invariant Lagrangian for the interactions between scalars, fermions, and F. It is given by

$$\mathcal{L}_{\text{int}} = \left(-\frac{1}{2} \mathcal{W}^{ij} \psi_i \psi_j + \mathcal{W}^i F_i \right) + \text{c.c.} \,, \tag{3.1.2}$$

where $\mathcal{W}^{ij}$ and $\mathcal{W}^i$ are polynomials in the scalar fields and have mass dimension 1 and 2, respectively. The $\mathcal{W}$s are further constrained to be holomorphic in the scalar fields, i.e. must not contain ϕ^* , and it can be shown that they can be written as derivatives

$$\mathcal{W}^i = \frac{\delta}{\delta \phi_i} \mathcal{W} \qquad \mathcal{W}^{ij} = \frac{\delta^2}{\delta \phi_i \, \delta \phi_j} \mathcal{W} \tag{3.1.3}$$

of a function $\mathcal{W}$, called the superpotential. The most general form of the superpotential is given by

$$\mathcal{W} = L^i \phi_i + \frac{1}{2} M^{ij} \phi_i \phi_j + \frac{1}{6} y^{ijk} \phi_i \phi_j \phi_k \,, \tag{3.1.4}$$

where M^{ij} are mass matrices for the scalars and y^{ijk} take over the role of the Yukawa couplings. The L_i term is forbidden in the MSSM due to the requirement of gauge invariance and will be omitted in the following. It might, however, show up in less minimal extensions of the SM where gauge singlets are introduced.

After combining $\mathcal{L}_{\text{free}}$ and $\mathcal{L}_{\text{int}}$ and removing the auxiliary fields by their equations of motion $F_i = -\mathcal{W}_i^*$ and $F_i^* = -\mathcal{W}_i$, one obtains

$$\mathcal{L}'_{\text{chiral}} = \mathcal{L}_{\text{free}} - \frac{1}{2} \left(\mathcal{W}^{ij} \psi_i \psi_j + \mathcal{W}^*_{ij} \psi^{\dagger i} \psi^{\dagger j} \right) - \mathcal{W}^i \mathcal{W}^*_i \,. \tag{3.1.5}$$

The scalar potential of this Lagrangian is given by

$$V(\phi,\phi^*) = \mathcal{W}^i\mathcal{W}_i^* = \left|\frac{\delta}{\delta\phi_i}\mathcal{W}\right|^2 = M_{ik}^* M^{kj}\phi^{*\,i}\phi_j + \frac{1}{4}y^{ijn}y_{kln}^*\phi_i\phi_j\phi^{*\,k}\phi^{*\,l} + \cdots\,, \tag{3.1.6}$$

with the ellipses indicating the terms containing the ϕ^3- and ϕ^4-terms. Now several important observations can be made. Since V is written as an absolute square of the derivatives of the superpotential, it can never get smaller than zero. It is thus automatically bounded from below. Further, one can observe that the mass matrices M_{ij} do not only give mass to the scalars but also to the fermions via the terms in the brackets in Eq. (3.1.5). The particles within one chiral supermultiplet are therefore mass degenerate. Moreover, both the ϕ^4 and the $\psi\phi^2$ couplings originate from the Yukawa terms of the superpotential and are therefore related. Together with the mass degeneracy this has the exact cancellation of the quadratic UV sensitivity of the Higgs mass as a direct consequence.

Clearly, the mass degeneracy is not present in nature because no supersymmetric particles have been found up to now, in particular not with the masses of the SM particles. Therefore SUSY cannot be a symmetry of nature at the electroweak scale, but must be somehow broken. From Eq. (3.1.4) it can also be seen why two Higgs doublets are needed in the MSSM. The Yukawa terms in the superpotential are needed to give mass to the SM fermions after electroweak symmetry breaking. Since the superpotential has to be holomorphic it can not contain the Higgs and its complex conjugate. Then the only way to couple both up- and down-type quarks and charged leptons in a gauge invariant way to a Higgs is via two different Higgs bosons with opposite hypercharge.

Next, the Lagrangian describing the fields of the gauge supermultiplet is considered. It is given by

$$\mathcal{L}_{\text{gauge}} = -\frac{1}{4}F_{\mu\nu}^a F^{a\,\mu\nu} + i\lambda^{\dagger\,a}\bar{\sigma}^\mu\nabla_\mu\lambda^a + \frac{1}{2}D^a D^a\,, \tag{3.1.7}$$

where $F_{\mu\nu}^a = \partial_\mu A_\nu^a - \partial_\nu A_\mu^a + g f^{abc}A_\mu^b A_\nu^c$ is the usual fieldstrength tensor with the structure constants f^{abc}, the second term is the kinetic term of the gaugino λ with the covariant derivative $\nabla_\mu\lambda^a = \partial_\mu\lambda^a + g f^{abc}A_\mu^b\lambda^c$, and D^a is again an auxiliary field introduced in analogy to F in Eq. (3.1.1).

In order to combine $\mathcal{L}'_{\text{chiral}}$ and $\mathcal{L}_{\text{gauge}}$, the derivatives in the former need to be replaced by the covariant derivatives given by

$$\nabla_\mu\phi_i = \partial_\mu\phi_i - igA_\mu^a\left(T^a\phi\right)_i\,, \tag{3.1.8}$$

$$\nabla_\mu\phi^{*i} = \partial_\mu\phi^{*i} + igA_\mu^a\left(\phi^*T^a\right)^i\,, \tag{3.1.9}$$

$$\nabla_\mu\psi_i = \partial_\mu\psi_i - igA_\mu^a\left(T^a\psi\right)_i\,, \tag{3.1.10}$$

with T^a being the generators of the gauge group in question. Further, additional terms, which introduce interactions among the fields of the chiral and the gauge supermultiplets,

have to be introduced. These terms are fixed by gauge invariance and SUSY and one obtains as a final result

$$\mathcal{L} = \mathcal{L}_{\text{chiral}} + \mathcal{L}_{\text{gauge}} - \sqrt{2}g\left(\phi^* T^a \psi\right)\lambda^a - \sqrt{2}g\lambda^{\dagger\, a}\left(\psi^\dagger T^a \phi\right) + g\left(\phi^* T^a \phi\right) D^a\,, \tag{3.1.11}$$

where $\mathcal{L}_{\text{chiral}}$ is obtained from $\mathcal{L}'_{\text{chiral}}$ in Eq. (3.1.5) by making the replacements (3.1.8-3.1.10). Replacing the D^a by their equations of motion $D^a = -g\left(\phi^* T^a \phi\right)$ in Eq. (3.1.11) extends the scalar potential which so far only consisted of so-called "F-terms" by the "D-terms"

$$V\left(\phi, \phi^*\right) = F^{*i} F_i + \frac{1}{2}\sum_a D^a D^a = \mathcal{W}_i^* \mathcal{W}^i + \frac{1}{2}\sum_a g_a^2 \left(\phi^* T^a \phi\right)^2\,, \tag{3.1.12}$$

where the sum is over the generators of the gauge groups of the theory. The above observation about the properties of the scalar potential and the cancellation of the quadratic UV sensitivity remain of course valid even in the presence of the D-terms.

The Lagrangian in Eq. (3.1.11) was constructed to be invariant under SUSY and therefore cannot be a viable description of nature at the electroweak scale. Consequently, SUSY breaking has to be introduced to complete the MSSM and to obtain a phenomenological Lagrangian. Explicit and viable models of SUSY breaking are, however, difficult to construct. If they are to contain only renormalizable interactions they predict very light supersymmetric particles via sum rules that link the masses of fermions and scalars. A common approach is therefore to assume that SUSY is broken in a hidden sector which is only weakly coupled to the MSSM. The breaking of SUSY is then mediated via a weak interaction to the MSSM sector and can be described by adding terms to the MSSM Lagrangian that explicitly break SUSY. At the same time, however, the cancellation of the quadratic divergences in the Higgs mass corrections must not be spoiled. This is achieved by breaking SUSY softly, meaning that only operators that have a coupling constant with positive mass dimension are allowed to break SUSY. In the effective field theory language those operators are relevant and their effect becomes less important at high energies. Thus they do not spoil the UV cancellation. It was shown that the soft SUSY breaking Lagrangian below does not induce quadratic divergences to all orders in perturbation theory [52]. For the field content of the MSSM this Lagrangian is

$$\mathcal{L}_{\text{soft}} = -\left(\frac{1}{2}M_a \lambda^a \lambda^a + \frac{1}{6}a^{ijk}\phi_i\phi_j\phi_k + \frac{1}{2}b^{ij}\phi_i\phi_j\right) + \text{c.c.} - \left(m^2\right)^i_j \phi^{*j}\phi_i\,. \tag{3.1.13}$$

Now all the ingredients for the MSSM are prepared. One just needs to replace the generic superfields in $\mathcal{W}$, $\mathcal{L}$ and $\mathcal{L}_{\text{soft}}$ by the MSSM fields listed in tables 3.1 and 3.2 and impose gauge invariance under the SM gauge group $SU(3)_C \times SU(2)_L \times U(1)_Y$. The MSSM superpotential

is then given in terms of the superfields[2] by

$$\mathcal{W}_{\text{MSSM}} = \bar{u}\mathbf{y_u}QH_u - \bar{d}\mathbf{y_d}QH_d - \bar{e}\mathbf{y_e}LH_d + \mu H_u H_d\,, \tag{3.1.14}$$

where a sum over the three generations is explicitly understood and the $\mathbf{y}_\psi$ are the usual Yukawa matrices in flavor space. The MSSM version of $\mathcal{L}_{\text{soft}}$ is given by

$$\mathcal{L}_{\text{soft}}^{\text{MSSM}} = -\frac{1}{2}\left(M_3\tilde{g}\tilde{g} + M_2\widetilde{W}\widetilde{W} + M_1\widetilde{B}\widetilde{B} + \text{c.c.}\right) \tag{3.1.15}$$

$$-\left(\tilde{\bar{u}}\,\mathbf{a_u}\,\widetilde{Q}H_u - \tilde{\bar{d}}\,\mathbf{a_d}\,\widetilde{Q}H_d - \tilde{\bar{e}}\,\mathbf{a_e}\,\widetilde{L}H_d + c.c\right) \tag{3.1.16}$$

$$-\widetilde{Q}^\dagger\mathbf{m_Q^2}\widetilde{Q} - \widetilde{L}^\dagger\mathbf{m_L^2}\widetilde{L} - \tilde{\bar{u}}\,\mathbf{m_{\bar{u}}^2}\,\tilde{\bar{u}}^\dagger - \tilde{\bar{d}}\,\mathbf{m_{\bar{d}}^2}\,\tilde{\bar{d}}^\dagger - \tilde{\bar{e}}\,\mathbf{m_{\bar{e}}^2}\,\tilde{\bar{e}}^\dagger \tag{3.1.17}$$

$$-m_{H_u}^2 H_u^* H_u - m_{H_d}^2 H_d^* H_d - (bH_u H_d + \text{c.c.})\,. \tag{3.1.18}$$

When comparing $\mathcal{W}_{\text{MSSM}}$ and $\mathcal{L}_{\text{soft}}$, it can be seen that except for μ all parameters that are not already present in the SM are introduced by the SUSY breaking part. This means that the 105 new parameters introduced in the MSSM [53] reflect our ignorance of the actual breaking mechanism. While they could in principle take any value, most of them lead to flavor or CP-violation and are severely restricted by experiments (see for example [54] and references therein). Besides the R-parity, which is well motivated by the non-observation of proton decay and leads to a dark matter candidate, the following assumptions are usually made in the MSSM to account for the experimental constraints.

- The tri-linear scalar mixing matrices in Eq. (3.1.16) are proportional to the Yukawa matrices $\mathbf{a}_\psi = A_\psi \mathbf{y}_\psi$,
- both, the proportionality factors A_ψ and the gaugino Masses M_i in Eq. (3.1.15) are real and
- the soft masses in Eq. (3.1.17) are diagonal in flavor space $\mathbf{m}_\psi^\mathbf{2} = \text{diag}\left(m_{\psi_1}^2, m_{\psi_2}^2, m_{\psi_3}^2\right)$, and the first and second generation are mass degenerate $m_{\psi_1}^2 = m_{\psi_2}^2$.

A careful count reveals that from the 105 parameters only 19 independent parameters are left. They describe the p(henomenological) MSSM [55]. Often, these parameters are even further constrained by assuming a specific SUSY breaking mechanism, which relates for example the gaugino masses.

3.2. Electroweak symmetry breaking and the Higgs potential

Having obtained the MSSM Lagrangian, the mechanism of electroweak symmetry breaking in this framework is now investigated. The Higgs potential in terms of the $SU(2)_L$

[2] This is equivalent to a superpotential where all superfields are replaced by their corresponding scalar field but the latter contains quite many sub- and superscripts.

components of the Higgs doublets $H_u = \left(H_u^+, H_u^0\right)$ and $H_d = \left(H_d^0, H_d^-\right)$ is given by

$$V = \left(|\mu|^2 + m_{H_u}^2\right)\left(\left|H_u^0\right|^2 + \left|H_u^+\right|^2\right) + \left(|\mu|^2 + m_{H_d}^2\right)\left(\left|H_d^0\right|^2 + \left|H_d^-\right|^2\right) \tag{3.2.1}$$

$$+ \left(b\left(H_u^+ H_d^- - H_u^0 H_d^0\right) + \text{c.c.}\right) \tag{3.2.2}$$

$$+ \frac{1}{8}\left(g^2 + g'^2\right)\left(\left|H_u^0\right|^2 + \left|H_u^+\right|^2 - \left|H_d^0\right|^2 - \left|H_d^-\right|^2\right)^2 \tag{3.2.3}$$

$$+ \frac{1}{2}g^2\left|H_u^+ H_d^{0*} + H_u^0 H_d^{-*}\right|^2 . \tag{3.2.4}$$

This potential gets contributions from very different parts of the MSSM Lagrangian that are a priori not related. In particular, there are the SUSY conserving contributions $|\mu|^2$ from the F-terms and the gauge couplings stemming from the D-terms on the one hand. On the other hand soft breaking effects enter through b, m_{H_u}, and m_{H_d}. The latter coefficients are expected to be all of the order $\mathcal{O}(m_{\text{soft}})$ where m_{soft} is the scale where SUSY breaking happens. To avoid the re-introduction of UV sensitivities of the Higgs mass, this scale should be not higher than a few TeV. The μ parameter, however, is not linked to SUSY or electroweak symmetry breaking and could be as high as M_{Planck}. This will lead to the so-called "μ-problem" of the MSSM, as is discussed below.

In order to find the minimum of the potential, firstly the gauge freedom is used to set $H_u^+ = 0$ at the minimum. By the minimum condition

$$\left.\frac{\partial V}{\partial H_u^+}\right|_{H_u^+=0} = \left(bH_d^- + \text{c.c.}\right) + g^2\left|H_u^0 H_d^{-*}\right| H_d^{0*} \stackrel{!}{=} 0\,, \tag{3.2.5}$$

it can be seen immediately that also H_d^- has to vanish at the minimum. This is necessary because the vev in the SM is not charge breaking and so should be the vev of the MSSM. Next one observes that any possible phase of b can be absorbed in the Higgs fields such that b is real and positive. At the same time, however, the only possibly negative contribution to the quadratic part of the potential comes from b. Since an over-all negative Higgs-squared contribution is needed for spontaneous symmetry breaking, $H_u^0 H_d^0$ has to be positive at the minimum. This means that H_u^0 and H_d^0 have to have opposite phases which can be rotated away by an $U(1)_Y$ transformation due to the opposite hypercharge assignment of the two doublets. After this rotation, no phases are left in the Higgs potential and therefore CP cannot be broken spontaneously at tree level by the Higgs sector.

Demanding that the potential remains positive even in the D-flat direction[3] and that the determinant of the Hesse-matrix is negative at the origin, i.e. the potential has a saddle

[3] The direction defined by $\left|H_u^0\right| = \left|H_d^0\right|$ where the D-term contribution to the Higgs potential vanishes. If the potential remains positive in this direction, it will be stable in all directions, since the D-terms contribute positively.

point there, yields

$$2b < 2\left|\mu\right|^2 + m_{H_u}^2 + m_{H_d}^2 \tag{3.2.6}$$

$$b^2 > \left(\left|\mu\right|^2 + m_{H_u}^2\right)\left(\left|\mu\right|^2 + m_{H_d}^2\right) . \tag{3.2.7}$$

From these constraints one can remark two things. First, if $m_{H_u}^2 = m_{H_d}^2$, both inequalities cannot be fulfilled simultaneously. Therefore they have to differ, at least at loop level. Second, without soft SUSY breaking ($b = m_{H_u^0} = m_{H_d^0} = 0$), Inequality (3.2.7) is violated. Consequently, broken SUSY is required for electroweak symmetry breaking.

By defining

$$\langle H_u^0 \rangle = \frac{v_u}{\sqrt{2}}, \quad \langle H_d^0 \rangle = \frac{v_d}{\sqrt{2}}, \quad \text{and} \quad \tan\beta = \frac{v_u}{v_d} \tag{3.2.8}$$

the relations

$$v_u = v\sin\beta, \quad v_d = v\cos\beta, \quad \text{and} \quad v_u^2 + v_d^2 = v^2 = \frac{4m_Z^2}{g^2 + g'^2} \tag{3.2.9}$$

are obtained and when requiring $\partial V/\partial H_u^0 = \partial V/\partial H_d^0 = 0$ one finds

$$m_Z^2 = \frac{\left|m_{H_d}^2 - m_{H_u}^2\right|}{\sqrt{1-\sin^2\beta}} - m_{H_u}^2 - m_{H_d}^2 - 2\left|\mu\right|^2 \qquad \text{and} \tag{3.2.10}$$

$$\sin 2\beta = \frac{2b}{m_{H_u}^2 + m_{H_d}^2 + 2\left|\mu\right|^2} . \tag{3.2.11}$$

It is straightforward to check that the minimum obtained in this way automatically fulfills the constraints (3.2.6) and (3.2.7). Eq. (3.2.10) illustrates the above mentioned μ problem in an even more severe way. Variables that originate from fundamentally different parts of the MSSM (m_{H_d} and m_{H_u} vs. μ) and are expected to be introduced at very different scales far above the electroweak scale ($\mathcal{O}(m_{\text{soft}}) \sim 1\,\text{TeV}$ and $\mathcal{O}(M_{\text{Planck}})$, respectively) combine such that they give the mass of the Z boson m_Z.

Now that it is known that the Higgs potential has a minimum, the Higgs masses can be computed. Since the MSSM has two complex doublets, there are eight degrees of freedom in the Higgs sector. After electroweak symmetry breaking, they correspond to three Goldstone bosons G^0 and $G^\pm$ giving mass to Z^0 and $W^\pm$, respectively, two neutral CP-even Higgs bosons h^0 and H^0 where the former is the lighter by definition, one neutral CP-odd Higgs A^0, and two charged Higgs bosons $H^\pm$. To obtain expressions for their masses one defines the transformation from the interaction basis to the mass basis

$$\begin{pmatrix} H_u^0 \\ H_d^0 \end{pmatrix} = \frac{1}{\sqrt{2}} R_\alpha \begin{pmatrix} h^0 \\ H^0 \end{pmatrix} + \frac{i}{\sqrt{2}} R_{\beta^0} \begin{pmatrix} G^0 \\ A^0 \end{pmatrix} \tag{3.2.12}$$

$$\begin{pmatrix} H_u^+ \\ H_d^{-*} \end{pmatrix} = R_{\beta^+} \begin{pmatrix} G^+ \\ H^+ \end{pmatrix} \tag{3.2.13}$$

with

$$R_\alpha = \begin{pmatrix} c_\alpha & s_\alpha \\ -s_\alpha & c_\alpha \end{pmatrix} \quad \text{and} \quad R_{\beta^x} = \begin{pmatrix} s_{\beta^x} & c_{\beta^x} \\ -c_{\beta^x} & s_{\beta^x} \end{pmatrix}, \tag{3.2.14}$$

where s_x and c_x are $\sin x$ and $\cos x$, respectively. Inserting the expressions (3.2.12) and (3.2.13) in the quadratic part of the Higgs potential and demanding that the mixing terms vanish, yields $\beta = \beta^0 = \beta^\pm$ and

$$\frac{\tan 2\alpha}{\tan 2\beta} = \frac{m_A^2 + m_Z^2}{m_A^2 - m_Z^2}, \tag{3.2.15}$$

and the masses of the Higgs bosons are

$$m_{G^0}^2 = m_{G^\pm}^2 = 0 \tag{3.2.16}$$

$$m_A^2 = \frac{2b}{\sin 2\beta} = 2\,|\mu|^2 + m_{H_u}^2 + m_{H_d}^2 \tag{3.2.17}$$

$$m_{H^\pm}^2 = m_A^2 + m_W^2 \tag{3.2.18}$$

$$m_{h^0,H^0}^2 = \frac{1}{2}\left(m_A^2 + m_Z^2 \mp \sqrt{\left(m_A^2 - m_Z^2\right)^2 + 2m_A^2 m_Z^2 \sin^2 2\beta}\right). \tag{3.2.19}$$

From Eq. (3.2.19), the tree-level upper bound for the lighter CP-even neutral Higgs h^0

$$m_{h^0}^2 \leq m_Z^2 \cos^2 2\beta \tag{3.2.20}$$

is deduced. This is clearly in contradiction with the experimental results. Nevertheless, this is not the end of the MSSM since it was calculated only at tree-level but the loop corrections are quite substantial. When including the corrections from the stops in the decoupling limit (see below) the Higgs mass becomes

$$m_{h^0}^2 = m_Z^2 \cos^2 2\beta \tag{3.2.21}$$

$$+ \frac{3}{4\pi^2} \sin^2\beta\, y_t^2 \left[m_t^2 \ln\left(\frac{m_{\tilde{t}_1} m_{\tilde{t}_2}}{m_t^2}\right) + c_{\tilde{t}}^2 s_{\tilde{t}}^2 \left(m_{\tilde{t}_2}^2 - m_{\tilde{t}_1}^2\right) \ln\left(\frac{m_{\tilde{t}_2}^2}{m_{\tilde{t}_1}^2}\right) \right. \tag{3.2.22}$$

$$\left. + c_{\tilde{t}}^4 s_{\tilde{t}}^4 \frac{\left(m_{\tilde{t}_2}^2 - m_{\tilde{t}_1}^2\right)^2 - \frac{1}{2}\left(m_{\tilde{t}_2}^4 - m_{\tilde{t}_1}^4\right) \ln\left(\frac{m_{\tilde{t}_2}^2}{m_{\tilde{t}_1}^2}\right)}{m_t^2} \right], \tag{3.2.23}$$

where $c_{\tilde{t}}$ and $s_{\tilde{t}}$ are the sine and cosine of the stop mixing angle. Including all corrections one finds the relaxed relation [56–58] (and references therein)

$$m_{h^0}^2 \lesssim 135\,\text{GeV}, \tag{3.2.24}$$

which is in good agreement with experiment.

The couplings of the light Higgs to the fermions are modified with respect to their SM value by two effects. Firstly the up- and down-type couplings are scaled by $\sin^{-1}\beta$ and $\cos^{-1}\beta$, respectively, corresponding to the ratio of v to the vev of the respective Higgs doublet which is given in Eq. (3.2.9). Secondly, since the mass eigenstates are obtained from rotating the up- and down-type Higgs bosons, but only one of them couples to the fermions in question, their couplings are again scaled by $\cos\alpha$ and $-\sin\alpha$, respectively, as can be read off of Eq. (3.2.12). After including both effects,

$$g_{htt} = g_{htt}^{SM}\frac{\cos\alpha}{\sin\alpha} \qquad \text{and} \qquad g_{hbb} = -g_{hbb}^{SM}\frac{\sin\alpha}{\cos\alpha} \tag{3.2.25}$$

is obtained.

One important limit in the MSSM (in particular in the light of LHC results) is given for $m_A \gg m_Z$. In this so-called decoupling limit, h^0 behaves like the SM Higgs boson and saturates its upper mass bound. All other Higgs bosons are nearly mass degenerate and decoupled from the dynamics at the electroweak scale.

3.3. Neutralino, chargino and stop masses

After electroweak symmetry breaking the neutral gauginos $\widetilde{B}$ and $\widetilde{W}^0$ are no longer mass eigenstates but mix with the higgsinos $\widetilde{H}_u^0$ and $\widetilde{H}_d^0$. The four mass eigenstates are called neutralinos $\widetilde{\chi}_i^0$ with $i = 1,2,3,4$, where $\widetilde{\chi}_1^0$ is the lightest and $\widetilde{\chi}_4^0$ the heaviest. In many breaking scenarios, $\widetilde{\chi}_1^0$ is the LSP and serves as a dark matter candidate if R-parity is conserved.

The mass matrix in the gauge basis $\left(\widetilde{B}, \widetilde{W}^0, \widetilde{H}_d^0, \widetilde{H}_u^0\right)$ is given by

$$\mathbf{M}_{\widetilde{\chi}^0} = \begin{pmatrix} M_1 & 0 & -c_\beta s_W m_Z & s_\beta s_W m_Z \\ 0 & M_2 & c_\beta c_W m_Z & -s_b c_W m_Z \\ -c_\beta s_W m_Z & c_\beta c_W m_Z & 0 & -\mu \\ s_\beta s_W m_Z & -s_\beta c_W m_Z & -\mu & 0 \end{pmatrix}. \tag{3.3.1}$$

In the limit where the 2×2 off-diagonal block matrix entries are small compared to the others, $m_Z \ll |\mu \pm M_1|, |\mu \pm M_2|$, the bino and wino are nearly mass eigenstates and the neutral higgsinos do barely mix with them. When further $m_Z \ll \mu \ll M_1, M_2$, the two higgsinos are nearly mass degenerate with $m_{\widetilde{\chi}_1^0} \approx m_{\widetilde{\chi}_1^0} \approx |\mu|$ and the two heaviest neutralinos have the masses M_1 and M_2.

The same discussion can be made for the mixing of the charged gauginos. Their mass

matrix is given by

$$\mathbf{M}_{\widetilde{\chi}^{\pm}} = \begin{pmatrix} 0 & 0 & M_2 & \sqrt{2}\, c_\beta\, m_W \\ 0 & 0 & \sqrt{2}\, s_\beta\, m_W & \mu \\ M_2 & \sqrt{2}\, s_\beta\, m_W & 0 & 0 \\ \sqrt{2}\, c_\beta\, m_W & \mu & 0 & 0 \end{pmatrix} \tag{3.3.2}$$

in the gauge basis $\left(\widetilde{W}^+, \widetilde{H}_u^+, \widetilde{W}^-, \widetilde{H}_d^-\right)$. As in the neutralino sector, the charginos have approximately the masses $m_{\chi_1^\pm} \approx |\mu|$ and $m_{\chi_2^\pm} \approx M_2$ if $M_2 > |\mu| \gg m_Z$.

The fermion sector can be substantially more complicated because in principle all the six up-type squarks can mix as well as the down-type squarks, the charged sleptons, and the sneutrinos. However, when constraining to flavor diagonal soft parameters and neglecting the Yukawa couplings of the first two generations, the picture simplifies a lot. Then the pairs of same-type sfermions of the first two generations $(\tilde{u}_R, \tilde{c}_R)$, $(\tilde{u}_L, \tilde{c}_L)$, etc. will be mass degenerate and only in the third family left- and right sfermions mix. Moreover, the masses of the third generation sleptons are affected by the Yukawa couplings in the β-functions and can therefore differ from the other sfermion masses.

For the stops, the mass matrix is given in the gauge basis $\left(\tilde{t}_L, \tilde{t}_R\right)$ as

$$\mathbf{M}_{\tilde{\mathbf{t}}}^{\mathbf{2}} = \begin{pmatrix} m_{Q_3}^2 + m_t^2 + \Delta_{\bar{u}_L} & m_t\left(A_t^* - \mu \cot\beta\right) \\ m_t\left(A_t - \mu^* \cot\beta\right) & m_{\bar{u}_3}^2 + m_t^2 + \Delta_{\bar{u}_R} \end{pmatrix}, \tag{3.3.3}$$

where $\Delta_{\bar{u}_L} = m_Z^2\left(1/2 - 2s_W^2/3\right)\cos 2\beta$ and $\Delta_{\bar{u}_R} = m_Z^2\left(2s_W^2/3\right)\cos 2\beta$. In order to obtain light stops that are needed to solve the hierarchy problem, small m_{Q_3} and $m_{\bar{u}_3}$ are needed. Through the RG running, the large Yukawa interactions of the third generation decrease these masses while the gluino mass increases them. Given the strong bounds on the gluino mass, this introduces a new source of fine tuning [59] into the MSSM. Possible solutions to this problem might include Dirac gauginos.

4. Composite Higgs models

Besides the electroweak symmetry there is another spontaneously broken symmetry present in the SM. This symmetry breaking works without the Higgs mechanism, is free of any hierarchy problem and in fact also breaks the electroweak symmetry. The mechanism in question is the spontaneous breaking of the axial symmetry in QCD by a quark condensate. In the chiral limit (massless quarks) the QCD Lagrangian with two flavors $q = (u, d)$,

$$\mathcal{L}_{\text{QCD}} = -\frac{1}{4} G^a_{\mu\nu} G^{a\,\mu\nu} + \bar{q}_L i \not{D} q_L + \bar{q}_R i \not{D} q_R \,, \tag{4.0.1}$$

exhibits a global $SU(2)_L \times SU(2)_R \times U(1)_L \times U(1)_R$ symmetry, where the $q_{L,R}$ transform in the fundamental representation of $SU(2)_{L,R}$ and $U(1)_{L,R}$ and are invariant under transformations of the other two groups. From the corresponding conserved currents, two vector currents $j^\mu_V = \bar{q}\gamma^\mu q$ and $j^{\mu\,a}_V = \bar{q}\gamma^\mu \tau^a q$ can be built, corresponding to baryon number and isospin, respectively[1], and two axial currents $j^{\mu\,5}_A = \bar{q}\gamma^\mu\gamma^5 q$ and $j^{\mu\,5\,a}_A = \bar{q}\gamma^\mu\gamma^5\tau^a q$. The former of the axial currents is anomalous and therefore does not correspond to a conserved quantity. The latter is, however, not observed in nature[2] despite being not anomalous and therefore has to be broken spontaneously. This is done by a quark condensate $\langle \bar{q}q \rangle = \langle \bar{q}_L q_R + \text{h.c.} \rangle$ at energies below $\Lambda_{QCD} \approx 200 - 300\,\text{MeV}$ where the strong force becomes non-perturbative. The condensate is invariant under the vectorial transformation where left- and right-handed quarks transform equally, but it breaks the axial symmetry. The three Goldstone bosons arising from the symmetry breaking are the pions. Their masses do not vanish completely because the chiral symmetry is broken explicitly by the quark masses and the only partly gauged $SU(2)_R$ but their Goldstone nature explains their lightness compared to the other QCD resonances.

Since the electroweak gauge group $SU(2)_L \times U(1)_Y$ is a subgroup of $SU(2)_L \times SU(2)_R \times U(1)_B$ with $Y = \tau^3_R + B/2$ and B being the baryon number, the only remaining gauge group after chiral symmetry breaking $SU(2)_L \times SU(2)_R \to SU(2)_V$ is the $U(1)_{\text{em}}$ with the generator $Q = \tau^3_L + Y$. When the explicit calculation is done, it can be seen that the pions are eaten by the electroweak gauge bosons and their masses are given by the same expressions as in the SM Higgs mechanism, except that the Higgs vev v is replaced by the

[1] $\tau^a \equiv \sigma^a/2$ are the generators of $SU(2)$.

[2] The left and right generators are related by parity. If the axial vector symmetry were present in nature, degenerate particles with opposite parity would be observed.

pion decay constant $f_\pi \approx 93\,\text{MeV}$. Obviously this cannot be the whole story as pions are actually observed in the particle spectrum and the masses of the gauge bosons are much heavier than predicted by QCD-induced EWSB only. Therefore there has to be an additional mechanism for the breaking of the electroweak symmetry. Nevertheless the QCD mechanism has one very appealing feature: It is free of the hierarchy problem since it needs no fundamental scalar. Unitarity in pion-pion scattering or equivalently the scattering of longitudinally polarized Ws is rather restored by an exchange of higher resonances, in particular the exchange of ρ and a_1 mesons. This lead to the suggestion of scaled-up versions of QCD [36, 60–63], called technicolor, where a $SU(N_{\text{TC}})$ gauge group exhibits the same symmetry breaking pattern $SU(2)_L \times SU(2)_R \to SU(2)_V$ as QCD. Despite being well motivated, the simplest technicolor models suffer from severe problems, namely their problem to find agreement with electroweak precision tests (EWPT) and constraints on flavor-changing neutral currents (FCNC) [64–67] as well as generating the fermion mass hierarchy [64, 68]. The worst problem for technicolor models is, however, the observation of a SM-like Higgs particle at the LHC which is difficult to explain within this framework.

An alternative setup, which takes the idea of some strongly coupled dynamics at a high scale but avoids the problems of simple technicolor models, are the (minimal) composite Higgs models ((M)CHM) [69–72]. They will be discussed in the following as an alternative explanation for EWSB besides SUSY. The CHM are an interpolation between technicolor and the SM and avoid both the hierarchy problem of the SM and the conflicts with e.g. FCNC observables in technicolor models. The former is avoided through the compositeness of the Higgs boson, which arises as a pseudo-Goldstone boson from a dynamically broken global symmetry of a strong sector. Due to its Goldstone nature, the Higgs will be naturally lighter than any other resonance of the strong sector and since it is composite, it is automatically insensitive to corrections from UV physics above the scale of the strong symmetry breaking, just like the QCD pions are insensitive to the Planck scale. The FCNC problems are attenuated by the concept of partial compositeness, which will be explained in Section 4.2.

Since the composite Higgs will have modified couplings to the gauge bosons, it will no longer fully unitarize the scattering of longitudinally polarized Ws, but only push the scale of unitarity violation to higher energies. Unitarity is then fully restored at this higher scale by an exchange of resonances of the strong sector [73]. Owing to the partially restored unitarity, the masses of these resonances can be large enough to avoid conflicts with EWPT.

Throughout the remaining part of this chapter the focus is on the EWSB part of the theory. The $SU(3)_C$ group of the SM, which does not play any role in the symmetry breaking, is therefore completely omitted. Nevertheless, it is of course always understood that it is still present in the theory. In fact, in order to obtain gauge invariant operators for the partial compositeness, the resonances of the strong sector need to be charged under

color.

4.1. Symmetry breaking in the MCHM

In the minimal[3] setup for a pseudo-Goldstone Higgs we start with a global symmetry group $G = SO(5) \times U(1)_X$, which is spontaneously broken by a condensate to $H = SO(4) \times U(1)_X \sim SU(2)_L \times SU(2)_R \times U(1)_X$ at a scale $\Lambda \approx 4\pi f$ with $f \sim 1\,\text{TeV}$ being the equivalent of the pion decay constant in QCD. The coset G/H contains four broken generators corresponding to the four real degrees of freedom of the Higgs, which at this level still is a massless Goldstone boson. As in the QCD case, the electroweak gauge group can be embedded into the global symmetry group H. Comparing the generators of H and G_{EW}, one finds that the hypercharge is given by $Y = T_R^3 + X$. The gauging of the SM group and interactions with the SM fermions, however, explicitly break G and generate a potential for the Higgs, which in turn triggers EWSB at the electroweak scale v. The ratio $\xi = v^2/f^2$ measures the separation of the two scales and quantifies the vacuum misalignment between G_{SM} and H in the true vacuum. The limit $\xi \to 0$ corresponds to infinitely heavy (decoupled) resonances and thus mimics the SM Higgs mechanism, while the other limit $\xi \to 1$ corresponds to a minimal technicolor model with no separation of the scales and no longer provides a natural explanation for the lightness of the Higgs compared to other resonances. Clearly, small values of ξ come along with some tuning because the Higgs mass will always receive corrections of the order of the strong scale, but has to remain light. But nevertheless with $\Lambda \sim 10\,\text{TeV} \ll M_{Planck}$, the tuning is much milder than in the SM. The presence of the $U(1)_X$ symmetry in the above described breaking pattern is needed to obtain the correct values for the hypercharges, but it plays no role in the breaking procedure.

4.1.1. Higgs coupling to gauge bosons

In order to obtain the effective Lagrangian describing the low energy dynamics of the pseudo-Goldstone bosons and their interactions with the gauge fields, the CCWZ formalism [78, 79] is used. For convenience, the representation where the six unbroken generators T_L^a and T_R^a $(a = 1, 2, 3)$ of $SO(4) \sim SU(2)_L \times SU(2)_R$ are given by

$$\left(T_{L,R}^a\right)_{ij} = -\frac{i}{2}\left(\frac{1}{2}\epsilon^{abc}\left(\delta_i^b\delta_j^c - \delta_j^b\delta_i^c\right) \pm \left(\delta_i^a\delta_j^4 - \delta_j^a\delta_i^4\right)\right) \tag{4.1.1}$$

[3] Considering the needed degrees of freedom, it would be sufficient to demand the even simpler pattern $G = SU(3) \to H = SU(2)_L \times U(1)_Y$. However, this smaller setting contains no custodial symmetry and therefore generally violates the experimental bounds on the electroweak T parameter. Of course, non-minimal breaking patterns leading to different coset spaces are conceivable, too. A list of possible patterns with references can be found in [74]. These different coset spaces often lead to more than the four needed (pseudo-) Goldstone bosons which could then act as dark matter candidates [75–77].

while the four broken generators of the coset are given by

$$\left(T^{\hat{a}}\right)_{ij} = -\frac{i}{\sqrt{2}}\left(\delta_i^{\hat{a}}\delta_j^5 - \delta_j^{\hat{a}}\delta_i^5\right) \tag{4.1.2}$$

is chosen. Since in this representation $\left(T^a_{R,L}\right)_{i5} = \left(T^a_{R,L}\right)_{5i} = 0 \neq \left(T^{\hat{a}}\right)_{5i} = \left(T^{\hat{a}}\right)^*_{5i}$, the Goldstone bosons can be parametrized in the coset space spanned by the broken generators via $\Sigma = U\,\Sigma_0$ with $\Sigma_0 = (0,0,0,0,1)^T$ and $U = \exp\left(-i\sqrt{2}T^{\hat{a}}h^{\hat{a}}/f\right)$. Simplifying the matrix exponential yields

$$\Sigma = \frac{\sin_h}{h}\left(h^1, h^2, h^3, h^4, h\frac{\cot_h}{f}\right)^T , \tag{4.1.3}$$

where $h = \sqrt{h^{\hat{a}}h^{\hat{a}}}$, $\sin_h \equiv \sin(h/f)$, and $\cot_h$ correspondingly. In lowest order in the derivatives, the Goldstone Lagrangian is then given by

$$\mathcal{L} = \frac{f^2}{2}\left(D_\mu\Sigma\right)^\dagger\left(D^\mu\Sigma\right) , \tag{4.1.4}$$

with the covariant derivative defined in analogy to the expression given in Eq. (2.1.14). From this equation the gauge boson masses and their interactions with the physical Higgs particle are obtained by going to unitary gauge where the unphysical particles are no longer present but appear as longitudinal degrees of freedom of the gauge bosons. In this gauge, the direction can be chosen such that all $h^{\hat{a}}$ vanish except for h^3, which is then equal to h. With this choice the Lagrangian from Eq. (4.1.4) becomes

$$\mathcal{L} = \frac{1}{2}\partial_\mu h\,\partial^\mu h + f^2\sin_h^2\left(\frac{g^2}{4}W^+_\mu W^{-\,\mu} + \frac{g^2}{8c_W^2}Z_\mu Z^\mu\right) . \tag{4.1.5}$$

The relation between the SM vev v and the vacuum expectation value of the Higgs $\langle h\rangle$ is obtained by comparing this Lagrangian with the expressions for the boson masses in the SM in Eq. (2.1.15)

$$v = f\sin\left(\frac{\langle h\rangle}{f}\right) \equiv f\sin_{\langle h\rangle} . \tag{4.1.6}$$

Expanding $\sin_h$ around the vev yields the operators for the Higgs-gauge interactions. Their structure is exactly the same as in the SM, they differ merely by a factor given by

$$g_{hVV} = g^{SM}_{hVV}\sqrt{1-\xi} \tag{4.1.7}$$

$$g_{hhVV} = g^{SM}_{hhVV}\left(1-2\xi\right) , \tag{4.1.8}$$

where V stands for the W and Z gauge bosons. From these factors it can be seen that in the limit where the scale of the strong sector goes to infinity, $\xi \to 0$, the Higgs has SM couplings and unitarity in scattering of longitudinally polarized Ws is restored. In the other limit, $\xi \to 1$, the g_{hVV} coupling vanishes and the Higgs can no longer unitarize the cross

section. This needs then to be done exclusively by the resonances of the strong sector. In the intermediate regime, however, the Higgs will partially unitarize the scattering as was pointed out in the beginning of this section.

Since the SM gauge bosons only partially gauge the $SO(5)$ group, they explicitly break it and thus generate a mass term for the now pseudo-Goldstone Higgs. In order to obtain the mass, the Coleman-Weinberg potential [80] generated by gauge boson loops needs to be calculated

$V(h) =$ 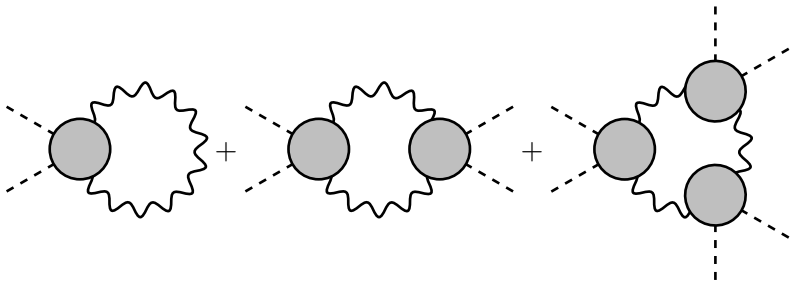 $+ \dots ,$ (4.1.9)

where the gray blobs indicate effects of the strong dynamics. Although being a strongly interacting theory, the potential can be calculated [72], e.g. in an effective theory that contains the light resonances. The result is given by [81]

$$V(h) = \alpha \sin_h^2 + \beta \sin_h^4 + \dots , \tag{4.1.10}$$

where α and β are constants depending on the masses of the resonances. One important feature of this potential is that α and thus the Higgs mass is positive and therefore the gauge bosons alone are not sufficient to trigger EWSB. Only when including the contributions from the SM fermions, in particular of the top quark, the Coleman-Weinberg potential will break the electroweak symmetry.

4.2. Fermions in CHM

The need for SM fermions to couple to the composite sector is two-fold. On the one hand they are needed to generate an EWSB triggering potential for the composite Higgs, since the gauge bosons alone are not sufficient for that, as was noted in the previous section. In Section 4.2.1 it will be shown that the Coleman-Weinberg potential generated from the top quark is such a potential. On the other hand, the composite Higgs is needed to provide a mass term with the observed hierarchy for the fermions.

Both of these effects are achieved by coupling the fermions linearly [82] to operators $\mathcal{O}_\psi$ of the strong sector

$$\mathcal{L}_{\text{linear}} = \lambda \bar{\psi} \mathcal{O}_\psi + \text{h.c.} . \tag{4.2.1}$$

Clearly, in order to construct singlets under the SM gauge groups, there needs to be at least one operator for each SM fermion multiplet. Unlike bilinear couplings $\mathcal{L}_{\text{bilinear}} = \lambda\bar{\psi}\psi\mathcal{O}$, which appear in technicolor theories and could in principle be introduced in the MCHM as well, the linear coupling allows for large quark masses while keeping the potentially dangerous four fermion operators suppressed and avoiding UV instabilities.

The fermion masses arise through the interactions with the composite operators which interpolate the Higgs field and can be estimated as[4]

$$m_q = v\frac{\sqrt{N}}{4\pi}\lambda_L(\mu)\lambda_R(\mu)\,. \tag{4.2.2}$$

The couplings $\lambda_{L,R}$ are subject to the RG evolution and can lead to very different masses. Assuming that the theory at a high scale is approximately conformal, one obtains for small and positive anomalous dimensions $\gamma_{L,R}$ of $\mathcal{O}_{L,R}$

$$m_q \sim v\frac{\sqrt{N}}{4\pi}\left(\frac{\Lambda_\rho}{\Lambda_{UV}}\right)^{\gamma_L+\gamma_R} \tag{4.2.3}$$

where $\Lambda_\rho \approx f$ is the scale of the light resonances and Λ_{UV} is the scale at which the linear interaction is generated. If $\Lambda_\rho \gg \Lambda_{UV}$, small differences in the anomalous dimensions of the composite operator generate large differences in the fermion masses and naturally explain the mass hierarchy of the SM fermions. Eq. (4.2.3) is, however, not sufficient to explain the large top mass. If conversely the $\gamma_{L,R}$ are negative, the coupling λ will grow and eventually arrive at an IR fixed point and the mass expression becomes

$$m_q \sim \frac{4\pi}{\sqrt{N}}v\sqrt{\gamma_L\gamma_R} \tag{4.2.4}$$

which can easily reproduce the top mass.

The linear coupling introduced in Eq. (4.2.1) has another interesting effect. The composite operator $\mathcal{O}$ will generate resonances of the strong sector which then mix with the SM elementary particles. The mass eigenstates are therefore no longer elementary or completely composite particles but a mixture of both. This effect is accordingly known as *partial compositeness* [82]. Since the Higgs will be a fully composite particle, it will couple the more to a particle the larger its composite fraction is. Light particles are therefore mostly elementary i.e. the quarks of the first generation, while heavy particles are mostly composite, in particular the top quark. As a side-effect this explains how the bounds on the compositeness of the first generation fermions are avoided.

[4]The two factors of $\lambda_{L,R}$ appear since both left and the right handed fermion fields couple to the strong sector to generate the mass, and the factor $\sqrt{N}/(4\pi)$ is the scaling of the amplitude for the excitation of a heavy resonance in the large N limit.

The resonances of the composite operator appear as new particles in the spectrum and are referred to as partner particles of the corresponding fermion, e.g. top partners. Since the elementary top quark is expected to mix substantially with its partners, the initially fully composite resonances will get a significant contribution from the elementary field and thus be much lighter than the mass of a purely composite state. Therefore the top partners are expected to be among the lightest composite objects beside the Higgs.

4.2.1. Higgs potential from top quarks

As noted above, the contributions of the top quark to the Higgs potential are needed to trigger EWSB. To obtain a straightforward description, the left-handed quark doublet q_L of the third generation and the right-handed top quark t_R are embedded in the fundamental representation of $SO(5)$

$$\mathcal{Q}_L = \begin{bmatrix} \begin{pmatrix} q'_L \\ q_L \end{pmatrix} \\ u'_L \end{bmatrix}, \qquad \text{and} \qquad \mathcal{Q}_R = \begin{bmatrix} \begin{pmatrix} q^t_R \\ q'^t_R \end{pmatrix} \\ t_R \end{bmatrix}, \tag{4.2.5}$$

where the first two entries correspond to doublets and the third to a singlet. All newly introduced fields in these multiplets are spurions and will be set to zero in a moment. They were only introduced to make it straightforward to construct a $SO(5) \times U(1)_X$ invariant Lagrangian. Instead of the fundamental representation, which is the smallest that protects the $Zb\bar{b}$ coupling, one could have chosen a different, non-minimal representation to embed the SM quarks into. Other common representations are e.g. the spinorial **4**, adjoint **10**, and the less minimal tensor **14**.

The most general $SO(5)\times U(1)_X$ invariant Lagrangian built out of the multiplets in (4.2.5) and the Σ defined in Eq. (4.1.3) is given at quadratic order in the fields in momentum space by

$$\mathcal{L} = \sum_{r=L,R} \bar{\mathcal{Q}}^i_r \not{p} \left[\delta^{ij}\Pi^r_0(p) + \Sigma^i\Sigma^j\Pi^r_1(p)\right] \mathcal{Q}^j_r + \bar{\mathcal{Q}}_L \left[\delta^{ij}M_0(p) + \Sigma^i\Sigma^j M_1(p)\right] \mathcal{Q}^j_R + \text{h.c.}\,, \tag{4.2.6}$$

where $\Pi^r_{0,1}$ and $M^r_{0,1}$ are form factors taking into account the effects of the composite sector. When now switching off the spurion fields one can read off the top mass

$$m_t \approx \frac{\sin_{\langle h\rangle}\cos_{\langle h\rangle}}{\sqrt{2}} \left.\frac{M_1(p)}{\sqrt{\left(\Pi^L_0 + \frac{\sin^2_{\langle h\rangle}}{2}\Pi^L_1\right)\left(\Pi^R_0 + \Pi^R_1 - \frac{\sin^2_{\langle h\rangle}}{4}\Pi^R_1\right)}}\right|_{p^2=0} \tag{4.2.7}$$

after normalizing the fields and setting h to its vev. The Higgs-top coupling

$$g_{h\bar{t}t} = g^{SM}_{h\bar{t}t}\frac{1-2\xi}{\sqrt{1-\xi}} \tag{4.2.8}$$

differs from the one of the SM and is obtained by expanding around the vev. Clearly, the coefficient in the modified top Yukawa interaction depends on the representation in which the SM quarks are embedded.

After switching off the spurions, the Feynman rules needed for the calculation of the Coleman-Weinberg potential can be retrieved from Eq. (4.2.6). The potential is then calculated analogously to Eq. (4.1.9) and one obtains [81]

$$V(h) = (\alpha - \beta)\sin_h^2 + \beta \sin_h^4 \,, \tag{4.2.9}$$

where α and β are integrals over the form factors. Neglecting the gauge contribution to the Higgs potential, one sees that $V(h)$ has a non-trivial minimum at

$$\sin^2_{\langle h\rangle} = \frac{\beta - \alpha}{2\beta} \tag{4.2.10}$$

for $\alpha - \beta < 0$ and $\beta > 0$. Now the Higgs mass is obtained from the second derivative of the potential

$$\begin{aligned} m_h^2 = V''(\langle h\rangle) &= \frac{8\beta}{f^2}\sin^2_{\langle h\rangle}\cos^2_{\langle h\rangle} && (4.2.11)\\ &\approx \frac{N_c}{\pi^2}\frac{m_t^2}{v^2}\xi\Lambda_\rho^2 && (4.2.12)\\ &\approx 125\,\text{GeV}\left(\frac{\xi}{0.2}\right)\left(\frac{\Lambda_\rho}{700\,\text{GeV}}\right)^2 && (4.2.13)\\ &\approx 125\,\text{GeV}\left(\frac{\xi}{0.1}\right)\left(\frac{\Lambda_\rho}{1\,\text{TeV}}\right)^2 , && (4.2.14) \end{aligned}$$

where the scale of the first fermionic resonances Λ_ρ enters the equation when approximating β. From the last equation it can be seen that the correct Higgs mass can be obtained with not too much fine tuning ($\xi \sim 0.1 - 0.2$) and that in this case resonances are expected at the lower TeV scale. Fortunately this is also the range which the LHC can cover within the next years and therefore, if the hierarchy problem of the SM is solved by a natural composite Higgs, signs of it should be found there.

This statement can be made more concrete by considering a realistic version of the MCHM where the top partners are explicitly included in the form of a $SO(5)$ multiplet of composite fermions $\Psi = (\psi_4, \psi_1)^T$ that decomposes as $\mathbf{5} \sim \mathbf{4} \oplus \mathbf{1}$ [83]. The top-sector Lagrangian of this model reads

$$\mathcal{L}_t = i\bar{q}_L \not{D} q_L + i\bar{t}_R \not{D} t_R + i\bar{\Psi}\not{D}\Psi - m_4\bar{\psi}_4\psi_4 - m_1\bar{\psi}_1\psi_1 - \left(\lambda_q \bar{\mathcal{Q}}_L U^T \Psi_R + \lambda_u \bar{\Psi}_L U \mathcal{Q}_R + \text{h.c.}\right) , \tag{4.2.15}$$

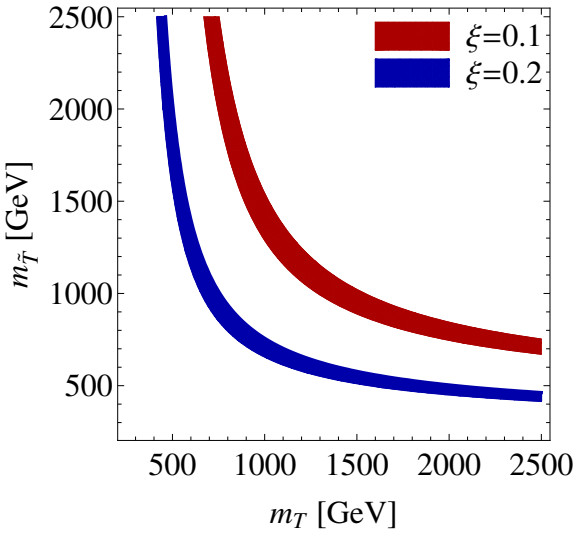

Figure 4.1.: Areas in the m_T-$m_{\tilde{T}}$-plane where the correct Higgs mass $m_h = 125 \pm 5\,\text{GeV}$ is obtained within the model described by the Lagrangian in Eq. (4.2.15). Red and blue correspond to $\xi = 0.1$ and $\xi = 0.2$, respectively. m_T and $m_{\tilde{T}}$ are the mass eigenstates of the composite sector. It can be seen that when one resonance becomes heavy, the other one gets simultaneously light. Further, the less fine-tuned the model is, i.e. the larger ξ, the lighter one of the resonances has to be.

where U is the Goldstone matrix. In this model, the Higgs mass can be calculated as a function of the mass eigenstates of the composite fermions $m_{T,\tilde{T}} = \sqrt{m_{4,1}^2 + \lambda_{q,u}^2}$ [84]

$$m_h^2 \approx \frac{2N_c}{\pi^2}\frac{m_t^2}{v^2}\xi\frac{m_T^2 m_{\tilde{T}}^2}{m_T^2 - m_{\tilde{T}}^2}\log\left(\frac{m_T}{m_{\tilde{T}}}\right)^2 . \tag{4.2.16}$$

In Fig. 4.1 we show for two different values of ξ the areas where the correct Higgs mass $m_h = 125 \pm 5\,\text{GeV}$ is obtained for $m_t = 150\,\text{GeV}$, corresponding to the running mass at $\sim 1\,\text{TeV}$. Clearly, one heavy resonance implies a light one and vice versa. Furthermore, we observe that as the LHC excludes light resonances the viable models need to have a smaller ξ and are therefore more fine-tuned.

For all the general properties of composite Higgs models derived above, only some strong coupling that breaks the $SO(5)$ symmetry was assumed and an effective description for the broken phase was employed. This is a very economic and useful approach for the collider signatures of these models but eventually a UV completion needs to be found. Although there was some progress in recent years [85–89] a fully consistent theory is not known yet. This should nevertheless not be seen too problematic but rather in analogy to SUSY breaking, which was introduced explicitly without knowing the exact mechanism that drives it.

5. Boosted Higgs couplings

The Higgs coupling to the top quark plays a central role in stabilizing the Higgs mass. Its precise measurement is therefore of great importance for the discovery of BSM dynamics. It can be either measured directly via the $t\bar{t}h$ cross section or indirectly via the top loop in gluon fusion or the decay of a Higgs into two photons. The cross section of the former $\sigma_{t\bar{t}h}^{14\,\mathrm{TeV}} \approx 0.6\,\mathrm{pb}$ [90–93] is almost two orders of magnitude smaller than the gluon fusion cross section $\sigma_{ggF}^{14\,\mathrm{TeV}} \approx 49\,\mathrm{pb}$ [93] and difficult to measure due to the high multiplicity final state. Nevertheless, several searches for Higgs production in association with top quark pairs (or with a single top) have been done and the latest results from ATLAS (CMS) give a best fit value for the signal strength of 1.7 ± 1.4 [94] (2.8 ± 1.0 [95]). Studies of the LHC experiments for the high-luminosity upgrade of the LHC estimate a sensitivity to the top Yukawa coupling of the order of 10% [96, 97] through the $t\bar{t}h$ channel.

In this chapter, we want to focus on the gluon fusion process to measure the top Yukawa coupling. Despite the loop suppression it has the advantage of the larger cross section and is the main production channel for Higgs bosons at the LHC. This process is, however, not only sensitive to the top Yukawa coupling but also to effects from new particles that appear in the loop. This is actually expected in most BSM models: In order to cancel the top contributions and stabilize the Higgs mass, new particles appear in loop corrections to the Higgs propagator. If these new particles couple to gluons[1], they will necessarily appear in gluon fusion. To see this, we only need to append two gluons to the loop in the Higgs propagator and replace one of the Higgs fields by its vacuum expectation value (see Fig. 5.1).

Given the fact that no BSM light degrees of freedom were discovered so far, it is likely that new particles are separated from the electroweak scale by a mass gap. In this case, a common tool to describe their effects without making too many assumptions on their nature are effective field theories (EFTs). In EFTs, deviations from the SM are encoded in higher dimensional operators, $\dim[\mathcal{O}] > 4$, built out of the SM fields and obeying the SM symmetries. We will adopt this approach in the following to describe the effect of the new loop particle by a direct gluon-Higgs interaction. While there is only one dimension 5 operator, which is irrelevant for Higgs physics, there are 59 different operators of dimension

[1] Considering the most prominent models for BSM physics, SUSY and CHM, these new particles are the stops and top partners, respectively. Both of these particles are charged under the strong force and therefore do appear in this loop process.

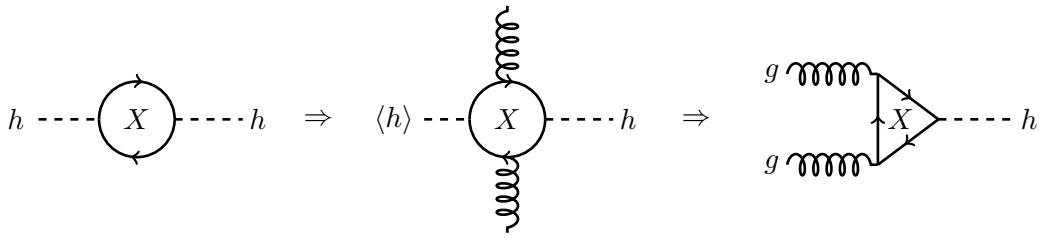

Figure 5.1.: New particles (X) that couple to the Higgs boson will appear as loop corrections to its propagator and can help to stabilize its mass. If these particles are charged under $SU(3)_C$ two gluons can couple to the loop. Replacing one of the external Higgs lines by the vacuum expectation value results in the gluon fusion diagram with the top loop replaced by the loop of a new particle.

6 (for one family of fermions) [98, 99]. Out of these operators, 30 encode BSM effects on Higgs physics [100–102], though 20 of them are already strongly constrained by electroweak measurements. From the remaining operators the following four affect the gluon fusion cross section:

$$\mathcal{O}_y = \frac{y_t}{v^2}\,|H|^2\,\bar{Q}_L \widetilde{H} t_R \qquad \mathcal{O}_H = \frac{1}{2\,v^2}\partial_\mu\,|H|^2\,\partial^\mu\,|H|^2 \tag{5.0.1}$$

$$\mathcal{O}_g = \frac{\alpha_S}{12\,\pi v^2}\,|H|^2\,G^a_{\mu\nu}G^{a\,\mu\nu} \qquad \mathcal{O}_{\tilde{g}} = \frac{\alpha_S}{8\,\pi v^2}\,|H|^2\,G^a_{\mu\nu}\widetilde{G}^{a\,\mu\nu}\,. \tag{5.0.2}$$

Here, Q_L and t_R are the $SU(2)_L$ doublet and singlet of the third quark generation, H and $\widetilde{H} = i\sigma_2 H^*$ denote the Higgs doublet, $G^a_{\mu\nu}$ is the $SU(3)_C$ fieldstrength tensor, and $\widetilde{G}^a_{\mu\nu} = \frac{1}{2}\,\epsilon_{\mu\nu\rho\lambda}G^{a\,\rho\lambda}$ its dual. The top Yukawa and the strong coupling constant are denoted by y_t and α_S, and $v \approx 246\,\text{GeV}$ is the SM vacuum expectation value of the Higgs field. The prefactors of the two effective gluon-Higgs operators $\mathcal{O}_g$ and $\mathcal{O}_{\tilde{g}}$ are chosen such that the amplitude for gluon fusion calculated with them is identical to the amplitude obtained from the full loop calculation in the limit of an infinitely heavy loop particle (heavy top limit).

Alternatively to writing down the operators corresponding to the heavy top limit, they can be derived from the low energy theorem [103–105], [106]: When writing the mass terms of the SM Lagrangian in a particular way (cf. Eq. (2.2.2))

$$\mathcal{L}_m = -\left(1+\frac{h}{v}\right)\sum_f m_f \bar{f} f - \left(1+\frac{h}{v}\right)^2\left(m_W^2 W\mu^+ W^{-\,\mu} + \frac{1}{2}m_Z^2 Z_\mu Z^\mu\right), \tag{5.0.3}$$

one can see that in the limit where the Higgs field is constant, i.e. carries no momentum, it can be included by a rescaling of the mass parameters by a factor $\left(1+\frac{h}{v}\right)$. Therefore, any amplitude involving a zero-momentum Higgs can be written in terms of the same amplitude without a Higgs boson

$$\mathcal{M}(\mathcal{A} \to \mathcal{B} + h) = \frac{1}{v}\left(\sum_f m_f \frac{\partial}{\partial m_f} + \sum_V m_V \frac{\partial}{\partial m_V}\right)\mathcal{M}(\mathcal{A} \to \mathcal{B})\,, \tag{5.0.4}$$

where the sums go over the fermions and bosons. When considering gluon fusion, the corresponding process without Higgs is just the gluon two-point function where masses enter through loop effects. For heavy quarks they can be included in the Lagrangian by adding

$$\delta\mathcal{L} = -\frac{\alpha_S}{24\,\pi} G^a_{\mu\nu} G^{a\,\mu\nu} \sum_f \log\left[\frac{\Lambda^2}{m_f^2}\right]. \tag{5.0.5}$$

Now, using Eq. (5.0.4) one obtains directly $\mathcal{O}_g$ as it was already given in Eq. (5.0.2).

Adding the operators from Eqs. (5.0.1) and (5.0.2) to the SM Lagrangian and keeping only the terms relevant for gluon fusion we obtain[2]

$$\mathcal{L}_{eff} = \mathcal{L}_{SM} + (c_y \mathcal{O}_y + h.c.) + c_H \mathcal{O}_H + c_g \mathcal{O}_g + \tilde{c}_g \mathcal{O}_{\tilde{g}} \tag{5.0.6}$$

$$\supset -\kappa_t \frac{m_t}{v} \bar{t}th + \kappa_g \frac{\alpha_S}{12\,\pi} \frac{h}{v} G^a_{\mu\nu} G^{a\,\mu\nu} + i\tilde{\kappa}_t \frac{m_t}{v} \bar{t}\gamma_5 th + \tilde{\kappa}_g \frac{\alpha_S}{8\,\pi} \frac{h}{v} G^a_{\mu\nu} \widetilde{G}^{a\,\mu\nu} + \mathcal{L}_{QCD}\,, \tag{5.0.7}$$

where the couplings κ_i are given in terms of the coefficients c_i by

$$\kappa_t = 1 - \mathrm{Re}(c_y) - \frac{c_H}{2}\,, \qquad \kappa_g = c_g\,, \tag{5.0.8}$$

$$\tilde{\kappa}_t = \mathrm{Im}(c_y)\,, \qquad \text{and} \qquad \tilde{\kappa}_g = \tilde{c}_g\,. \tag{5.0.9}$$

In the limit $\kappa_t = 1$ and all other $\kappa_i = 0$, the SM Lagrangian is obtained. The operators multiplied by the κ_i without tilde in Eq. (5.0.8) are invariant under CP and the ones multiplied by the $\tilde{\kappa}_i$ in Eq. (5.0.9) are CP-violating. Since the CP-even and CP-odd amplitudes do not interfere in gluon fusion, we can treat the two cases independently. We will make use of this fact and focus on the CP-conserving part and correspondingly set $\tilde{\kappa}_g = \tilde{\kappa}_t = 0$ for the rest of this chapter unless mentioned otherwise. In the remaining effective Lagrangian, we have now two parameters that encode new physics effects: κ_t controls modifications of the top Yukawa coupling and thus modifications to gluon fusion via top loops and κ_g quantifies the direct Higgs-gluon interaction, which results from loops of heavy (unknown) particles.

In the effective theory defined by Eq. (5.0.6), the amplitude for $gg \to h$ in terms of $\tau = (4m_t^2)/m_h^2 \approx 7.7$ is given by [107–110]

$$\mathcal{M}(\kappa_t, \kappa_g) \propto \kappa_g + \kappa_t \frac{3}{2}\tau \left(1 + (1-\tau)\,\arcsin^2\left[\frac{1}{\sqrt{\tau}}\right]\right). \tag{5.0.10}$$

Here, the first term corresponds to the direct Higgs-gluon interaction and the second term is obtained from the full calculation of the top loop. Expanding the loop function in the

[2] In principle, all Yukawa-type operators for the 6 quarks contribute. However, since the coupling of the fermions to the Higgs is proportional to their mass, already the contribution of the bottom loop is much smaller than the one of the top loop and will be neglected here.

squared amplitude in $1/\tau$ and normalizing the amplitude by the SM value ($\kappa_t = 1,\ \kappa_g = 0$) yields

$$\frac{|\mathcal{M}(\kappa_t,\kappa_g)|^2}{|\mathcal{M}(1,0)|^2} = (\kappa_t+\kappa_g)^2\left[1-\frac{7}{15}\frac{\kappa_g}{\tau(\kappa_t+\kappa_g)}+\mathcal{O}\left(\frac{1}{\tau^2}\right)\right] \approx (\kappa_t+\kappa_g)^2\,. \tag{5.0.11}$$

The combination of a large value for τ and a small prefactor of the second term in the square brackets pushes the effects of this term beyond the reach of the LHC [111]. We therefore omitted it in the second equation and will continue to do so throughout the remaining part of this chapter. The physical interpretation of Eq. (5.0.11) is that, due to the relatively light Higgs, the low energy theorem is already a very good approximation for the top loop and not only for even heavier new particles. Unfortunately this means that the effects from IR- and UV physics encoded in κ_t and κ_g, respectively cannot be disentangled in gluon fusion.

When we want to break the degeneracy present in Eq. (5.0.11), we have to make the effective description of the top loop no longer a good one. We achieve this by introducing a new scale into the process that is high enough to demand a full description of the top loop but still low enough to keep the effective description valid for new heavier particles. To introduce the new scale, we simply demand a very boosted Higgs which recoils against another particle. Earlier studies which made use of the transverse momentum of the Higgs are for example [112–114].

The recoiling particle can not be a photon due to Furry's theorem [115]: If a photon is appended to the top loop, the color structure of the loop remains trivial. It is contributing only a global factor $\frac{1}{2}\,\delta^{ab}$ where $a,b = 1\ldots 8$ are the color coefficients of the gluons. Replacing the initial gluons by photons therefore yields the same amplitude apart from this global factor. However, any amplitude for a QED process with an odd number of external photons has to vanish due to Furry's theorem. Thus also $gg \to H+\gamma$ has to vanish. A way out could be to demand two instead of only one final state photon. Yet, this process is only induced by a dimension 10 operator

$$\mathcal{O} \sim \frac{1}{16\pi^2}\frac{v}{m_t^2}F_{\mu\nu}F^{\mu\nu}G^a_{\mu\nu}G^{a\,\mu\nu}H \tag{5.0.12}$$

and a rough estimate reveals a tiny cross section of about 0.5-1 fb, making this channel very challenging.

The cross section for a boost from Z emission is dominated by the Higgs radiated off a Z and the diagrams depending on the top Yukawa contribute only about 10% to the total cross section of this final state. Thus the hZ final state is difficult as well. Nevertheless two studies looked into this process and analyzed is capabilities [116, 117].

In the following, we will consider a third possibility where the Higgs recoils against a final state parton. If the initial partons are gluons, the recoiling parton has to be a gluon, too.

At low transverse momenta this process will be the dominating one. At higher transverse momenta, the (anti-)quark-gluon initial state becomes more and more important. In these processes the recoiling parton is the initial (anti-)quark. Irrespective of the initial partons, all diagrams for the $h+jet$ final state contain a top loop and thus show the same degeneracy in the low energy limit. See Fig. 5.4 for example Feynman diagrams.

5.1. Boosted Higgs in BSM models

In our analysis in sections 5.2 to 5.4, we employ a model independent approach and describe the effects of new physics by modified couplings only. In this section, however, we want to show that the breaking of the above mentioned degeneracy in κ_t and κ_g is not merely of academic interest but might be necessary in both, supersymmetric and in particular in composite Higgs models. Both of these models have in common that they modify the top Yukawa coupling on the one hand and introduce new heavy particles that will generate a non-zero κ_g on the other hand. In realistic ranges of the SUSY parameter space and in a very generic composite Higgs setup, these two effects conspire and cancel mutually. Therefore, despite being present in the gluon fusion process, new physics could hide in the inclusive cross section. An independent measurement of κ_t and κ_g is therefore crucial to disclose the new physics effects and draw conclusions on the mass spectrum of the BSM models.

5.1.1. Boosted Higgs in the MCHM

In a very broad class of MCHMs the contribution to gluon fusion from the top partners cancels with the modified top Yukawa coupling such that the overall cross section experiences a rescaling but is completely independent of the mass of the top partners [118–122]. The scaling is given by a function $g(\xi)$ which fulfills $g(\xi \to 0) = 1$. For small values of $\xi \equiv v^2/f^2$ the rescaling might be therefore very hard to detect at the LHC.

The combination of couplings, which is measured in the inclusive cross section, is given in the MCHM by [119]

$$\kappa_t + \kappa_g = v \left(\frac{\partial}{\partial h} \log \det \mathcal{M}_t(h) \right)_{\langle h \rangle} , \tag{5.1.1}$$

where $\mathcal{M}_t(h)$ is the mass matrix describing the top sector of the model. Assuming partial compositeness, i.e. that the SM fermions couple linearly to the resonances, the mass matrix can be written in a block-diagonal form [122]

$$\mathcal{M}_t(h) = \begin{pmatrix} 0 & \mathbf{F}_L^T(h) \\ \mathbf{F}_R(h) & \mathbf{M}_C \end{pmatrix} . \tag{5.1.2}$$

Here $\mathbf{F}_{L,R}(h)$ are vectors coming from the mixing terms and $\mathbf{M}_C$ is the mass matrix of the composite sector. The determinant of $\mathcal{M}_t(h)$ can be factorized and assuming that $\mathbf{M}_C$ is independent of h,

$$\kappa_t + \kappa_g = v \left(\frac{\partial}{\partial h} \log m_t^0(h) \right)_{\langle h \rangle} \tag{5.1.3}$$

is obtained with $m_t^0(h) = -\mathbf{F}_L^T(h)\mathbf{M}_C^{-1}\mathbf{F}_R(h)$ being the top mass before wave function renormalization. It can be further shown [120] that $m_t^0(h)$ can be written as

$$m_t^0(h) = \sum_i C_i \, I_i \left(\frac{h}{f} \right) , \tag{5.1.4}$$

where the sum goes over all possible $SO(5)$ invariants $I_i(h/f)$ that can be built out of the embeddings of the left- and right-handed top quarks. The C_i are independent of h and contain the information on the elementary-composite mixing and the composite mass parameters. If only one $SO(5)$ invariant $I(h/f)$ can be built as is the case in most viable and popular choices $\mathbf{5}_L + \mathbf{5}_R$, $\mathbf{10}_L + \mathbf{10}_R$, or $\mathbf{14}_L + \mathbf{1}_R$[3], which all have $I(h/f) \propto \sin(2h/f)$, Eq. (5.1.4) becomes simply $m_t^0(h) \propto I(h/f)$. The proportionality factor containing all the interesting information on the spectrum of the composite sector then drops out of $\kappa_t + \kappa_g$ due to the logarithm in Eq. (5.1.3), making gluon fusion insensitive to the composite spectrum. In the above cases with $I(h/f) \propto \sin(2h/f)$, we obtain

$$\kappa_t + \kappa_g = v \left(\frac{\partial}{\partial h} \log \sin(2h/f) \right)_{\langle h \rangle} = \frac{1 - 2\xi}{\sqrt{1-\xi}} \, . \tag{5.1.5}$$

Clearly, as soon as more than one (different) invariant exists, as e.g. in $\mathbf{5}_L + \mathbf{14}_R$, the h dependence of $m_t^0(h)$ becomes less trivial and the gluon fusion will depend to some extent on the spectrum of the composite sector. Interestingly, the above observed insensitivity of $\kappa_t + \kappa_g$ can be observed in some Little Higgs models as well [119].

For a concrete example we will now consider the MCHM introduced in Eq. (4.2.15) in the previous section. In the limit where the right-handed top quark is mostly composite, one obtains in this model [121]

$$\kappa_g = \xi \sin^2\theta_R \left(\frac{m_1^2 - m_4^2}{m_4^2} \right) + \mathcal{O}\left(\sin^2\theta_L\right) \tag{5.1.6}$$

$$= \xi \sin^2\theta_R \frac{m_{\tilde{T}}^2 \cos\theta_R^2 - m_T^2}{m_T^2} + \mathcal{O}\left(\sin^2\theta_L\right) , \tag{5.1.7}$$

with $\sin\theta_{R,L} = \lambda_{u,t}/\sqrt{m_{1,4}^2 + \lambda_{u,q}^2}$ being the sine of the elementary-composite mixing angle. From Eq. (5.1.7) it can be seen that large values of $|\kappa_g| \gtrsim \xi$ are only possible for $m_{\tilde{T}} \gg m_T$, thus implying a light resonance. This can be seen as well in Fig. 5.2, where the distributions

[3] This notation specifies in which representation the left- and right-handed fermions are embedded.

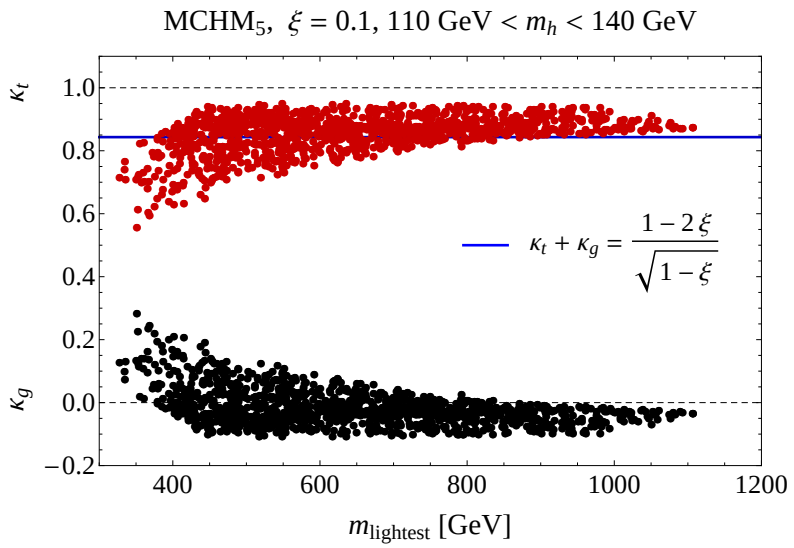

Figure 5.2.: Distribution of κ_t and κ_g against the mass of the lightest resonance. We observe that large values of κ_g are only obtained for light resonances and that the sum $\kappa_g + \kappa_t$ is indeed independent of m_{lightest} as given in Eq. (5.1.5)

of κ_t and κ_g, obtained from a numerical scan over the parameters of the Lagrangian in Eq. (4.2.15), are shown against the mass of the lightest resonance. From this figure we can see moreover that the sum $\kappa_t + \kappa_g$, which is measured in the inclusive cross section, is indeed independent of the mass spectrum.

As a final application of the concrete model, we will now establish the validity of the EFT approach in the presence of a high cut on the Higgs p_T. In Section 5.3, we will describe the effect of top partners by an effective ggh interaction but impose a cut of $p_T > 650\,\text{GeV}$. Naively the effective theory is expected to break down if the mass of the lightest top partner is smaller or of the order of the p_T cut. Fortunately this is not the case. In Fig. 5.3 the ratio of the effective to the full cross section

$$\frac{\sigma_{\text{EFT}}(pp \to h + jet)}{\sigma_{\text{full}}(pp \to h + jet)} \tag{5.1.8}$$

with a minimal Higgs transverse momentum of 650 GeV is shown against the mass of the lightest top partner. The full cross section was calculated within the model described by Eq. (4.2.15). In the left plot the ratio is shown for the different initial states. While the effective gg initiated process is within a few % deviation from the full result even in the presence of top partners as light as 400 GeV the $q\bar{q}$ initiated process deviates substantially even if $m_{\text{lightest}} > p_T^{\text{min}}$ as was already noted previously [123]. Since, however, the $q\bar{q}$ initiated process contributes only 1-2% to the total cross section while gg and $qg+\bar{q}g$ contribute about equally at a p_T cut of 650 GeV (see Table 5.2) the total cross section of the effective theory

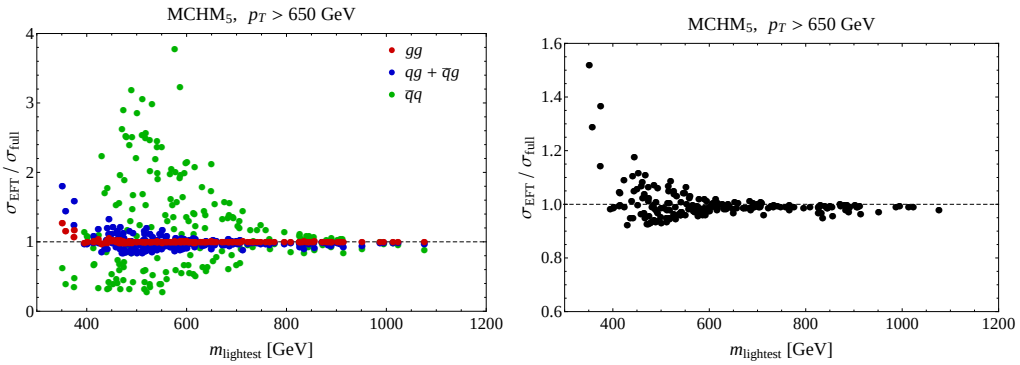

(a) **(b)**

Figure 5.3.: Ratio of the effective to the full cross section in $pp \to h + jet$ with minimal transverse momentum of the Higgs $p_T^{\min} = 650\,\text{GeV}$ against the mass of the lightest composite resonance. The left plot shows the ratio for the different initial states gg (red), $qg + \bar{q}g$ (blue), and $\bar{q}q$ (green) separately and the right plot shows it for the total combined cross section.

yields a result within 10% of the full calculation for top partners as light as 500 GeV. Since the lower limit on the top partner masses is already at $600 - 800\,\text{GeV}$ [124–135], we conclude that the utilization of the effective description is safe for our study.

5.1.2. Boosted Higgs in SUSY

For our supersymmetric example we choose the MSSM where additional D- or F-terms are present to lift the Higgs mass to the measured value while any degrees of freedom beyond the MSSM do not have any significant impact on the phenomenology of the CP-even lightest Higgs. In this framework both the inclusive [136–140] as well as the boosted [141–144] cross section are modified by diagrams where the top loop is replaced by squark loops and by completely new topologies. Example Feynman diagrams with SM topologies are shown in Fig. 5.4 and with MSSM topologies in Fig. 5.5.

Assuming that the CP-odd Higgs is decoupled, the inclusive signal strength can be written as [103, 145–148]

$$\frac{\Gamma(gg \to h)}{\Gamma(gg \to h)_{\text{SM}}} = (1 + \Delta_t)^2 \,, \tag{5.1.9}$$

where

$$\Delta_t \approx \frac{m_t^2}{4}\left(\frac{1}{m_{\tilde{t}_1}^2} + \frac{1}{m_{\tilde{t}_2}^2} - \frac{(A_t - \mu/\tan\beta)^2}{m_{\tilde{t}_1}^2\, m_{\tilde{t}_2}^2}\right) \tag{5.1.10}$$

is obtained in the limit where the loop particles are much heavier than the Higgs and small contributions from the D-terms are neglected. Due to the relative minus sign in Eq. (5.1.10) the MSSM contributions can cancel and lead to a SM-like inclusive cross section if the

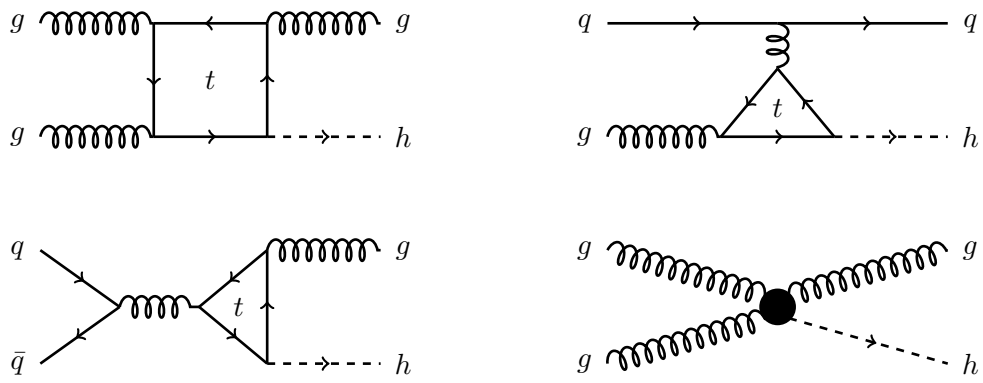

Figure 5.4.: Example Feynman diagrams for $pp \to h + jet$ in the SM and with the contact term.

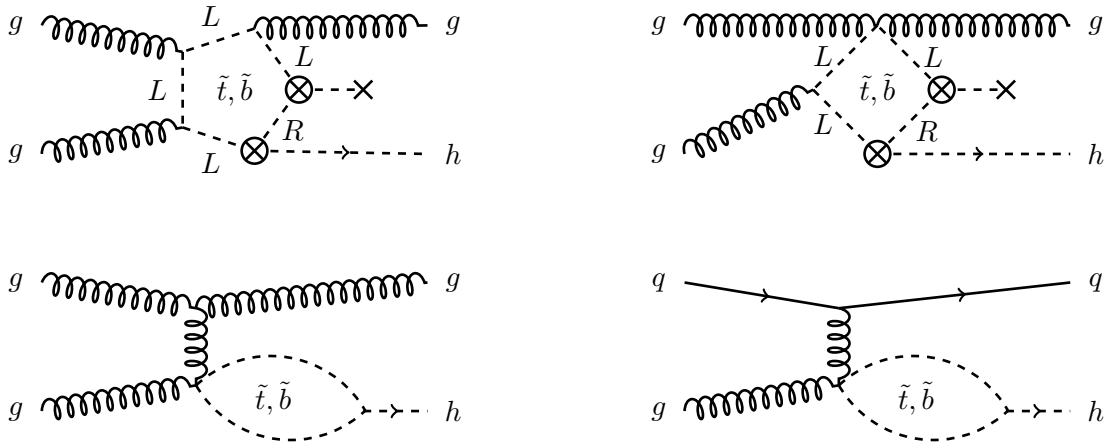

Figure 5.5.: Example Feynman diagrams for $pp \to h + jet$ in the MSSM. Besides the SM diagrams in Fig. 5.4 with stops and sbottoms replacing the top in the loops, new topologies contribute to the cross section. The upper two diagrams contain a flip from one interaction eigenstate to the other and are proportional to the trilinear mixing A_t.

trilinear coupling A_t is large. The flat direction in the A_t-$m_{\tilde{t}_2}$-plane is shown for different choices of $m_{\tilde{t}_1}$ in Fig. 5.6. Parameter regions where the soft masses are no longer real and thus are excluded are shaded in red.

Terms proportional to the trilinear coupling A_t appear with a negative sign in the scalar potential $V \supset -A_t\, h\, \tilde{t}_L \tilde{t}_R^*$ and if A_t is large, this might lead to a charge and color breaking minimum. Clearly, the vacuum in the universe is charge and color conserving and either it is the global minimum of the potential or the tunneling time to the true vacuum is longer than the lifetime of the universe. This stability constraint can be estimated by [149, 150]

$$A_t^2 < a\left(m_{\tilde{t}_1}^2 + m_{\tilde{t}_2}^2\right) - 3\mu^2\,, \tag{5.1.11}$$

where $a \approx 3$. The second reference even argues that a value as large as $a = 7.5$ is still suffi-

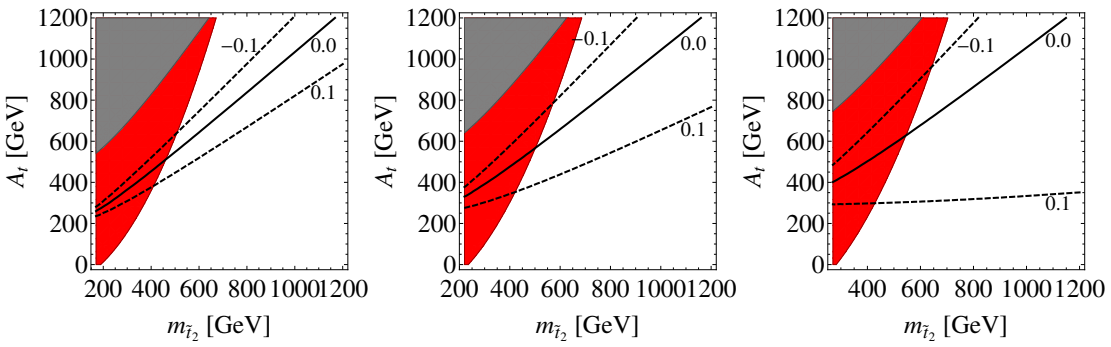

(a) $m_{\tilde{t}_1} = 170\,\text{GeV}$ **(b)** $m_{\tilde{t}_1} = 220\,\text{GeV}$ **(c)** $m_{\tilde{t}_1} = 270\,\text{GeV}$

Figure 5.6.: Lines of constant Δ_t (cf. Eq. (5.1.10)) for different values of $m_{\tilde{t}_1}$. Solid and dashed correspond to $\Delta_t = 0.0$ and $\Delta_t = \pm 0.1$, respectively. The deviations from the SM value ($\Delta_t = 0$) are small when $A_t \approx m_{\tilde{t}_2}$. The red shaded regions are excluded because there the soft parameters are no longer real (red). In gray we show the region excluded due to the vacuum stability constraint from Eq. (5.1.11) with $a = 3$.

cient when taking the tunneling rates into account. The excluded region for a conservative choice of $a = 3$ is shown in gray in Fig. 5.6.

Severe constraints on the parameter space also arise from direct searches at ATLAS [151–158] and CMS [159–162] and put strong limits on the squark masses. These limits are, however, relaxed if the LSP is heavy, the decay chains are long or the missing transverse energy E_T is not as large as expected in the minimal approaches (see for example Refs [163–166]). In particular, if the stop and LSP mass are such that the stop decay into a top quark is just kinematically open $m_{\tilde{t}} \approx m_t + m_{\tilde{\chi}_0}$, the LSP will only carry little transverse momentum. This region of parameter space is hard to tackle and is only poorly constrained.

In the following, we want to verify that light stops might be seen in boosted Higgs production even if their contribution to the inclusive cross section cancels. The advantage of tracing them in gluon fusion is that we do not need to make any assumptions on their decay. To re-analyze all existing searches in terms of boosted Higgs channels goes, however, far beyond the scope of this thesis and is left for future work.

The cross section for boosted Higgs production in the MSSM was calculated with `FeynArts` version 3.7 [167, 168] and `FormCalc` version 8.0 [169] and the `MSTW 2008 LO PDFs` [170] were interfaced with `LHAPDF` version 5.8.9 [171]. We chose the transverse mass at the p_T cut

$$\mu = \sqrt{m_h^2 + \left(p_T^{\text{min}}\right)^2} \tag{5.1.12}$$

as factorization and renormalization scale. We cross-checked the results with `HIGLU` [172] and found good agreement. The cross section, normalized by the SM value, is shown in

Point	$m_{\tilde{t}_1}$ [GeV]	$m_{\tilde{t}_2}$ [GeV]	A_t [GeV]	Δ_t
P_1	171	440	490	0.0026
P_2	192	1224	1220	0.013
P_3	226	484	532	0.015
P_4	226	484	0	0.18

Table 5.1.: The benchmark points that are used for the cross sections shown in Fig. 5.7. All points have the common values $\tan\beta = 10$, $M_{A^0} = 500\,\text{GeV}$, $M_2 = 1\,\text{TeV}$, $\mu = 200\,\text{GeV}$ and all trilinear couplings are set to the indicated value of A_t. The remaining sfermion masses are set to 1 TeV and the mass of the lightest CP-even Higgs is set to the experimental value of 125 GeV.

Fig. 5.7 for four different benchmark points. The first three points P_1–P_3 were chosen to have one light stop near the top mass and A_t such that Δ_t vanishes. The fourth point P_4 has the same stop masses as P_3 but differs by the choice $A_t = 0$. Even for P_1–P_3 where the inclusive cross section is SM-like, the boosted cross section deviates from the SM value at large p_T^{min}. A precision measurement could therefore uncover a hidden 'stealth' stop. However, in the example with one heavy stop, P_2, only small deviations are observed. In order to draw sound conclusions even in the presence of heavy stops, also the theoretical uncertainties need to be reduced and higher order calculations, taking the top mass effects into account, are necessary. Allowing small deviations in the inclusive cross section could alleviate the situation as larger deviations in the boosted cross section can then be expected.

Comparing the curves for P_3 and P_4, we see that they have roughly the same p_T^{min} dependence and differ only by a constant shift. We conclude that mainly the A_t independent diagrams are responsible for the breaking of the degeneracy. Of course it would be preferable to have an analytic expression for the MSSM cross section to trace the different p_T dependencies of the A_t dependent and independent parts and not only to motivate them from the different topologies involved. However, due to the large number of diagrams involved, compared to the SM case, this task is non-trivial and computationally demanding.

5.2. Calculating $pp \to h + jet$

The Higgs + jet final state has three different classes of processes at the parton level that we will distinguish by their initial states in the following. The most important one is $gg \to hg$ followed by $qg \to qh$ and $\bar{q}g \to \bar{q}h$ (both will be denoted by qg in the following) and finally $\bar{q}q \to gh$. The last process class is included for completeness but contributes only about 1% to the total cross section. Example Feynman diagrams for these processes as well as for the contact interaction are shown in Fig. 5.4. The effective interaction appears of course in all types of diagrams by just shrinking the top loop to a point.

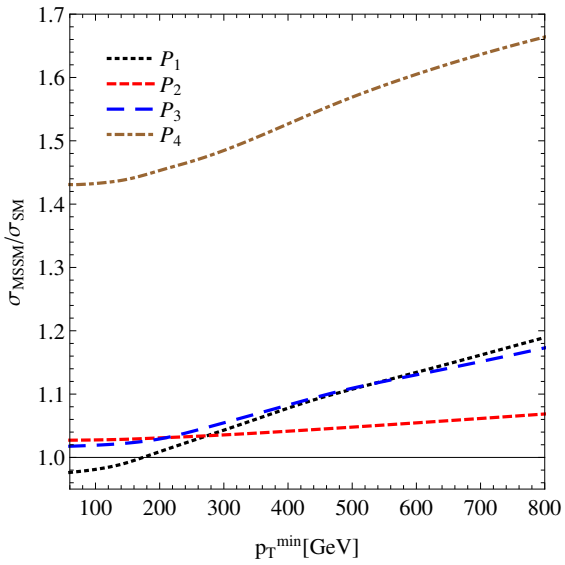

Figure 5.7.: Cross section for boosted Higgs in the MSSM as a function of the p_T-cut for four benchmark points corresponding to different choices of the stop masses and A_t. Their values are given in Table 5.1. The cross section is normalized by the SM value.

To obtain the cross section for Higgs + jet production within the theory described by the Lagrangian in Eq. (5.0.7), we need to scale the SM expression $\mathcal{M}_{ij}^{IR}(m_t)$ for the amplitudes with a top loop and initial partons $i, j \in \{g, q, \bar{q}\}$ by κ_t and the amplitudes with the contact interaction $\mathcal{M}_{ij}^{UV}$ by κ_g

$$\mathcal{M}_{ij}(\kappa_t, \kappa_g) = \kappa_t \mathcal{M}_{ij}^{IR}(m_t) + \kappa_g \mathcal{M}_{ij}^{UV} \,. \tag{5.2.1}$$

The matrix elements with the full top mass dependence for CP-conserving couplings were first calculated at leading order in QCD in Ref. [173] and shortly afterwards with a different notation in Ref. [174]. Since the K-factors in gluon fusion are known to be large it would increase the reliability of the following calculations if the Higgs + jet cross section were known at NLO, too. However, while higher order calculations for gluon fusion in the heavy top limit are available since some time a full calculation of the p_T-dependent cross section taking the top mass effects into account is not yet available. Attempts in this direction have been made firstly in Ref. [123] and recent progress is presented in Refs. [175–177]. Since the full top mass dependence is crucial for the idea of the calculation, we will only use the LO cross section, rescaled by a K-factor that is obtained in the heavy top limit. The full hadronic cross section for $pp \to h + jet$ with a minimal transverse momentum $p_T^{\min}$ of the

Higgs[4]

$$\sigma_{\text{total}}^{p_T^{\min}}(\kappa_t, \kappa_g) = \sum_{i,j=g,q,\bar{q}} \sigma_{ij}^{p_T^{\min}}(\kappa_t, \kappa_g) \tag{5.2.2}$$

is then obtained from Eq. (5.2.1) by

$$\sigma_{ij}^{p_T^{\min}}(\kappa_t, \kappa_g) = \int_{s_{\min}/s}^{1} \mathrm{d}\tau \int_{t_{\min}}^{t_{\max}} \mathrm{d}t \, \frac{1}{16\,\pi(\tau s)^2} \mathcal{L}_{ij}(\tau s, \mu_{\text{fac}}) \, |\mathcal{M}_{ij}(\kappa_t, \kappa_g)|^2 \tag{5.2.3}$$

where $\mathcal{M}_{ij}$ is the amplitude defined in Eq. (5.2.1), $\mathcal{L}_{ij}$ the parton luminosity for the initial partons i and j depending on the available energy of the partonic system and the factorization scale μ_{fac}, and $s_{\min}$ and $t_{\max/\min}$ are the extreme values of the Mandelstam variables s and t. The latter are determined by energy and momentum conservation and are given by

$$t_{\max/\min} = \frac{1}{2}\left(m_H^2 - \tau s \pm \sqrt{m_H^4 - 2\,\tau s\,\left(m_H^2 + 2p_T^2\right) + (\tau s)^2}\right) \tag{5.2.4}$$

$$s_{\min} = m_H^2 + 2p_T^2 + 2\sqrt{m_H^2 p_T^2 + p_T^4}\,, \tag{5.2.5}$$

for a demanded minimal transverse momentum p_T and Higgs mass m_H. Throughout the whole calculation we neglected the contribution from a bottom loop or modified bottom Yukawa couplings. This is done because at large transverse momenta $p_T^{\min} \gtrsim 50\,\text{GeV}$ their contribution is of the order of only a few percent [114, 178, 179]. We explicitly checked this statement for a few points and found a negligible effect of the bottom for the large boosts that we demand in the following.

From Eq. (5.2.1) it can be seen that the cross section can be written as polynomial of degree 2 in both κ_t and κ_g

$$\frac{\sigma^{p_T^{\min}}(\kappa_t, \kappa_g)}{\sigma^{p_T^{\min}}(1,0)} = (\kappa_t + \kappa_g)^2 + \delta\kappa_t\kappa_g + \epsilon\kappa_g^2\,, \tag{5.2.6}$$

where the expression in the bracket is what would be obtained in the inclusive case and δ, ϵ are numerical constants quantifying the deviations for nonzero $p_T^{\min}$. For the LHC center of mass energy of $\sqrt{s} = 14\,\text{TeV}$ and several choices of $p_T^{\min}$ the values for δ and ϵ are given in Table 5.2. These numbers were calculated using the parton distribution functions and the strong coupling constant α_S from the `MSTW 2008 LO PDFs` [170] with factorization and renormalization scale set to the transverse mass of the partonic system

$$\mu = \mu_{\text{fac}} = \mu_{\text{ren}} = m_T = \sqrt{m_H^2 + p_T^2}\,, \tag{5.2.7}$$

[4] since we do not include additional initial or final state radiation in this analytic treatment, the Higgs will have the same absolute transverse momentum as the accompanying jet

where $p_T^2 = \hat{t}\hat{u}/\hat{s}$ is calculated from the partonic values of the mandelstam variables[5]. The scalar integrals in the amplitudes were evaluated with `LoopTools` version 2.8 [169]. We cross checked the values for the cross section for the parameter choice $(\kappa_t, \kappa_g) = (1, 0)$ with `HIGLU` [172] for the parameter choice $(\kappa_t, \kappa_g) = (0, 1)$ with `MCFM` version 6.6 [180] and found very good agreement over the full p_T range. The table also shows in the sixth column the relative contributions of the different initial state classes to the SM cross section. While the gluon-gluon initial state is the most important at low p_T cuts, the (anti-)quark-gluon initial state becomes increasingly important and contributes to about 60% at the very high p_T cuts. The third category of initial states, $q\bar{q}$, contributes only between 1-2%.

We also show two sets of values for a 100 TeV collider to give a rough impression of the capabilities of such a machine. Clearly the large values for δ and ϵ at $p_T^{\min} = 2000\,\text{GeV}$ look very promising. However, the separation in the ϕ-η-plane of the decay products of a boosted Higgs scales approximately like $\Delta R = \sqrt{\Delta\phi^2 + \Delta\eta^2} \sim \frac{2m_h}{p_T}$ if $m_h \ll p_T$ and the mass of the decay products is negligible. A large boost therefore demands a very high resolution of a future detector. For a thorough analysis of the 100 TeV example, we need the efficiencies of the detector involved in the measurement. Since this is not known yet, we do not consider these numbers any further.

Finally, we also quote numbers for the CP-violating couplings generated by the operators in Eq. (5.0.7) where the coefficients $(\tilde{\gamma}, \tilde{\delta}, \tilde{\epsilon})$ are defined via

$$\frac{\sigma^{p_T^{\min}}(\tilde{\kappa}_t, \tilde{\kappa}_g)}{\sigma_{SM}^{p_T^{\min}}} = \frac{9}{4}\left[(\tilde{\kappa}_t + \tilde{\kappa}_g)^2 + \tilde{\gamma}\tilde{\kappa}_t^2 + \tilde{\delta}\tilde{\kappa}_t\tilde{\kappa}_g + \tilde{\epsilon}\tilde{\kappa}_g^2\right] \tag{5.2.8}$$

in the style of Eq. (5.2.6). The overall coefficient 9/4 appears because in the unboosted case we obtain the relation

$$\frac{\sigma^{\text{incl}}(\tilde{\kappa}_t, \tilde{\kappa}_g)}{\sigma_{SM}^{\text{incl}}} = \frac{9}{4}\left(\tilde{\kappa}_t + \tilde{\kappa}_g\right)^2 \ . \tag{5.2.9}$$

The numbers for the CP-violating coefficients were calculated with the analytic expressions for the helicity amplitudes quoted in the appendix A and the values for $\tilde{\gamma}$ and $\tilde{\epsilon}$ were successfully cross checked with `MCFM` and `HIGLU`. Note the equality of $\tilde{\epsilon}$ and ϵ over the whole p_T range. This is not by accident but is due to the fact that the operators $\mathcal{O}_g$ and $\mathcal{O}_{\tilde{g}}$ in Eq. (5.0.2) lead to the same expression for the squared amplitude for $pp \to h + jet$ when defined with the appropriate normalization.

[5] The relation $p_T^2 = \hat{t}\hat{u}/\hat{s}$ holds in the limit where at most one massive particle appears in the initial and final state. Since the valence quarks of the proton are much lighter than the Higgs and the center of mass energy, this expression is valid even in the qg initial state.

$\sqrt{s}$ [TeV]	$p_T^{\min}$ [GeV]	$\sigma_{p_T^{\min}}^{\mathrm{SM}}$ [fb]	δ	ϵ	gg, qg [%]	$\tilde{\gamma} \cdot 10^2$	$\tilde{\delta}$	$\tilde{\epsilon}$
14	100	2180	0.0031	0.031	67, 31	2.6	0.033	0.031
	150	837	0.070	0.13	66, 32	1.7	0.094	0.13
	200	351	0.20	0.30	65, 34	0.28	0.22	0.30
	250	157	0.39	0.56	63, 36	0.20	0.41	0.56
	300	74.9	0.61	0.89	61, 38	1.0	0.64	0.89
	350	37.7	0.85	1.3	58, 41	2.2	0.91	1.3
	400	19.9	1.1	1.7	56, 43	3.4	1.2	1.7
	450	10.9	1.4	2.3	54, 45	4.6	1.5	2.3
	500	6.24	1.7	2.9	52, 47	5.6	1.8	2.9
	550	3.68	2.0	3.6	50, 49	6.5	2.2	3.6
	600	2.22	2.3	4.4	48, 51	7.3	2.5	4.4
	650	1.38	2.6	5.2	46, 53	7.9	2.9	5.2
	700	0.871	3.0	6.2	45, 54	8.4	3.2	6.2
	750	0.562	3.3	7.2	43, 56	8.8	3.6	7.2
	800	0.368	3.7	8.4	42, 57	9.1	3.9	8.4
100	500	964	1.8	3.1	72, 28	5.0	1.9	3.1
	2000	1.01	14	78	56, 43	7.0	15	78

Table 5.2.: SM cross sections for $pp \to h + jet$ with different choices for the minimal transverse momentum of the Higgs $p_T^{\min}$ and a center of mass energy of $\sqrt{s} = 14\,\mathrm{TeV}$ and $\sqrt{s} = 100\,\mathrm{TeV}$. The coefficients δ, ϵ, $\tilde{\gamma}$, $\tilde{\delta}$, and $\tilde{\epsilon}$ quantify the deviation from the inclusive cross section and are defined in Eqs. (5.2.6) and (5.2.8). The column before the double bar gives the relative contribution of the gluon-gluon and the (anti-)quark-gluon initial states to the SM cross section.

5.3. Resolving the couplings in boosted Higgs production

From Table 5.2 we can see that the coefficients δ and ϵ increase with increasing $p_T^{\min}$ and thus lead to a deviation from the inclusive cross section. On the other hand however, the cross section drops drastically and we therefore need to find a good compromise between a large enough boost to break the degeneracy and a reasonably large cross section to observe enough events. To compensate for the small cross section, we will only consider in the following the decay $h \to \tau\tau$, which has a large branching ratio and also a reasonable reconstruction efficiency. A full analysis should of course make use of as many decay channels as possible. In Section 5.4, we will discuss as an interesting alternative channel the decay $h \to WW$.

The decay channel with the largest branching ratio $h \to b\bar{b}$ suffers unfortunately from a large QCD background and will be hard to resolve. Nevertheless, jet substructure techniques which can resolve the two collimated b-jets from the boosted Higgs might provide a handle

on this final state. The decay $h \to ZZ^* \to 4\ell$ would be very interesting due to its very small background, however, the branching ratio is only 0.21%. Therefore, even with 100% reconstruction efficiency, we could only expect to see about nine events with $p_T > 650\,\text{GeV}$ at $3\,\text{ab}^{-1}$. This is too few for a measurement and we therefore do not consider this channel any further.

Since $m_\tau \approx 1.7\,\text{GeV} \ll m_H$ [181] and the Higgs mass is small compared to the boost $m_H/p_T \ll 1$, we can use $\Delta R \approx 2m_H/p_T$ for the typical separation of the decay products. In our case, we can therefore expect a jet-radius of about 0.5 if at least one of the taus decays hadronically. This is too small to resolve the decay products so that the standard tau tagging techniques will fail. Fortunately, there is already a study [182] to adapt the tau tagging to highly boosted taus whose efficiencies we will use here. Specifically, they applied the tau tagging to a decaying Higgs originating from a heavy Z'. We will use the efficiencies obtained for a Z' mass of 2 TeV, which will result in Higgs bosons with about the same boost as in our analysis. In Ref. [182], they quoted two different numbers for di-tau tagging. One with a cut on the reconstructed Higgs mass and one without. Since we assume that the cut on the Higgs mass will be helpful to reduce the background, we employ the numbers with the cut. We then arrive at an estimated total efficiency of

$$\epsilon_{\text{tot}} = \text{BR}(h \to \tau\tau) \cdot \left(\sum_{i=\tau_l\tau_l,\tau_l\tau_h,\tau_h\tau_h} BR(\tau\tau \to i)\, \epsilon_i \right) \approx 2 \cdot 10^{-2}\,, \tag{5.3.1}$$

when using the SM value for $\text{BR}(h \to \tau\tau)$ [183].

To break the degeneracy between κ_t and κ_g and determine them independently, we need to have two observables. On the one hand, we will take the signal strength for inclusive Higgs production

$$\mu_{\text{incl}}(\kappa_t, \kappa_g) = \frac{\sigma^{\text{incl}}(\kappa_t, \kappa_g)}{\sigma^{\text{incl}}_{\text{SM}}} \approx (\kappa_t + \kappa_g)^2 \tag{5.3.2}$$

and on the other hand we will take the ratio

$$\mathcal{R}(\kappa_t, \kappa_g) = \frac{\sigma^{650\,\text{GeV}}(\kappa_t, \kappa_g) K_{650\,\text{GeV}}}{\sigma^{150\,\text{GeV}}(\kappa_t, \kappa_g) K_{150\,\text{GeV}}}\,, \tag{5.3.3}$$

where $K_{p_T^{\text{min}}}$ is the QCD NLO K-factor obtained for a given minimal transverse momentum. The K-factors were calculated with `MCFM` version 6.6, which provides an NLO cross section for $h + jet$ production (process 204). This cross section is calculated in the heavy top limit and thus does not apply directly to our case but at least it gives an approximate result, actually the best we can get at the moment. We take the ratio $\mathcal{R}$ instead of just the boosted cross section to cancel systematic and theoretical uncertainties. The two values for p_T^{min} were chosen to have a combination of a boosted and a basically unboosted cross section which still has similar uncertainties. The specific value was determined through a rough optimization,

$\mu = \mu_{\text{ren}} = \mu_{\text{fac}}$	$\sigma^{150\,\text{GeV}}$ [fb]	$K_{150\,\text{GeV}}$	$\sigma^{650\,\text{GeV}}$ [fb]	$K_{650\,\text{GeV}}$	$\mathcal{R} \cdot 10^3$
$m_T/2$	$1.2 \cdot 10^3$	1.16	2.0	1.14	1.66
m_T	$0.83 \cdot 10^3$	1.41	1.4	1.44	1.69
$2\,m_T$	$0.60 \cdot 10^3$	1.64	0.96	1.70	1.66

Table 5.3.: SM QCD K-factors, LO cross sections and ratios $\mathcal{R}$ obtained for different choices of renormalization and factorization scale. Clearly $\mathcal{R}$ is very stable under the variations.

testing for which values the limits are most stringent. While the cross sections and the K-factors are quite scale-dependent, $\mathcal{R}$ is very stable under scale variations as can be seen from table 5.3.

For our scenario, we choose the high luminosity phase of the LHC with an integrated luminosity of $\int \mathcal{L}\text{d}t = 3\,\text{ab}^{-1}$ at $\sqrt{s} = 14\,\text{TeV}$. We further assume[6] a systematic uncertainty of 10%, $\delta_{\text{sys}} = 0.1$, for both the inclusive signal strength μ_{incl} and the two cross sections appearing in $\mathcal{R}$ (cf. Eq. (5.3.3)). While we expect a negligible statistical uncertainty in the inclusive measurement, we include the statistical uncertainty on the number of boosted events $N_{p_T^{\text{min}}} = \sigma^{p_T^{\text{min}}}(\kappa_t, \kappa_g) K_{p_T^{\text{min}}} \epsilon_{\text{tot}} \int \mathcal{L}\text{d}t$. Finally, we combine the two observables in a simple χ^2 function

$$\chi^2(\kappa_t, \kappa_g) = \left(\frac{\mu_{\text{incl}}(\kappa_t, \kappa_g) - \mu_{\text{incl}}^{\text{obs}}}{\delta\mu_{\text{incl}}} \right)^2 + \left(\frac{\mathcal{R}(\kappa_t, \kappa_g) - \mathcal{R}^0}{\delta\mathcal{R}} \right)^2 , \tag{5.3.4}$$

where

$$\frac{\delta\mu_{\text{incl}}}{\mu_{\text{incl}}^{\text{obs}}} = \delta_{\text{sys}} \qquad \text{and} \qquad \frac{\delta\mathcal{R}}{\mathcal{R}^0} = \sqrt{\frac{1}{N_{150\,\text{GeV}}} + \frac{1}{N_{650\,\text{GeV}}} + 2\delta_{\text{sys}}} \,. \tag{5.3.5}$$

We consider three different benchmark points where the observed inclusive signal strength is $\mu_{\text{incl}}^{\text{obs}} = 0.8, 1.0, 1.2$ and pick for each of the points the three values for the top Yukawa modification $\kappa_t^0 = 0.8, 1.0, 1.2$. This fixes immediately $\kappa_g^0 = \sqrt{\mu_{\text{incl}}^{\text{obs}}} - \kappa_t^0$ and then $\mathcal{R}^0 = \mathcal{R}(\kappa_t^0, \kappa_g^0)$. For each of the choices of $\mu_{\text{incl}}^{\text{obs}}$ and κ_t^0 we draw in the κ_t-κ_g-plane the contours for $\chi^2(\kappa_t, \kappa_g) = Q_{0.95}^{\chi^2(2)} \approx 3.84$, where $Q_{0.95}^{\chi^2(2)}$ is the 95% CL quantile of the χ^2-distribution with two degrees of freedom[7]. The resulting plots are shown in figure 5.8a-(c). There the blue, red, and black contours correspond to $\kappa_t = 0.8$, 1.0, and 1.2, respectively, and the gray band shows the constraint obtained from the inclusive cross section only. The black star indicates the SM parameters. From Fig. 5.8b, we can see that even in the worst case with a

[6] As this section describes an exploratory study and is supposed to give only a rough estimate of the resolving power of boosted Higgs, we do not include background events but estimate the uncertainties. For the results of a more realistic study including background see section 5.4

[7] Actually, in general the contours are drawn for $\Delta\chi^2 \equiv \chi^2(\kappa_t, \kappa_g) - \chi^2_{\text{min}} = Q_{0.95}^{\chi^2(2)}$ with χ^2_{min} being the minimum of $\chi^2(\kappa_t, \kappa_g)$. Since $\chi^2_{\text{min}} = 0$ here, we omitted it.

SM inclusive signal strength $\mu_{\text{incl}}^{\text{obs}} = 1.0$, a top Yukawa that deviates by $\pm 20\%$ from the SM value (black and blue contour) can be excluded at 95% CL with an integrated luminosity of $3\,\text{ab}^{-1}$.

In Fig. 5.8d the scale dependence of the contour lines is shown for SM input parameters $\mu_{\text{incl}}^{\text{obs}} = 1.0$, $\kappa_t = 1.0$. The three contours correspond to the three different choices for the renormalization and factorization scale $\mu = 0.5\,m_T$, m_T, and $2\,m_T$ with m_T defined in Eq. (5.2.7). In agreement with the numbers presented in table 5.3, the contours depend hardly on the scale.

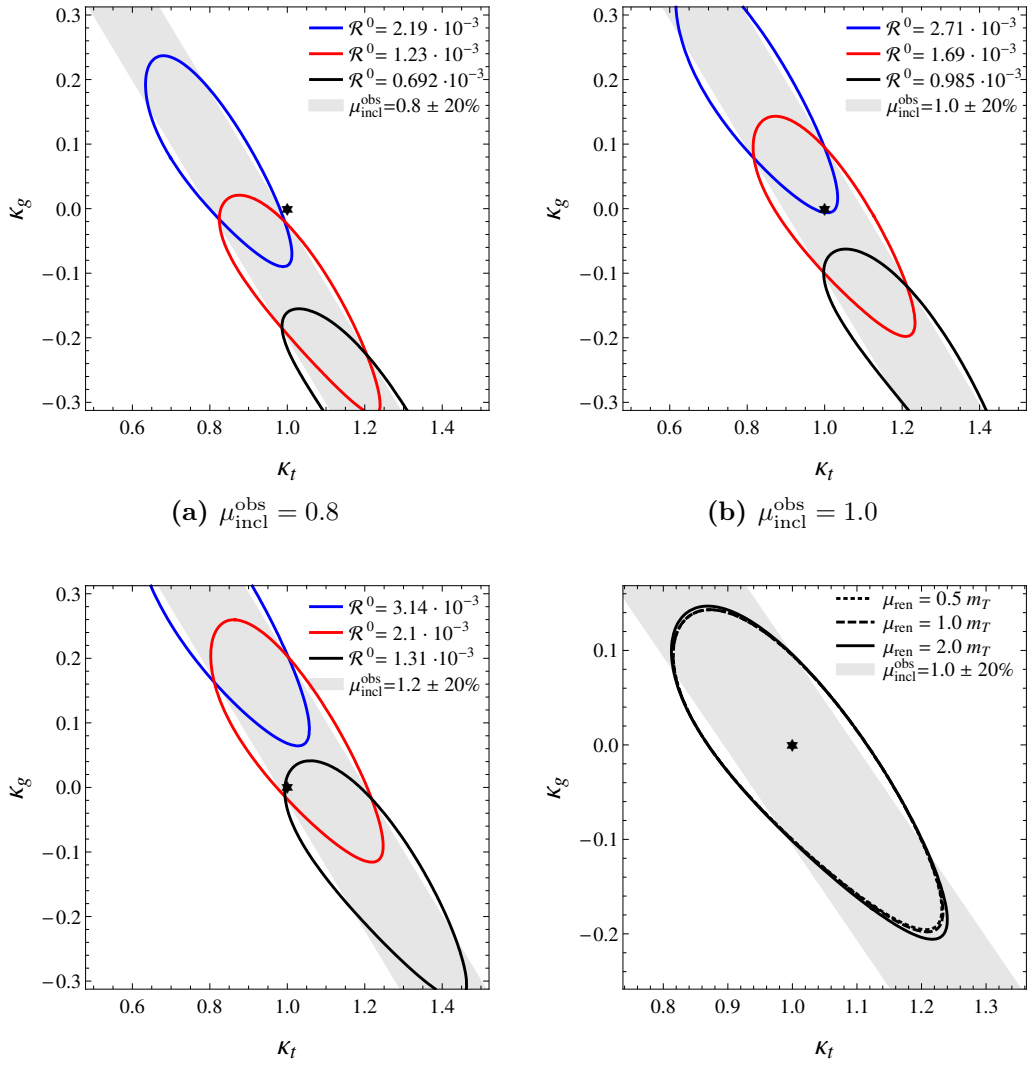

(a) $\mu_{\rm incl}^{\rm obs} = 0.8$ **(b)** $\mu_{\rm incl}^{\rm obs} = 1.0$

(c) $\mu_{\rm incl}^{\rm obs} = 1.2$ **(d)** Scale variation

Figure 5.8.: Figures (a)-(c) show the 95% CL contours obtained from the χ^2 in Eq. (5.3.4) for different choices of the actual parameters κ_t^0 and κ_g^0, or equivalently of $\mu_{\rm incl}^{obs}$ and $\mathcal{R}^0$. The colors blue, red and black correspond to $\kappa_t^0 = 0.8$, 1.0, and 1.2, respectively, or equivalently to the indicated values of $\mathcal{R}^0 = \mathcal{R}(\kappa_t^0, \sqrt{\mu_{\rm incl}^{obs}} - \kappa_t^0)$. The gray band is obtained by considering only the inclusive measurement $\mu_{\rm incl}^{\rm obs} \pm 20\%$. The SM point is indicated by the black star. Figure (d) shows the variation of the 95% CL contours for SM parameters and different choices of the renormalization and factorization scale μ. For all plots we assumed an integrated luminosity of $\int \mathcal{L} dt = 3\,\text{ab}^{-1}$ and $\sqrt{s} = 14\,\text{TeV}$.

5.4. Realistic collider study

Up to now we based the boosted Higgs analysis purely on signal properties and estimated efficiencies for the reconstruction of the Higgs decay products but neglected the contribution from background processes. To put the results on a more solid footing, we will discuss a reconstruction-level analysis that includes a realistic background simulation in the following[8]. For this study, we assume a worst-case scenario where the inclusive cross section is equal to the SM value, i.e. $\kappa_t + \kappa_g = 1$, and try to get sensitive to the individual couplings through the boosted channel. If the composite Higgs model ansatz is realized in nature, the inclusive cross section will receive small corrections and therefore ameliorate the situation. Also in SUSY, an exact cancellation would need a specific relation among the stop masses. Small deviations from this relation would lead to modifications of the inclusive cross section. Our results will therefore give an estimate of what one could expect at least.

To suppress the large QCD background present at the LHC, we will consider clean channels where the boosted Higgs decays into two leptons plus missing energy. The main contributions to this channel come from the Higgs decay via $W_\ell W_\ell^*$ ($BR = 1.4\%$) and $\tau_\ell \tau_\ell$ ($BR = 0.77\%$) where the ℓ subscript denotes a subsequent decay into a lepton $\ell = e, \mu$. The decay via two Z bosons where one decays into neutrinos and the other one into leptons barely contributes to this channel ($BR = 0.08\%$) and is therefore omitted.

For the generation of the signal events, we used `MadGraph5` version 1.5.15 [184] and showered with `Herwig++` [185–187]. Since `MadGraph5` does not take into account the top mass dependence (which is crucial for the extraction of the couplings) but only provides the effective Higgs-gluon interaction via the 'HEFT' model file, we reweighted the events. Given that the generated cross section is proportional to $|\mathcal{M}(0,1)|^2$, defined in Eq. (5.2.1), the reweighting factor is $w(\kappa_t, \kappa_g) = |\mathcal{M}(\kappa_t, \kappa_g)|^2 / |\mathcal{M}(0,1)|^2$. Finally we normalize the cross section to the NNLO+NNLL result by rescaling it with a K-facor of 1.71 [188–191]. As before, this K-factor does not include the top mass effects but is the best result available to date.

As background processes, we consider $W + jets$, $Z + jets$, and $t\bar{t} + jets$, where we demand that both the direct Ws and those from the top decay, decay leptonically. The Z, however, has to decay into taus since this is the only channel where two final state leptons are produced and the Z-peak cannot be reconstructed to reject the event. The events are generated with `ALPGEN` [192] and `PYTHIA` [193]. The gauge boson + jets events are matched up to two partons and the $t\bar{t}$ events up to one parton, all with the MLM matching scheme [194, 195]. The $t\bar{t}$ cross section is rescaled to the NLO value [196–198].

[8] As described in the declaration on page ix, I was involved in this collider study but did not implement the analysis. I will therefore only focus on the main ideas of the analysis and present the results but refer to Ref. [2] for more details.

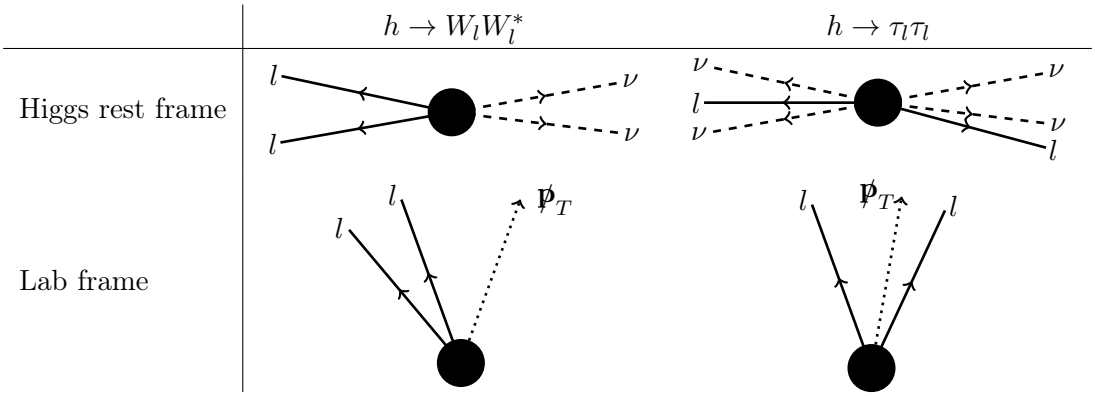

Figure 5.9.: Topology of the W and tau decay mode of the Higgs boson. A spin correlation in the W mode makes the charged leptons of the decay go in one similar direction. In the tau mode no such correlation is present and the neutrinos will go mostly in the same direction as the charged leptons due to the large boost from the mass difference. In the lab frame this leads to a different direction of the missing momentum compared to the directions of the two leptons. We can then distinguish the decay modes by this topology difference.

For the jet clustering in the event reconstruction, we used the Cambridge-Aachen algorithm [199, 200] implemented in `FastJet` version 3.0.4 [201].

In the event selection, we demand exactly two leptons in agreement with the selected final state. In the parton picture of a boosted Higgs event we expect a Higgs and a parton, both with a large p_T. The parton will radiate off other partons and produce a large jet. A fat jet as with radius $R = 1.5$ is expected to capture all those radiated off particles and correspondingly we demand one such jet with $p_T > 200\,\text{GeV}$. On the other hand, the Higgs transverse momentum can be reconstructed by summing the transverse momentum of the two leptons and the missing energy. Since the Higgs is recoiling against the fat jet, the Higgs reconstructed transverse momentum is demanded to exceed 200 GeV as well.

At this point, we split the analysis in two signal regions, one for each decay mode. To achieve this, we use a spin correlation in the W decay mode that makes the two final state charged leptons go in a similar direction as well as the two neutrinos. In the tau decay mode, however, the taus go in opposite directions in the Higgs rest frame and will be boosted due to the mass gap. Therefore, the tau decay products – two neutrinos and a charged lepton – will be very collimated for each tau. In the lab frame, the missing transverse momentum will therefore be mostly outside (inside) the area spanned by the two leptons in the W (tau) mode, see Fig. 5.9. We use this criterion to distinguish the two cases.

In the tau mode, we can reconstruct the neutrino momenta by assuming that they are parallel to the lepton momenta and have to sum up to the missing transverse momentum. This works particularly well in the boosted regime when the tau momenta are not back-to-

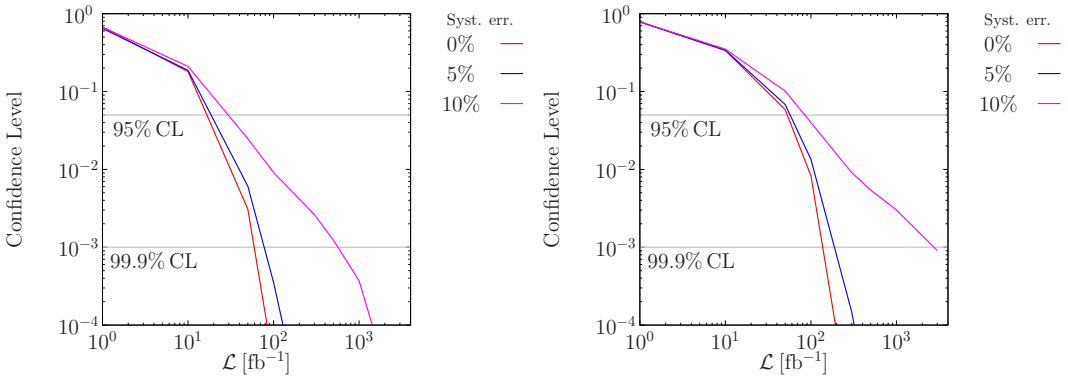

(a) tau mode, $\kappa_g = 0.5$ **(b)** W mode, $\kappa_g = 0.5$

Figure 5.10.: CL_s for signal plus background against the background only hypothesis as a function of integrated luminosity. The parameter point is $\kappa_g = \kappa_t = 0.5$ for both plots. The signal can be excluded at 95% confidence level at 20-60 fb, depending on the assumed systematic uncertainty.

back and provide a good basis. Within this collinear approximation [173], we can reconstruct the four-momentum of the Higgs and thus its mass. In fact, this reconstructed mass peaks at the Higgs mass and allows to estimate the background, the main contribution being $Z \to \tau_l \tau_l$, by looking at the side-bands. After keeping only the events with a reconstructed mass within 10 GeV of the actual Higgs mass, we achieve $S/B \sim 0.4$ with $S/\sqrt{B} > 9$ for 300 fb^{-1}.

In the W mode, a mass reconstruction on an event base is not possible and the kinematics of the signal is very similar to the two most dominant backgrounds of this mode: W and $t\bar{t} + jets$. We achieve some discrimination by looking into the transverse mass

$$m_{T,ll} = m_{ll}^2 + 2\left(E_{T,ll}\not{E}_T - \mathbf{p}_{T,ll} \cdot \not{\mathbf{p}}_T\right) , \tag{5.4.1}$$

which gives the greatest lower bound on the Higgs mass [202]. Here m_{ll} is the invariant mass of the dilepton system, $E_{T,ll} = \sqrt{m_{ll}^2 + p_{T,ll}^2}$ its transverse energy, and $\not{E}_T = |\not{\mathbf{p}}_T|$ the missing transverse energy. After demanding $m_{T,ll} < m_h$ and demanding further that the leptons go into a similar direction $\Delta R_{ll} < 0.4$ we obtain $S/B \sim 0.4$ and $S/\sqrt{B} > 6$ for 300 fb^{-1}.

Finally, we perform a binned likelihood analysis with the CL_s method described in [11] where we assume Gaussian errors on the cross section normalization. A brief sketch of the CL_s method is given in Appendix B. In Fig. 5.10, we show the p-value for the signal plus background against the background-only hypothesis as a function of the integrated luminosity for the tau mode (left) and W mode (right). Clearly, the tau mode is more sensitive as expected from the better value for $S/\sqrt{B}$. In this mode, we see the signal at 95% confidence level already at an integrated luminosity of 20-60 fb^{-1}, depending on the

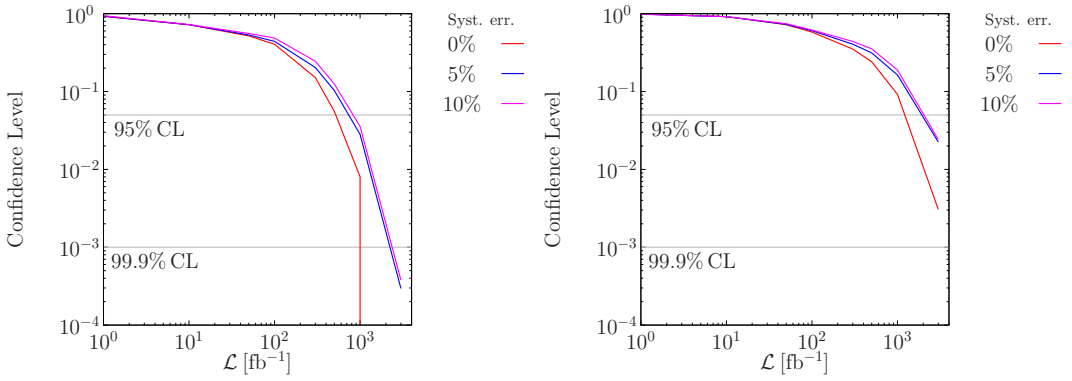

(a) tau mode, $\kappa_g = 0.5$ **(b)** tau mode, $\kappa_g = -0.5$

Figure 5.11.: CL_s for non-SM signal plus background against SM signal plus background hypothesis as a function of integrated luminosity. In both plots only the tau mode is considered.

assumed systematic uncertainty. The better performance of the tau mode compared to the W mode, which has a twice as large branching ratio, is due to the excellent Higgs-momentum reconstruction by the collinear approximation.

Distinguishing a non-SM signal from the SM signal is clearly much more difficult. We show in Fig. 5.11 the expected p-values as a function of the integrated luminosity for non-SM signal plus background hypothesis against the SM-signal plus background hypothesis. We only show the better performing tau mode for the parameter points $\kappa_g = 0.5$ (left) and $\kappa_g = -0.5$ (right). Since for negative κ_g the cross section decreases (cf. Eq. (5.2.6)), the performance in this case is worse than for positive κ_g. Still, we can exclude a non-SM signal with $\kappa_g = \pm 0.5$ at 95% confidence level with an integrated luminosity of roughly $3\,\text{ab}^{-1}$.

In Fig. 5.12 we show the p-value for the test of signal plus background against SM-signal plus background as a function of κ_g. The integrated luminosity is set to $3\,\text{ab}^{-1}$. Assuming 10% systematic uncertainty, we can exclude $\kappa_g < -0.4$ and $\kappa_g > 0.3$ at 95% confidence level.

5.5. Final remarks

From the plots in Figs. 5.11 and 5.12 one might conclude that the boosted Higgs channel is not very promising to disentangle the coupling coefficients κ_g and κ_t. However, a few points should be kept in mind to put this conclusion in perspective. In this study we assumed a worst case scenario with an *exact* SM inclusive cross section while it is expected to deviate slightly in BSM models. Further, we only focused on the decay of $H \to 2\ell + \not{p}_T$. Including also the hadronic decay of the taus [182, 203] and combining the different channels will

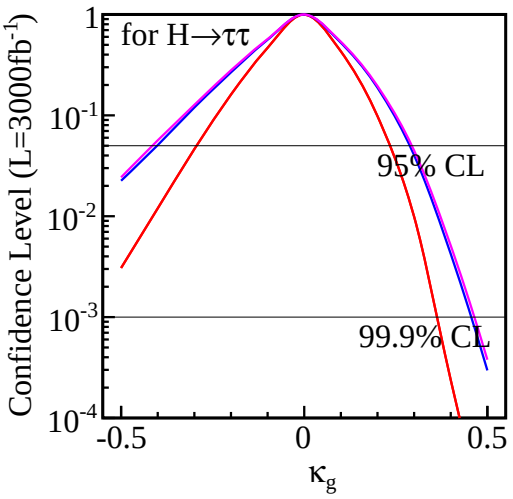

Figure 5.12.: CL_s for non-SM signal plus background against SM signal plus background hypothesis as a function of κ_g at an integrated luminosity of $\int \mathcal{L} dt = 3\,\mathrm{ab}^{-1}$. The red, blue, and violet curve correspond to 0, 5, and 10% systematic uncertainty, respectively.

certainly improve the situation although being far from trivial when coping with correlated uncertainties. Finally, the boosted Higgs channel is so far the only channel to complement the also very challenging $t\bar{t}H$ channel in measuring κ_t independently of κ_g. This alone makes the channel a very important and interesting one.

6. Scale invariant stop and sbottom searches

If SUSY is realized in nature, there are necessarily scalar partners (squarks and sleptons) to the fermions of the SM in the spectrum. As pointed out in Chapter 3, the stops and thus also one of the sbottoms need to be light in order to solve the hierarchy problem. Consequently the stops and sbottoms are intensively sought for at the LHC. Despite these intense attempts they have not been found yet and both ATLAS [151–158] and CMS [159–162, 204–207] already excluded light stops and sbotttoms and cut deeply into the well-motivated parameter space.

Having no hint for the squark and neutralino/LSP masses besides naturalness arguments, it is useful to employ search strategies that capture very general properties of SUSY and make as few assumptions on the realized model as possible. Simplified toplogies that shrink the decay chains down to the minimal requirements provide such an approach while remaining still flexible and allowing for different branching ratios. Within this simplified setup we consider the stop and sbottom pair production, followed by a direct decay into a hadronically decaying top or a bottom and a higgsino. Whether the higgsino is a neutralino or chargino is determined by charge conservation. A Feynman diagram depicting such a process is shown in Fig. 6.1. Of course, simplified topologies might be too simplifying to capture the properties of long decay chains that arise if the mass spectrum is more elaborate. On the other hand, however, this setup is motivated by a naturalness argument that demands light stops, higgsinos and gluinos and allows all the other SUSY particles of the spectrum to be heavy and decouple [208].

Within this simplified setup the event shape depends on the mass difference between the initially produced squarks and the higgsinos. If this difference is smaller than the top mass, only the decay into bottoms is kinematically allowed and therefore this channel makes up for all the decay width. Once the difference is big enough to allow the decay into top quarks, this channel contributes considerably. If the decay is only just allowed, $m_{\tilde{t}} \approx m_{\tilde{\chi}^0} + m_t$, the neutralino will hardly generate missing transverse energy and the top will be indistinguishable form the SM $t\bar{t}$ production. See [209] for a study trying to close this gap in the parameter space by precisely measuring the $t\bar{t}$ cross section. If the mass difference is large, boosted top or bottom quarks and large missing transverse energy will be generated.

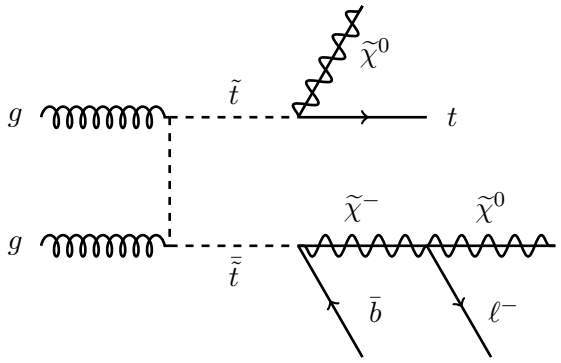

Figure 6.1.: Generic Feynman diagram for stop production and decay. The initially produced squarks can be any of the two stops or the lighter sbottom. They decay subsequently into a top or a bottom and a higgsino, such that the electric charge is conserved.

Since the mass difference is unknown, it is preferable to design a search strategy that is scale invariant and thus sensitive over a large range from the unboosted to the very boosted regime. Besides allowing to scan a large region of the parameter space, such an analysis has the advantage that it captures the final state particles from the three possible initial squarks $\tilde{t}_{1,2}$ and $\tilde{b}_1$ even if they have different masses. Therefore the effective signal cross section is increased compared to a search strategy which is only sensitive within a narrow mass range. Of course, scale invariance is only fulfilled approximately. At some point the squark masses become just too heavy and can no longer be detected at the LHC due to the tiny production cross section.

The core of the analysis will be to tag the top quarks with several jet substructure techniques, which are efficient at different boosts. For the very boosted top quarks we use the HEPTop Tagger [210, 211], for medium boosted top quarks the BDRS Tagger [212], and the unboosted ones we try to reconstruct from separated jets. By using incrementally increasing cone sizes for the jets to be tagged, we manage to tag the minimal content of a top decay without collecting too many particles from the underlying event. Previous studies using top taggers for the reconstruction of hadronic top quarks include [210, 211, 213–228]. Although they employ top tagging techniques, none of them combines the different techniques to obtain a scale invariant analysis for stop searches.

6.1. Event generation

6.1.1. Signal sample

As explained in the introduction to this chapter, not only $\tilde{t}_1$ but also $\tilde{t}_2$ and $\tilde{b}_1$ production contributes to the signal. For all these three production channels we consider the decay

into a higgsino $\widetilde{\chi}_1^{\pm}$, $\widetilde{\chi}_{1,2}^0$ and a top or bottom quark. Since in the natural SUSY setup the higgsinos are nearly mass degenerate, it is sufficient to generate only the decay in the lightest neutralino $\tilde{q} \to q + \widetilde{\chi}_1^0$ and the chargino $\tilde{q} \to q' + \widetilde{\chi}_1^{\pm}$, where q, q' stands for t or b. The decay of the second lightest neutralino $\widetilde{\chi}_2^0 \to \widetilde{\chi}_1^{0,\pm} + X$ and of the chargino to one of the neutralinos $\widetilde{\chi}_1^{\pm} \to \widetilde{\chi}_{1,2}^0 + X$ does not leave any trace in the detector since the emitted particles X will be extremely soft. Thus, the event topologies for $\tilde{t}_1 \to t + \widetilde{\chi}_{1,2}^0$ will be the same and the different cross section for this topology can be obtained by rescaling it with the appropriate branching ratios. This allows us to introduce a shorthand notation for each topology: The production of a pair of squarks S with their subsequent decay into the quarks q_1 and q_2, respectively, will be denoted by the shorthand notation Sq_1q_2, where q_1 and q_2 are alphabetically ordered. The emission of the appropriate higgsinos in the decay is always understood.

We consider the following points in the MSSM parameter space. At fixed $A_t = 200\,\text{GeV}$, $\mu = 300\,\text{GeV}$, and $\tan\beta = 10$ we scan in steps of 50 GeV over a grid defined by $300\,\text{GeV} \leq m_{Q_3}, m_{u_3} \leq 1\,400\,\text{GeV}$. The gaugino masses as well as the other squark mass parameters are set to 5 TeV while the remaining trilinear couplings are set to zero. For each grid point we calculate the spectrum and the branching ratios with `SUSY-HIT` [229]. Subsequently, we use `fastlim`, version 1.0 [230] to check which of the points are already excluded by existing searches.

Since the squark production cross section only depends on the squark mass, and the branching ratios are given in the `SUSY-HIT` output, we can now determine which event topologies are the most dominant. In Fig. 6.2 we show in the left panels from top to bottom the relative contribution to the total SUSY cross section for the three processes contributing to Stt, Sbt, and Sbb, respectively. Here, we define the total SUSY cross section as the sum of the squark pair production cross sections $\sigma_{\text{SUSY}} \equiv \sum_{S=\widetilde{T}_1,\widetilde{T}_2,\widetilde{B}_1} \sigma_{S\bar{S}}$. In the right panels we show in color code the coverage defined as the sum of these relative contributions. The larger the coverage the more of the cross section we can capture by looking into these channels. In the top figure we show the coverage of the tt final state only. In the middle figure we additionally include the bt final state and in the bottom figure all three final states tt, bt, and bb are taken into account. The gray shaded areas correspond to the already excluded parameter points, which are determined by `fastlim`. The red dashed lines show the mass of the lightest stop $m_{\tilde{t}_1}$.

In the regions where the soft masses are below 500 GeV the initial squarks are too light to allow the decay into top quarks and correspondingly they are only covered after taking the bb final state into account. In this case where all three final states are taken into account, the worst coverage is nearly 100% except along the line where the top decay channel opens up. There it is between 70–80% because in this narrow region also the direct decay to a W

boson $\tilde{t} \to W + b + \widetilde{\chi}^0$ has a significant branching ratio. In the regions where the decay into top quarks is kinematically allowed and $m_{u_3} > m_{Q_3}$, the tt final state alone allows to capture most of the cross section as the coverage is above 80%, see the upper right plot of Fig. 6.2. This happens because there the lighter stop has a large branching ratio into top quarks. In the other half of the plot, it is the heavier stop that has the larger branching ratio into top quarks and therefore the final states with bottom quarks dominate there. Once the analysis is sensitive to the mixed final state bt the region with $m_{Q_3} > m_{u_3}$ is covered to about 60% instead of 30–40% in the tt only case.

For six parameter points $(m_{Q_3}[\text{GeV}], m_{u_3}[\text{GeV}]) = (550, 550)$, $(900, 900)$, $(1\,400, 1\,400)$, and $(550, 900)$, $(550, 1\,400)$, $(900, 1\,400)$ we separately generate events for each of the nine signal processes using `MadGraph5_aMC@NLO`, version 2.1.1 [231] at a center of mass energy $\sqrt{s} = 13\,\text{TeV}$. No cuts are applied at the generator level. The matching up to two jets is done with the MLM method in the shower-k_T scheme [194, 195] with `PYTHIA` version 6.426 [193]. We set the matching and the matrix element cutoff scale, *Qcut* and *xqcut*, respectively, to the same value determined from the mass of the initial squark $\widetilde{m}$

$$\text{Qcut} = \text{xqcut} = \frac{\widetilde{m}}{6}\,. \tag{6.1.1}$$

We checked and found that the differential jet distributions [232] are smooth with this scale choice.

The cross section for the signal processes is eventually rescaled by the NLO QCD and NLL K-factors obtained from `NLL-fast`, version 3.0 [233–235]. Moreover, to correct for the omission of the decay of a squark into the second lightest neutralino and the corresponding quark, we multiply the cross section by a factor

$$\mathcal{F} = \frac{BR_{\widetilde{\chi}_1^0} + BR_{\widetilde{\chi}_2^0}}{BR_{\widetilde{\chi}_1^0}} \tag{6.1.2}$$

for each quark in the final state that has the same flavor as the initial squarks. Here, $BR_{\widetilde{\chi}_i^0}$ denotes the branching ratio of the corresponding squark to the same flavor quark and the neutralino $\widetilde{\chi}_i^0$.

6.1.2. Background sample

In our analysis we want to use different top tagging methods, which are based on jet substructure techniques. We therefore focus on the decay of the squarks into a hadronically decaying top and a neutralino. The former will generate between one to three distinct jets, depending on its boost, and the latter will generate missing energy. Our final state therefore consists of missing energy and up to six jets. As background we therefore considered the following four processes

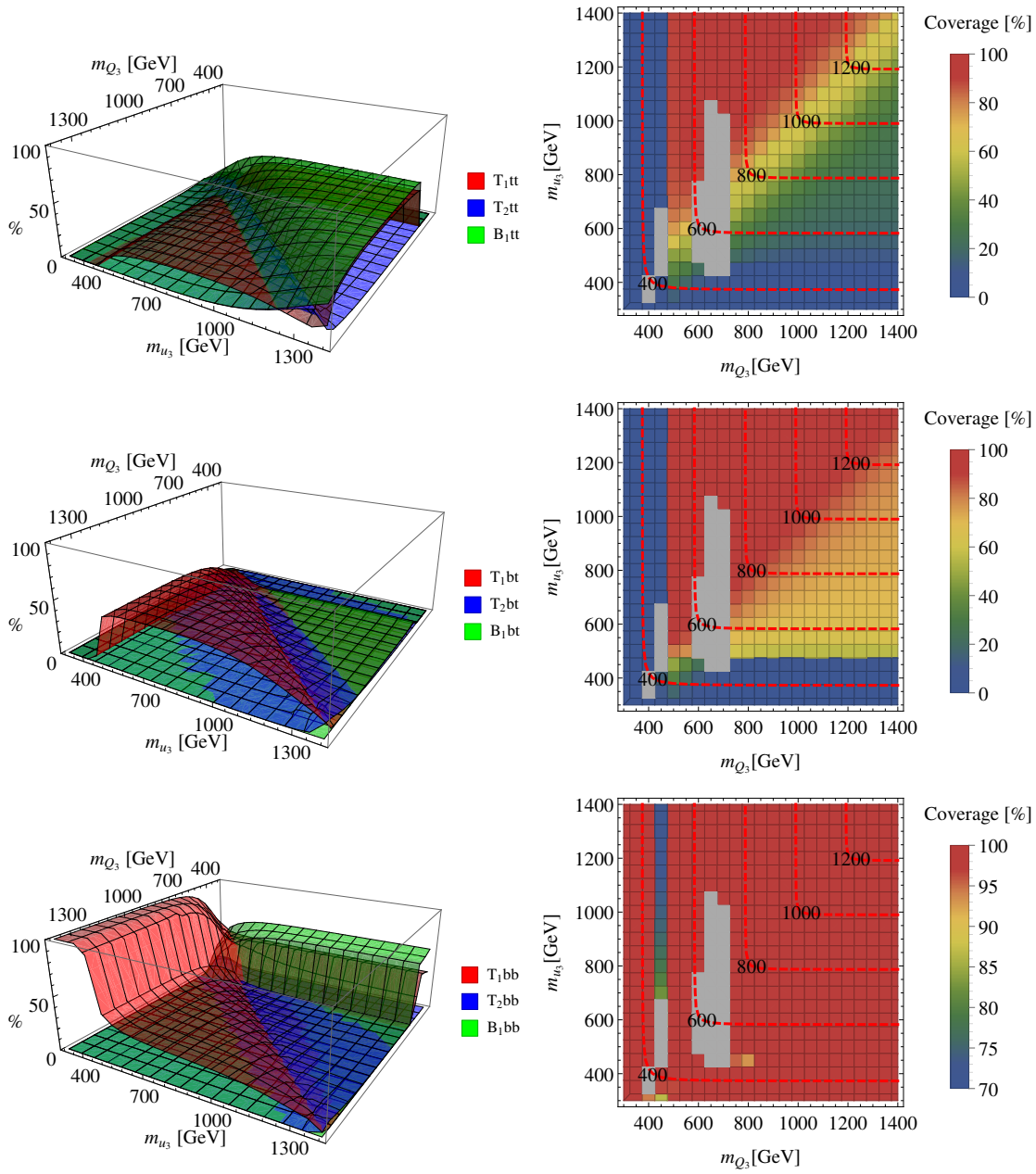

Figure 6.2.: Left panels: The relative contribution of the different processes to the total SUSY cross section, i.e. in red $100 \cdot \sigma_{T_1 q_1 q_2}/\sigma_{SUSY}$ as a function of m_{Q_3} and m_{u_3} and similar for the other colors. Right panels: Coverage, i.e. sum of the relative contributions of the considered processes to the total SUSY cross section. From top to bottom the considered channels are only tt final states, tt and bt final states, and tt, bt and bb final states. Note the different color scale of the lower right plot. The gray shaded areas show the points that are already excluded. Red dashed lines indicate the mass of the lightest stop in GeV.

(m_{Q_3}, m_{u_3})	$m_{\tilde{t}_1}$	$m_{\tilde{t}_2}$	$m_{\tilde{b}_1}$	σ_{SUSY} [fb]
(550, 550)	545.6	590.7	553.1	348
(900, 900)	897.2	925.0	901.9	12.6
(1 400, 1 400)	1 398	1 416	1 401	0.388
(550, 900)	566.7	912.4	553.1	210
(550, 1 400)	567.2	1 408	553,1	204
(900, 1 400)	910.4	1 408	901.9	8.36

Table 6.1.: Stop and sbottom masses as well as the cross section in fb summed up for all 9 channels at the chosen parameter points. All masses, including the soft masses that define the parameter point, are given in GeV. The higgsinos $\tilde{h} = \chi_1^{0,\pm}, \chi_2^0$ are nearly mass degenerate with $m_{\tilde{h}} \approx \mu = 300\,\text{GeV}$ for all parameter points.

- ***Wj*:** $pp \to W_\ell + 3\,\text{jets}$, where the W decays into leptons (including taus) such that the neutrino accounts for the missing energy. The cross section is multiplied by the K-factor 1.37 to rescale it to the NNLO QCD value [236].
- ***Zj*:** $pp \to Z_\nu + 4\,\text{jets}$, where the Z decays into two neutrinos and hence generates missing energy. This cross section is known at NNLO QCD as well [236] and rescaled to this value by a K-factor 1.2.
- ***Ztt̄*:** $pp \to Z_\nu + t + \bar{t}$, where both top quarks decay hadronically, faking the top quarks from the squark decay and the Z decays again into two neutrinos to generate missing energy. This cross section is known at NLO QCD [237] and rescaled by a K-factor of 1.39 to this value.
- ***tt̄*:** $pp \to t\bar{t} + 2\,\text{jets}$, where one top decays hadronically and the other one leptonically to emit a neutrino, which accounts for missing energy. The NNLO+NNLL QCD K-factor 1.41 is obtained from `Top++` version 2.0 [238].

The background events are all generated with `MadGraph5_aMC@NLO` version 2.1.1 [231] and showered with `PYTHIA` version 6.426 [193]. The cross sections for these four background processes are given in Table 6.2.

6.2. Analysis

6.2.1. Reconstruction

For the reconstruction of the events we use `ATOM` [239], based on `Rivet` [240], which links to `FastJet` version 3.1.0 [201] for jet clustering. We use both the Cambridge-Aachen (C/A)

Process	LO Cross section [pb]	K-factor	Order
Wj	78.3	1.37	NNLO [236]
Zj	24.8	1.20	NNLO [236]
$Zt\bar{t}$	8.13×10^{-3}	1.39	NLO [237]
$t\bar{t}$	13.75	1.41	NNLO+NNLL [238]

Table 6.2.: LO cross sections in pb and K-factors for the background processes.

[199, 200] and the anti-k_t [241] algorithm with several radii for the clustering. Electrons and muons are reconstructed as leptons if their transverse momentum is greater than 25 GeV and their pseudo-rapidity $\eta = \frac{1}{2}\log\left(\frac{|\boldsymbol{p}|+p_z}{|\boldsymbol{p}|-p_z}\right)$ is within $|\eta| < 2.47$ for electrons and $|\eta| < 2.4$ for muons, where $\boldsymbol{p}$ is the three-momentum and p_z the momentum along the beam direction. Furthermore, we demand the leptons to be isolated. For the electrons we enforce this by not reconstructing them if the scalar sum of track momenta within a cone of radius $R = \sqrt{\Delta\phi^2 + \Delta\eta^2} = 0.2$ around the electron exceeds 10 % of the electron energy. Muons are only reconstructed if this sum is smaller than 1.8 GeV. This lepton reconstruction follows the one presented in Ref. [242]. For the jet clustering we use tracks with $p_T > 20$ GeV and with $|\eta| < 2.5$.

In the end we want to be sensitive over a large range of stop masses leading to very different boosts for the top quarks. If the top is produced nearly at rest in the lab frame its decay products will be very well separated and lead to three distinct jets. For a medium boosted top we expect the b quark to produce a separated jet while the decay products of the W will generate one fat jet. In the very boosted case, all three final partons will be within a small area and the three jets can no longer be resolved. To reconstruct all possible top quarks we need to use very different reconstruction techniques.

In the boosted case the HEPTop Tagger [210, 211] is an efficient tool. This tagger takes a fat C/A jet and checks if two of the subjets have an invariant mass close to the W mass. If the invariant mass obtained after including a third subjet is close to the top mass, this fat jet is tagged as a top candidate. For a more detailed description of the algorithm see the original release papers [210, 211]. The radius of the fat jet is the bigger the less boosted the top is. We therefore increase the cluster radius gradually to pick the smallest possible radius for a top candidate to avoid collecting unnecessary nearby tracks.

In the medium boosted regime the BDRS Tagger [212] becomes efficient. This is a mass-drop tagger that takes a fat C/A jet and undoes the last clustering step such that two subjets are obtained. If the two subjets are well separated and their invariant masses are at most 33% of the invariant mass of the fat jet this fat jet is tagged. This way one expects to capture hadronically decaying W bosons which are so boosted that the two final state

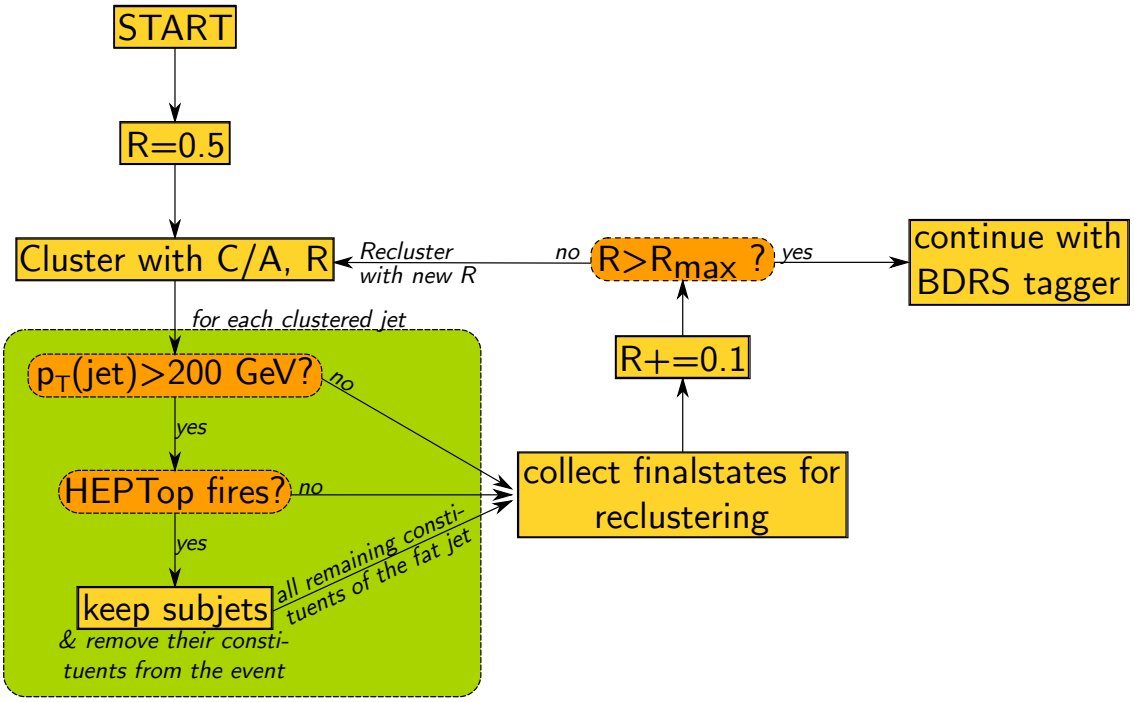

Figure 6.3.: Flowchart of the top reconstruction with the HEPTop Tagger. The reconstruction with the BDRS Tagger is done similarly, except that the initial radius is $R = 0.6$.

jets are too close to be reconstructed in two individual jets. The exact reconstruction and tagging procedure is described in the following and visualized in the flowchart in Fig. 6.3.

We start with clustering C/A jets with a small radius $R_0 = 0.5$ and check for each jet if its transverse momentum is bigger than 200 GeV. If this is the case, it is handed over to the HEPTop Tagger. When the tagger fires, we keep the subjets as top candidates and remove their constituents from the event. All remaining constituents of the fat jet are kept and collected with the constituents of the fat jets that are either not tagged by the HEPTop Tagger or do not even pass the $p_T > 200$ GeV criterion. Once all jets are checked we increase the clustering radius by $\Delta R = 0.1$, recluster the remaining tracks of the event, and start the procedure again until the radius exceeds the maximal value $R_{\text{max}} = 1.5$. Then the whole procedure starts again with the remaining tracks except that now the initial radius is $R_0 = 0.6$ and instead of the HEPTop Tagger we take the BDRS Tagger. All the tracks that are left after the BDRS tagging is done are finally clustered with the anti-k_t algorithm with a radius $R_{k_t} = 0.4$. A minimal transverse momentum of $p_T > 20$ GeV is demanded for the anti-k_t jets.

All anti-k_t jets and subjets of the tagged fat jets are eventually passed to a simple b-tagger which mimics the output of a real b-tagger with efficiency 0.7 and rejection 50 [243]. These

values are defined as ratios of the number of b-tags and the truth-level number of b-jets and non-b-jets

$$\text{efficiency} = \frac{\#\text{correct b-tags}}{\#\text{truth b-jets}} \qquad \text{and} \qquad \text{rejection} = \frac{\#\text{truth non-b-jets}}{\#\text{false b-tags}}\,. \tag{6.2.1}$$

Our tagger code checks if any constituent of the (sub-)jet in question has a b-hadron among its ancestors. If there is a bottom quark in its history this (sub-)jet is b-tagged with a probability of 70%. Otherwise it is b-tagged with a probability of 2%, corresponding to a rejection of 50. In the case of subjets from a very boosted fat jet these numbers are clearly optimistic [244]. Later we will however only use this information of HEPTop tagged subjets if their summed transverse momentum is below 250 GeV. In this case the three subjets of the tagged fat jet are still relatively far apart and therefore we assume that the actual tagging efficiency and the rejection is still comparable. The b-tag results of the subjets of BDRS jets are as well only used in the lower p_T region and moreover we then only demand that none of the subjets is b-tagged. Therefore only the overall b-tag information of the BDRS tagged jet is used and could as well be obtained by passing the fat jet to the b-tagger.

6.2.1.1. Filtering HEPTop tagged candidates

Clearly, as every real tagger, the HEPTop Tagger has a fake rate and provides top candidates that do not always correspond to top quarks at the truth level. In the left panel of Fig. 6.4 we show the minimal distance $\Delta R = \sqrt{\Delta\phi^2 + \Delta\eta^2}$ between a top candidate of the HEPTop Tagger and a truth top of the event against their difference in energy. Like all plots of Figs. 6.4, 6.5, and 6.6, this plot is based on the T_1tt, (900,900) sample after vetoing events that have a reconstructed lepton.

While most of the top candidates actually are close to a truth top, some lie far off. From now on we will consider a candidate which lies within $\Delta R < 0.5$ and $\Delta E < 300\,\text{GeV}$ of a truth top as a correct tag while all other tags are considered mis-tags.

In the central plane of Fig. 6.4, we show in green and red the distribution of the correctly and mis- tagged top candidates in the p_T-η-plane, respectively. We can see that the mis-tags lie predominantly in the low p_T region[1]. Since the HEPTop Tagger specifies which of the subjets it considers to originate from the decaying W and which to be a b-jet, we have an additional handle to purify the sample. We filter the sample of HEPTop candidates by demanding that if the transverse momentum of the top candidate is less than 250 GeV the correct jet (correct according to the HEPTop Tagger output) has to be b-tagged while the

[1] Note that although only fat jets with $p_T > 200\,\text{GeV}$ were passed to the HEPTop Tagger, the top candidates themselves can have slightly less transverse momentum as they are built out of the three tagged subjets of the fat jet and miss some of the constituents of the fat jet which contribute to its transverse momentum.

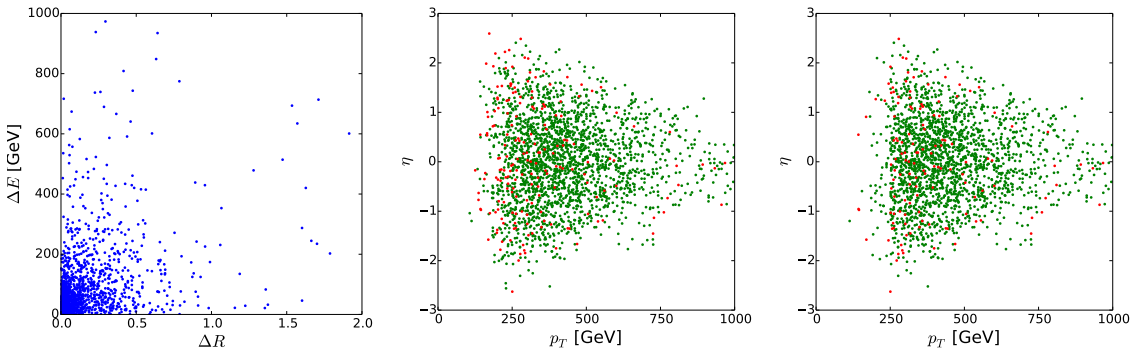

Figure 6.4.: Output of the HEPTop Tagger. Left panel: Minimal distance in terms of ΔR between a tagged candidate and a truth level top. For each such pair the difference in energy is plotted on the y-axis. Central panel: Distribution of the top candidates in the p_T-η-plane before additional filtering. Green dots correspond to correctly tagged candidates, red dots to all other candidates. Right panel: The same distribution as in the central plane but after filtering.

		$(900, 900),\ T_1tt$		$(550, 550),\ T_1tt$		Wj
		$\mathcal{R}_T$	ϵ	$\mathcal{R}_T$	ϵ	$\mathcal{R}_E$
HEPTop Tagger	unfiltered	8.9 %	20.5 %	18.3 %	7.8 %	1.34 %
	filtered	6.8 %	19.0 %	12.9 %	5.5 %	0.70 %
BDRS Tagger	unfiltered	7.3 %	2.0 %	11.0 %	0.9 %	0.04 %
	filtered	5.8 %	1.9 %	9.2 %	0.8 %	0.04 %
Resolved tops	unfiltered	57.4 %	1.5 %	50.2 %	5.8 %	1.32 %
	filtered	52.7 %	1.4 %	46.3 %	5.5 %	0.98 %

Table 6.3.: The effect of filtering the top candidates. $\mathcal{R}_T$, ϵ, and $\mathcal{R}_E$ are defined in Eqs. (6.2.2), (6.2.1), and (6.2.3), respectively. The filters for each tagger are described in the corresponding subsections.

other two must not be b-tagged. The distribution after this filtering is plotted in the right panel of Fig. 6.4.

It can be seen directly that some mis-tags are rejected by the filter but at the same time also correct tags do not pass it. To quantify this win-loss behavior we show in Table 6.3 the mis-tag ratio defined as the ratio of mis-tags to all tags

$$\mathcal{R}_T = \frac{\#\text{ mis-tags}}{\#\text{ mis-tags} + \#\text{ correct tags}}\,, \tag{6.2.2}$$

the efficiency ϵ as defined in Eq. (6.2.1), and the mis-tag rate

$$\mathcal{R}_E = \frac{\#\text{ tags}}{\text{event}}\,, \tag{6.2.3}$$

which gives the average number of tags on a top-less event. Clearly, $\mathcal{R}_T$, ϵ, and $\mathcal{R}_E$ diminish by applying the filter but the $\mathcal{R}_i$ more than the efficiencies. We therefore continue to use this filter in the analysis. In the last column of the table we $\mathcal{R}_E$ for the Wj sample which contains no truth top quarks.

6.2.1.2. Reconstructing and filtering BDRS tagged candidates

As a mass-drop tagger the BDRS Tagger tags on fat jets which seem to originate from a heavy boosted particle, e.g. W or h, decaying into two light collimated partons. In our case we expect to find the W bosons from a top decay where the top is only medium boosted. Then the b-jet is too far separated from the W for its decay products to be found by the HEPTop Tagger but the W itself is still boosted enough to be captured in one fat jet.

To eventually find good top candidates we first demand that the invariant mass m_{jet} of the BDRS tagged jet with the largest p_T is close to the W mass $|m_{\text{jet}} - m_W| < 10\,\text{GeV}$. Next we take the b-tagged anti-k_t jet with the largest p_T and check if the invariant mass of the W candidate and the b-jet together is close to the top mass $|m_{b+W} - m_t| < 25\,\text{GeV}$. If this is the case we keep the combination as a top candidate otherwise we take the next to hardest b-jet and repeat the procedure until either a top candidate is found or all b-jets failed. Then we proceed with the next-to-hardest BDRS tagged jet and repeat the procedure until all BDRS jets were tested. The minimal distance ΔR and the energy difference of these top candidates to a true top is shown in the left panel of Fig. 6.5. As in the HEPTop Tagger procedure we consider a tag to be correct if the candidate is within $\Delta R < 0.5$ and $\Delta E < 300\,\text{GeV}$ of a true top quark. In the central panel of this Figure we show the distribution of the BDRS jets that passed this reconstruction in the p_T-η-plane. Again, the low-p_T region is the one with the largest share of false tags. We consequently employ a similar filter as in the HEPTop Tagger filtering and introduce an additional requirement in the top candidate reconstruction: If the transverse momentum of the top candidate is below 300 GeV both of the two BDRS subjets must not be b-tagged. This threshold was found by a rough optimization. In the right panel we plot the distribution of the BDRS tagged jets after this filtering. As can be seen from Table 6.3, the effect of this filtering is not drastic but the mis-tag rage reduces more than the tagging rate.

6.2.1.3. Reconstructing and filtering fully resolved top quarks

An unboosted hadronically decaying top generates three distinct jets which can generally not be captured by the HEPTop or the BDRS Tagger. We try to reconstruct these top quarks by combining a b-tagged jet with two non-b-tagged jets[2]. In order to avoid too

[2]Here and in the following we drop the *anti-k_t* in front of the jets. By a *jet* we mean an *anti-k_t* jet and when we address fat jets we will make it clear.

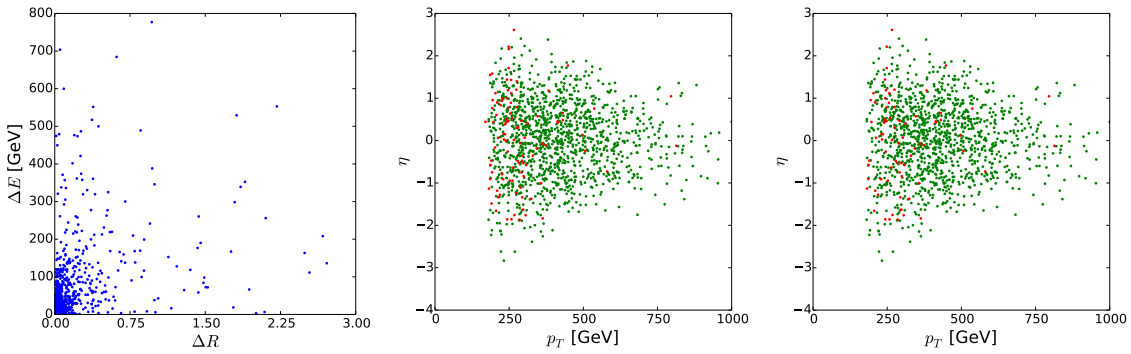

Figure 6.5.: Output of the BDRS Tagger. Left panel: Minimal distance in terms of ΔR between a tagged top candidate and a truth level top. For each such pair the difference in energy is plotted on the y-axis. Central panel: Distribution of the BDRS tagged jets in the p_T-η-plane before additional filtering. Green dots correspond to correctly tagged top candidates, red dots to mis-tagged candidates. Right panel: The same distribution as in the central plane but after filtering.

many background events faking top candidates, we apply this method only to events where the two hardest jets have at least a transverse momentum of 60 and 80 GeV, respectively.

First, we construct all possible combinations of one b-tagged jet and two non-b-tagged jets and sort them by p_T. Then, starting with the most boosted one, we check for each combination if its invariant mass is close to the top mass $\left|m_{\text{jet}_1+\text{jet}_2+b} - m_t\right| < 25\,\text{GeV}$ and if the invariant mass of the two non-b-jet system is close to the W mass $\left|m_{\text{jet}_1+\text{jet}_2} - m_W\right| < 10\,\text{GeV}$. If these two mass criteria are fulfilled and none of the three jets was part of a top candidate before, it is considered as a candidate. The minimal distance and the energy difference of these candidates to a true top quark is shown in the right panel of Fig. 6.6. Many candidates are mis-tags and lie far from any true top quark. Nevertheless, there is still a cluster of correct tags clearly visible in the lower left corner.

The distribution of the candidates in the p_T-m_{bj}-plane is shown in the central plot of the same Figure. m_{bj} is the invariant mass of the system consisting of the b-jet and the hardest of the two non-b-jets and obeys $m_{bj} \lesssim \sqrt{m_t^2 - m_W^2} \approx 150\,\text{GeV}$. To take this property of m_{bj} into account and improve the mis-tag rate, we filter the candidates and reject those with $m_{bj} > 150\,\text{GeV}$. Moreover, we introduce two cuts motivated from this plot: Firstly, a cut on $m_{bj} > 60\,\text{GeV}$ and secondly a cut on a minimal p_T of 30 GeV of the top candidate. Unless the sum of top and neutralino mass is within a few GeV of the stop mass, the top quarks should be at least slightly boosted and pass this cut. Correspondingly this minimal p_T requirement rather rejects the background than the signal. The distribution of the top candidates after filtering with these cuts on m_{bj} and p_T is shown in the right panel of Fig. 6.6.

The mis-tag rate is clearly reduced by these filters while the efficiency changes only mod-

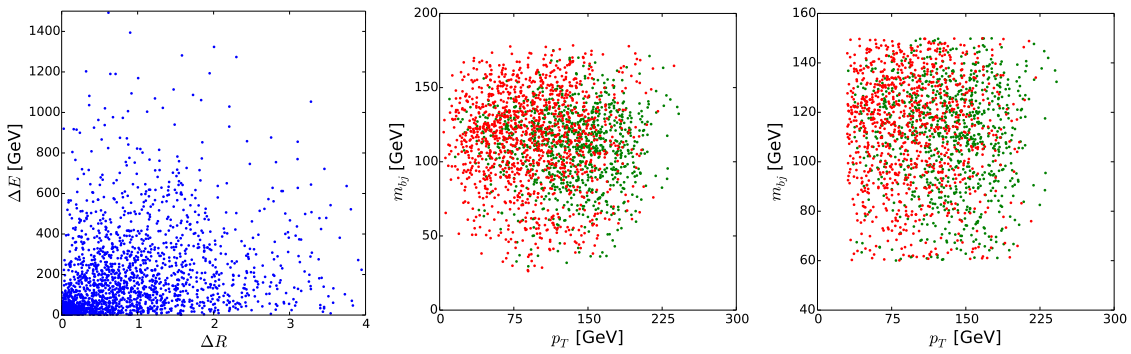

Figure 6.6.: Output of the reconstruction of resolved top quarks. Left panel: Minimal distance in terms of ΔR between a tagged top candidate and a truth level top. For each such pair the difference in energy is plotted on the y-axis. Central panel: Distribution of the top candidates in the p_T-m_{bj}-plane before additional filtering. Green dots correspond to candidates belong to correctly t 2576| 14| 3| 38agged top candidates, red dots to mis-tagged candidates. Right panel: The same distribution as in the central plane but after filtering.

erately. The overall small efficiency shown in Table 6.3 needs to be understood in the appropriate context. In the (900,900) sample, the top quarks are already boosted and therefore hard to find in the resolved method. Moreover, the HEPTop and BDRS Taggers already tagged many top quarks, such that less remain for the resolved reconstruction. When applying these cuts to the (550,550) sample which has less boosted top quarks, we obtain the better values $\epsilon = 5.5\,\%$ and $\mathcal{R}_T = 46.3\,\%$. Both of these numbers are obtained after filtering, which improves the rates also in this unboosted regime.

By comparing the numbers in Table 6.3 we observe that the HEPTop Tagger is by far the most efficient tagger as it correctly finds about 10–20 % of the top quarks in a sample compared to a few % for the other taggers. The fraction of mis-tags in the total number of tags is for both the HEPTop as well as the BDRS Tagger comparable and well below 10% in the medium boosted sample (900,900). Only in the unboosted sample (550,550) the mis-tag rates become bigger. The resolved top tagger provides about 50 % mis-tags which is only reduced slightly after filtering. Yet, in the unboosted sample its efficiency is greater than that of the BDRS Tagger.

In order to take these results into account, we prefer top candidates obtained from the HEPTop or the BDRS Tagger over fully reconstructed top candidates, and more boosted candidates over unboosted ones. This is realized by sorting the HEPTop and BDRS tagged candidates together by their transverse momentum and picking the hardest ones. If more candidates are demanded than provided by the HEPTop or BDRS Tagger, we pick the hardest from the fully reconstructed set. A sketch of this choosing procedure is shown in Fig. 6.7.

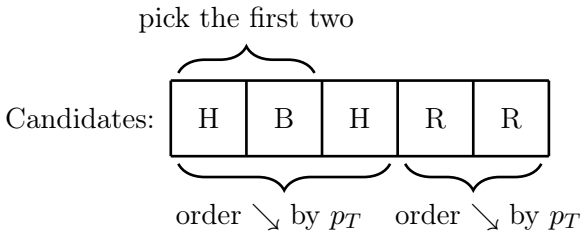

Figure 6.7.: Sorting of the top candidates. H and B stand for a HEPTop and BDRS tagged candidate, respectively. They are sorted together by descending p_T such that the hardest candidate is on the left side. R stands for a resolved candidate. They are ordered by descending p_T as well but not mixed with the former. Only when there are less than two candidates in the first category, the resolved candidates are used.

6.2.2. Analysis cuts

Once the reconstruction of the event and the top candidates is done, we can continue and increase the signal over background ratio S/B by imposing cuts on the events. As our premise is to make a scale invariant analysis, we must avoid to introduce scales through the cuts. We propose the following ones.

1. **Zero leptons:** The leptons or other particles that are emitted by the decaying chargino or second lightest neutralino are too soft to be seen by the detector. Moreover, since we want to reconstruct the hadronic top quarks to employ the jet substructure techniques, no leptons should be present in the signal events. In the Background however, they are produced in the leptonic decays which are necessary to generate missing energy. We therefore demand zero reconstructed electrons or muons. In Fig. 6.8a we see that about 20% of the background events contain at least one reconstructed lepton while this is only the case for about 10% of the signal events, irrespective of the considered parameter point.

2. **Two top candidates:** So far, we focus on the channels where both squarks decay into a top and a corresponding higgsino. Thus we demand at least two top candidates, where more than two are only allowed if the additional ones are candidates from the resolved reconstruction. This takes the large fake rate of the resolved method into account. Only the first two candidates, denoted by c_1 and c_2 in the following, are then considered further. The distribution before this cut is shown in Fig. 6.8b, but it needs to be taken with a grain of salt. The signal considered so far contains also the events where one or both of the stops and sbottoms decay directly into bottom quarks. Clearly, these events hardly pass this cut and lead to the very high rejection. When considering only the events where both squarks decay into top quarks, more than 4%

of the events pass this cut which is compatible with the 20% reconstruction efficiency of the HEPTop Tagger. The only exception to this are the samples with a light stop $m_{\tilde{t}} \approx 550\,\text{GeV}$. Here, the top quarks are too soft to efficiently trigger the taggers and only about 1% of the events passe this cut.

Once we have top candidates from the HEPTop or BDRS tagger, we know that there was at least one fat jet with a minimal transverse momentum of 200 GeV. Together with the missing energy from the escaping neutralino, this is enough to pass the trigger threshold of the experiments. Only if all top candidates originate from the resolved reconstruction, one might fear that the event contains too few hard objects to pass the trigger. We checked explicitly that all of these events pass one of the jet/$\not{E}_T$ trigger thresholds: $p_T > 200\,\text{GeV}$ or four jets all with $p_T > 60\,\text{GeV}$ or one jet with $p_T > 150\,\text{GeV}$ and missing transverse energy $\not{E}_T > 150\,\text{GeV}$ or only $\not{E}_T > 250\,\text{GeV}$ [245]. In addition, we will see later that after the cuts hardly any top candidates from the resolved reconstruction remain. Therefore the trigger thresholds should not pose any problems.

3. **Zero b-jets:** Besides the b-jets that pair up with a fat BDRS jet or two other jets to form a top candidate, no further b-jets are allowed in the event. From Fig. 6.8c we see that this further rejects the background events.

4. **Less than four jets:** In the signal process, additional jets to the top candidates can only arise from initial and final state radiation or from beam remnants. We therefore expect not too many jets and reject events with more than three jets that are not part of a top candidate. The normalized distribution of the number of jets, shown in Fig. 6.8d confirms that this cut prefers the signal.

5. **Zero jets with $p_T > 100\,\text{GeV}$:** This cut is based on the same assumptions as cut #4. Jets from the underlying event must not dominate the event and are thus required have at most $p_T = 100\,\text{GeV}$. The corresponding distribution is plotted in Fig. 6.8e

6. **$m_{bj} < 150\,\text{GeV}$ for both candidates:** As mentioned previously, the invariant mass m_{bj} of the b-jet combined with the hardest non-b-jet of a top decay is always smaller than about 150 GeV from kinematical considerations. Events with top candidates that have a larger m_{bj} are therefore probably based on fake top quarks which are consequently rejected. This can be seen in Fig. 6.8f.

7. **$\Delta\phi(\vec{p}_{Tc_1} + \vec{p}_{Tc_2}, \vec{\not{E}}_T) > 0.9\pi$:** Since we cannot determine the two neutralino momenta individually, it is impossible to reconstruct the momenta of the initial squarks. Yet, we can make use of the total event shape. In the signal, the transverse missing

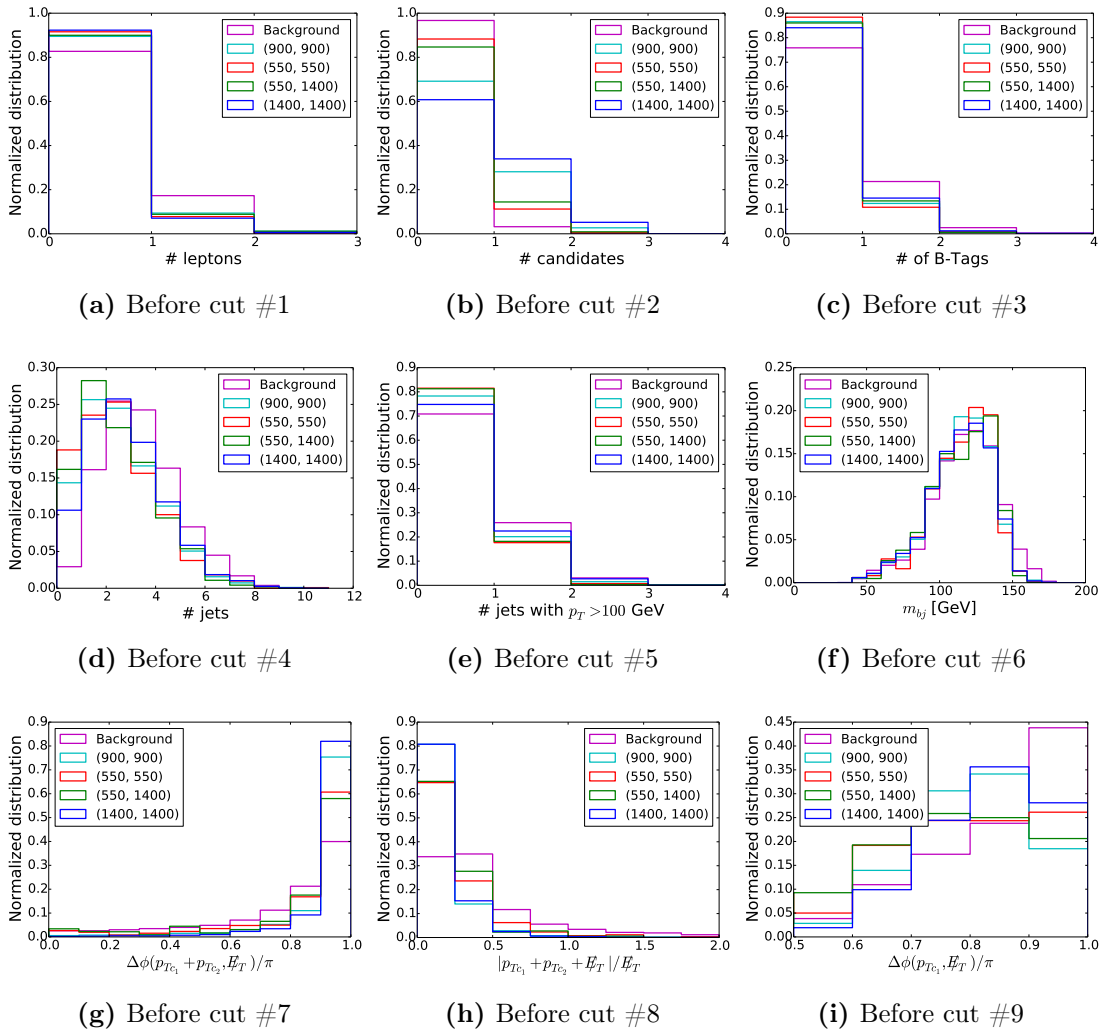

(a) Before cut #1 **(b)** Before cut #2 **(c)** Before cut #3

(d) Before cut #4 **(e)** Before cut #5 **(f)** Before cut #6

(g) Before cut #7 **(h)** Before cut #8 **(i)** Before cut #9

Figure 6.8.: Normalized distributions of the background and signal processes before the cut on the respective observable. The sums in Subfigs. (g) and (h) are understood to be vectorial.

energy is the combination of the two neutralino momenta and therefore balances the transverse momenta of the two top quarks. Consequently the vectorial sum of the candidate's momenta has to point in the opposite direction of the missing energy. Although we already constrained the additional components of the event by the previous cuts, this is not necessarily taking place in the background events, as can be seen in Fig. 6.8g.

8. $\left|\vec{p}_{Tc_1}+\vec{p}_{Tc_2}+\vec{\not{E}}_T\right|/\not{E}_T < 0.25$**:** This cut is based on the same reasoning as the previous one. The absolute value of the summed candidate's transverse momenta and the missing transverse energy needs to be small. In order to maintain scale invariance

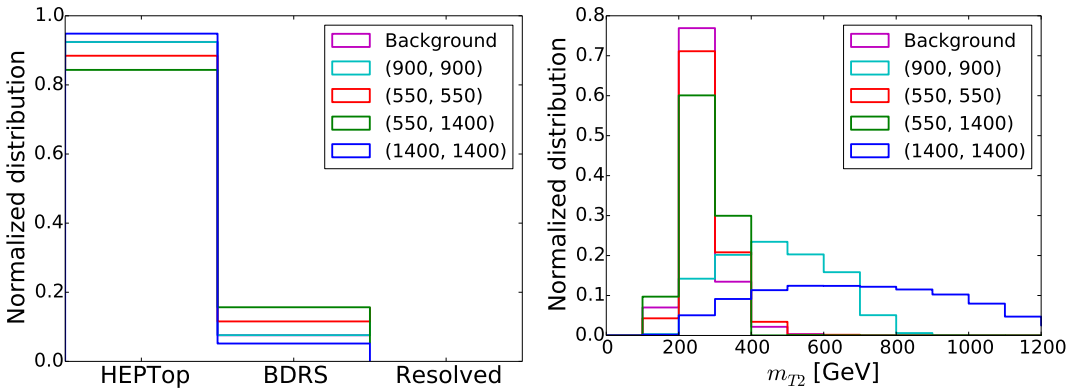

(a) Type of top tags after cut #9 **(b)** After cut #9

Figure 6.9.: Normalized distribution of the type of top tags of the candidates and of m_{T2} after the last cut.

and take into account that a hard jet might loose more energy by final state radiation than a soft jet, we normalize the result by $\not{E}_T$. Despite the fact that we used a very similar idea in cut #7, we can further reject background events as can be seen in Fig. 6.8h.

9. $\boldsymbol{\Delta\phi(\vec{p}_{Tc_1}, \vec{\not{E}}_T) < 0.9\pi}$**:** By this last cut we demand that the missing transverse energy and the transverse momentum of the hardest of the two candidates are not back-to-back. Since the two produced squarks are of the same type and the higgsinos are mass degenerate, the recoil of the top quarks against the respective higgsino will be the same in the squark rest-frame. Therefore, the two neutralinos should contribute about equally to the missing energy and spoil the back-to-back orientation that is present for each top neutralino pair individually. We therefore reject events where one top candidate recoils against an invisible particle and the second candidate does not. Moreover we can thus reject events where the missing energy comes from a mismeasurement of the jet momentum. From Fig. 6.8i it is clear that this further reduces the background.

The cutflows for background, signal, and the signal over background ratios S/B are given in Tables 6.4 and 6.5, respectively. After all cuts, the dominant background is $t\bar{t}$+jets, which is approximately one order of magnitude greater than the other background processes. The values for S/B range from about 0.3 in the samples where the stops have a mass around 550 GeV to $4 \cdot 10^{-3}$ in the (1 400,1 400) sample. In Fig. 6.9a we show the relative contribution of the types of the two top candidates after all cuts. The candidates from the HEPTop Tagger contribute most, which is not surprising considering the reconstruction efficiencies

cut	$Zt\bar{t}$	Zj	Wj	$t\bar{t}$
0. no cut	$1.13 \cdot 10^{-2}$	$2.98 \cdot 10^{1}$	$1.07 \cdot 10^{2}$	$1.94 \cdot 10^{1}$
1. 0 leptons	$1.13 \cdot 10^{-2}$	$2.98 \cdot 10^{1}$	$8.14 \cdot 10^{1}$	$1.57 \cdot 10^{1}$
2. 2 candidates	$4.23 \cdot 10^{-4}$	$2.94 \cdot 10^{-3}$	$5.10 \cdot 10^{-3}$	$7.29 \cdot 10^{-2}$
3. 0 b-jets	$3.90 \cdot 10^{-4}$	$2.59 \cdot 10^{-3}$	$4.57 \cdot 10^{-3}$	$5.26 \cdot 10^{-2}$
4. ≤ 3 jets	$3.65 \cdot 10^{-4}$	$1.86 \cdot 10^{-3}$	$3.44 \cdot 10^{-3}$	$3.54 \cdot 10^{-2}$
5. 0 jets with $p_T > 100\,\mathrm{GeV}$	$3.17 \cdot 10^{-4}$	$1.27 \cdot 10^{-3}$	$2.49 \cdot 10^{-3}$	$2.52 \cdot 10^{-2}$
6. $m_{bj} < 150\,\mathrm{GeV}$	$3.11 \cdot 10^{-4}$	$1.07 \cdot 10^{-3}$	$2.08 \cdot 10^{-3}$	$2.28 \cdot 10^{-2}$
7. $\Delta\phi(\boldsymbol{p_{Tc1}} + \boldsymbol{p_{Tc2}}, \not{\boldsymbol{E}}_{\boldsymbol{T}}) > 0.9\pi$	$2.40 \cdot 10^{-4}$	$4.48 \cdot 10^{-4}$	$8.11 \cdot 10^{-4}$	$8.98 \cdot 10^{-3}$
8. $\left\lvert \boldsymbol{p_{Tc1}} + \boldsymbol{p_{Tc2}} + \not{\boldsymbol{E}}_{\boldsymbol{T}} \right\rvert / \not{E}_T < 0.25$	$1.76 \cdot 10^{-4}$	$1.88 \cdot 10^{-4}$	$3.04 \cdot 10^{-4}$	$2.87 \cdot 10^{-3}$
9. $\Delta\phi(\boldsymbol{p_{Tc_1}}, \not{\boldsymbol{E}}_{\boldsymbol{T}}) < 0.9\pi$	$1.39 \cdot 10^{-4}$	$1.42 \cdot 10^{-4}$	$2.20 \cdot 10^{-4}$	$1.49 \cdot 10^{-3}$

Table 6.4.: Cutflow for the background processes. The numbers give the cross section in pb after the respective cut.

	(550,550)		(900,900)		(1 400,1 400)		(550,1 400)	
cut No.	σ	S/B	σ	S/B	σ	S/B	σ	S/B
0	$6.57 \cdot 10^{-1}$	$4.20 \cdot 10^{-3}$	$2.69 \cdot 10^{-2}$	$1.72 \cdot 10^{-4}$	$8.43 \cdot 10^{-4}$	$5.39 \cdot 10^{-6}$	$4.45 \cdot 10^{-1}$	$2.85 \cdot 10^{-3}$
1	$6.01 \cdot 10^{-1}$	$4.74 \cdot 10^{-3}$	$2.42 \cdot 10^{-2}$	$1.91 \cdot 10^{-4}$	$7.71 \cdot 10^{-4}$	$6.07 \cdot 10^{-6}$	$4.02 \cdot 10^{-1}$	$3.17 \cdot 10^{-3}$
2	$3.16 \cdot 10^{-3}$	$3.88 \cdot 10^{-2}$	$7.21 \cdot 10^{-4}$	$8.87 \cdot 10^{-3}$	$3.91 \cdot 10^{-5}$	$4.81 \cdot 10^{-4}$	$3.58 \cdot 10^{-3}$	$4.40 \cdot 10^{-2}$
3	$2.79 \cdot 10^{-3}$	$4.65 \cdot 10^{-2}$	$6.14 \cdot 10^{-4}$	$1.02 \cdot 10^{-2}$	$3.29 \cdot 10^{-5}$	$5.48 \cdot 10^{-4}$	$3.08 \cdot 10^{-3}$	$5.12 \cdot 10^{-2}$
4	$2.33 \cdot 10^{-3}$	$5.66 \cdot 10^{-2}$	$5.00 \cdot 10^{-4}$	$1.22 \cdot 10^{-2}$	$2.61 \cdot 10^{-5}$	$6.34 \cdot 10^{-4}$	$2.56 \cdot 10^{-3}$	$6.24 \cdot 10^{-2}$
5	$1.90 \cdot 10^{-3}$	$6.49 \cdot 10^{-2}$	$3.92 \cdot 10^{-4}$	$1.34 \cdot 10^{-2}$	$1.95 \cdot 10^{-5}$	$6.67 \cdot 10^{-4}$	$2.08 \cdot 10^{-3}$	$7.12 \cdot 10^{-2}$
6	$1.84 \cdot 10^{-3}$	$7.03 \cdot 10^{-2}$	$3.79 \cdot 10^{-4}$	$1.45 \cdot 10^{-2}$	$1.89 \cdot 10^{-5}$	$7.20 \cdot 10^{-4}$	$2.05 \cdot 10^{-3}$	$7.81 \cdot 10^{-2}$
7	$1.12 \cdot 10^{-3}$	$1.07 \cdot 10^{-1}$	$2.86 \cdot 10^{-4}$	$2.73 \cdot 10^{-2}$	$1.55 \cdot 10^{-5}$	$1.48 \cdot 10^{-3}$	$1.19 \cdot 10^{-3}$	$1.13 \cdot 10^{-1}$
8	$7.23 \cdot 10^{-4}$	$2.05 \cdot 10^{-1}$	$2.31 \cdot 10^{-4}$	$6.52 \cdot 10^{-2}$	$1.25 \cdot 10^{-5}$	$3.53 \cdot 10^{-3}$	$7.75 \cdot 10^{-4}$	$2.19 \cdot 10^{-1}$
9	$5.34 \cdot 10^{-4}$	$2.69 \cdot 10^{-1}$	$1.88 \cdot 10^{-4}$	$9.46 \cdot 10^{-2}$	$8.98 \cdot 10^{-6}$	$4.52 \cdot 10^{-3}$	$6.15 \cdot 10^{-4}$	$3.10 \cdot 10^{-1}$

Table 6.5.: Cutflow for the signal processes. The cross section is given in pb after each cut.

from Table 6.3 and the preference of the HEPTop and BDRS candidates over the resolved candidates. However, in the samples with light stops the BDRS Tagger provides between 10 and 15% of the candidates. It thus increases the amount of reconstructed signal events and hence improves the power of the analysis. The background has almost the same split as the $(900, 900)$ sample and is therefore hardly visible under the turquoise line.

6.3. Discussion

To continue further, we consider the m_{T2} [246, 247] distribution that is shown in Fig. 6.9b (normalized) and Fig. 6.10 (stacked). m_{T2} is designed to give a lower bound on the squark mass. This is reflected in the plotted distribution, where the upper edge of the signal distribution is just at the actual squark mass. It is defined as

$$m_{T2}^2(m_{\tilde{\chi}_1^0}) \equiv \min_{\boldsymbol{p}_T^1 + \boldsymbol{p}_T^2 = \not{\boldsymbol{E}}_{\boldsymbol{T}}} \left[\max \left\{ m_T^2 \left(\boldsymbol{p}_T^1, \boldsymbol{p}_{Tc_1}, m_{\tilde{\chi}_1^0} \right), m_T^2 \left(\boldsymbol{p}_T^2, \boldsymbol{p}_{Tc_2}, m_{\tilde{\chi}_1^0} \right) \right\} \right] , \tag{6.3.1}$$

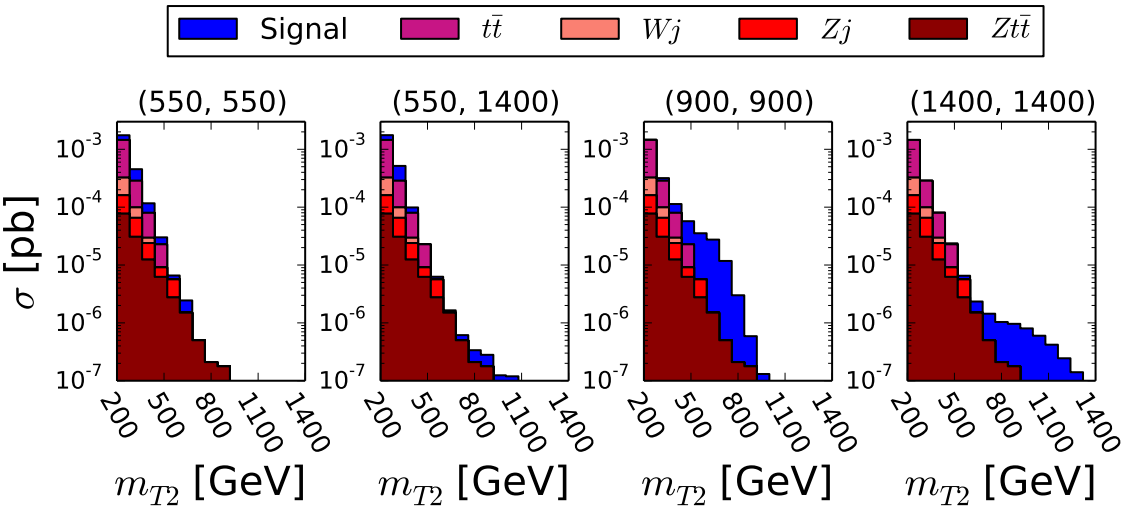

Figure 6.10.: Stacked distribution of m_{T2} after cut #9.

where $\boldsymbol{p}_{Tc_{1,2}}$ are the transverse momenta of the candidates, $\boldsymbol{p}_T^{1,2}$ are trial momenta for the two escaping invisible particles and need to sum up to the missing transverse energy, $m_{\tilde{\chi}_1^0}$ is the mass of the invisible particle, which we set to zero since we do not know it a priori, and finally,

$$m_T^2(\boldsymbol{p}_T^a, \boldsymbol{p}_{Tc_i}, m_{\tilde{\chi}_1^0}) = m_{c_i}^2 + m_{\tilde{\chi}_1^0}^2 + 2\left(E_T^{c_i} E_T^a - \boldsymbol{p}_T^{c_i} \cdot \boldsymbol{p}_T^a\right) \tag{6.3.2}$$

is the transverse mass with $E_T^{c_i} = \sqrt{m_{c_i}^2 + \left|\boldsymbol{p}_T^{c_i}\right|^2}$. For the calculation of m_{T2} we use a code described in Ref. [248] and provided by the authors of this reference.

The S/B value of the heavy samples could be improved substantially by making a hard cut on m_{T2}. But then we would lose scale invariance and reject the events from the light samples. We rather use a different approach and make a binned likelihood analysis using the CL_s technique described in Ref. [11] and briefly summarized in Appendix B. For the calculation we employ the code `MCLimit` [249]. The CL_s method has the advantage that it does not need an overall large S/B but it automatically gains sensitivity from the region where the signal contributes to the event rate. This way the analysis becomes sensitive over a large squark mass range. For light squark masses, the total S/B value is large enough to find the signal despite the large background and for heavy squark masses, the signal lies in the large m_{T2} region where the background contribution is low. In Fig. 6.11 we show the p-values for some of the parameter points against the integrated luminosity assuming different Gaussian errors on the background cross section. Moreover, in the calculation with a non-vanishing Gaussian error we always include a Monte Carlo error of 10^{-3} fb on each bin, corresponding to the largest weight of the background events. Without mentioning

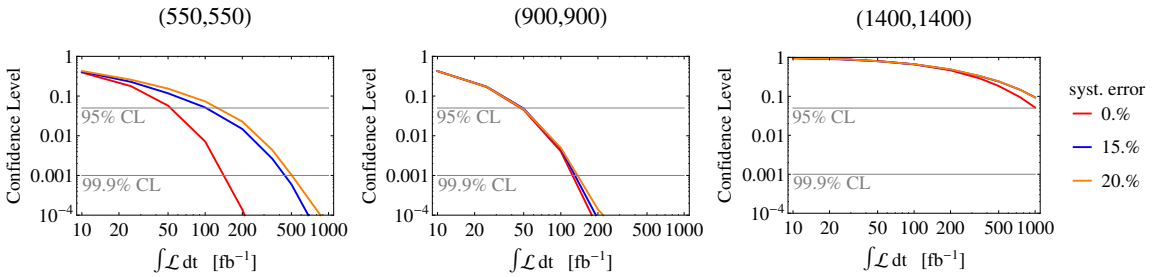

Figure 6.11.: p-values for the parameter points (550, 550), (900, 900), and (1 400, 1 400) against integrated Luminosity assuming different systematic errors.

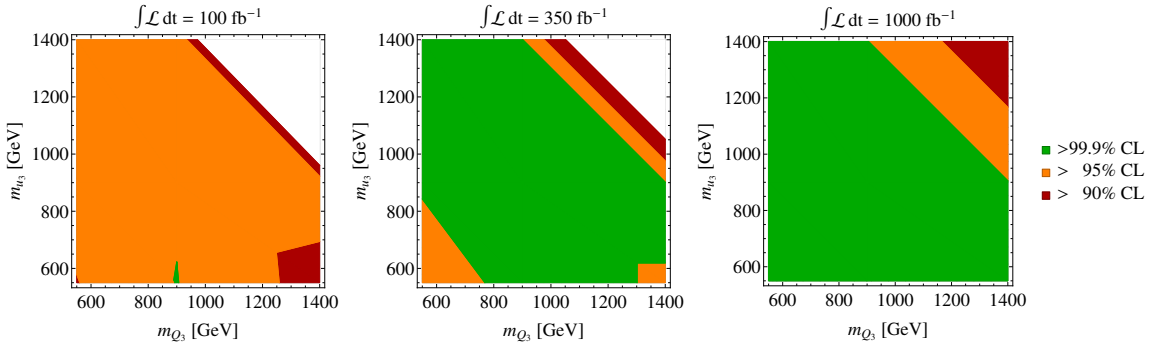

Figure 6.12.: Exclusion limits in the m_{Q_3}-m_{u_3}-plane. A Monte Carlo error and a systematic error of 15% on the background normalization is assumed. The higgsinos have a mass of about 300 GeV.

it further, this MC error is still considered in the results below. The light stops, benefit from the greater production cross section and can be excluded at 95% CL with less than 130 fb^{-1}, even when a systematic error of 20% is assumed. For the intermediate and heavy stop samples the signal lies in the regions with hardly any background event and therefore the error on the background normalization has almost no effect. The (900, 900) sample happens to be in the region where the production cross section is still relatively large but the background contribution is low. Stops around this parameter point can already be excluded with about 50 fb^{-1} at 95% CL. In the last sample, (1 400, 1 400), the error on the normalization has no effect as the signal region contains no background events. Generating more background events could ameliorate the situation but is computationally intensive. Alternatively a cut at the generator level could be introduced to populate the large m_{T2} region, however this introduces new systematic errors. We therefore rather rely on the included Monte Carlo error that pushes the exclusion limit for 1 000 fb^{-1} above the 95% CL line.

In Fig. 6.12 we show the exclusion limits in the m_{Q_3}-m_{u_3}-plane for an integrated luminosity of 100 fb^{-1}, 350 fb^{-1} and 1 000 fb^{-1}, respectively. For all plots we assume a systematic

uncertainty of 15%. The m_{T2} distributions for the CL_s computation of the points in the lower half of this plot are obtained from those of the upper half by reweighting with the appropriate branching ratios. As we saw earlier, the light stops in this lower half decay dominantly into a bottom quark and a chargino, a final state we are not sensitive to. Then the sensitivity of the analysis can be driven by both the heavy and the light stops. If the mass difference between the two is large, the much bigger production cross section for the light stop compensates the low branching ratio and gives the important contribution. If the mass difference is small, it is the heavy stop that yields more events in the final state due to the bigger branching ratio into top quarks. We see that already with the luminosity that is expected to be collected during the current run, stops with masses up to 1.1 TeV can be excluded at 95% CL along the diagonal, and more in the areas with a large hierarchy (left plot). After the third run (central plot), the exclusion is even at 99.9% CL for large parts of the parameter space and the high luminosity phase will further ameliorate the situation.

6.4. Final remarks

So far we computed CL_s for the points given in Table 6.1. For them we showed that it is in deed possible to design an analysis that is sensitive to supersymmetric signals over a large range of possible squark masses. In order to draw finer exclusion lines in the m_{Q_3}-m_{u_3}-plane and also taking different higgsino masses into account, events need to be generated for more of the grid points. Another improvement of the analysis will come from taking also the mixed decay—one top and one bottom quark—into account. This allows us to recover a larger part of the available signal cross section, in particular in the region where $m_{Q_3} > m_{u_3}$.

The generalization of the applied cuts to this scenario is straightforward: Instead of two candidates and no b-jet we demand one candidate and one b-jet. Also the other proposed cuts could be generalized as the basic picture does not change. Only the specific value for the kinematic cuts could change. Results for the same stop masses but with different higgsino masses can be obtained by identifying the point in the above considered parameter space that has the same mass difference between the squarks and the higgsinos, i.e. the same event shape, and rescale the weight of the events to account for the different production cross section.

The main idea behind this analysis was to obtain a scale invariant setup. In the first step we achieved this by employing the HEPTop and BDRS Taggers together with varying radii. Thereby we managed to pick the minimal content of a hadronically decaying top quark for a large range of top momenta. In the second step we avoided introducing scales in the cuts and only exploited the event properties that are independent of the mass spectrum. After this proof of concept it will now be interesting to apply this principle to other searches where

top quarks with various boosts appear in the final state as for example in little Higgs models with T-parity [250–252].

7. Conclusion

In this thesis we presented two strategies for searches for new physics at the LHC. As benchmark models and motivation for the strategies we took the minimal composite Higgs model and the minimal supersymmetric extension of the SM. These models are the two most discussed theories to solve the hierarchy problem, which is one of the best theoretical arguments for TeV-scale physics. A brief review of their basic ideas and electroweak symmetry breaking sector was given in the first part of this document.

The first strategy focuses on the Higgs couplings that enter in the gluon fusion cross section, namely its coupling to the top quark and to gluons, the latter being generated by new particles charged under color. This project is particularly motivated in the composite Higgs setup, where modifications of these couplings cancel in a broad class of models and lead to a SM-like inclusive cross section that provides no information on the top partner masses. We showed that this degeneracy can be broken by measuring the cross section of very boosted Higgs + jet production, i.e. the production of a Higgs with a large transverse momentum of at least 650 GeV recoiling against a hard jet. We provided a semi-numerical formula for the boosted cross section in the presence of modified couplings and analytic expressions for the matrix elements for the Higgs + jet production in the presence of CP-violating couplings. The results were used to estimate the possible determination of the two couplings in the high luminosity phase of the LHC in the $h \to \tau\tau$ channel. We found that even in the worst case scenario where the inclusive cross section is in agreement with the SM, the top Yukawa coupling modifier κ_t can be constrained at 95% CL to lie within about 0.8–1.3. Due to the small cross section of the boosted Higgs process, an integrated luminosity of $3\,000\,\text{fb}^{-1}$ is needed for this constraint. Finally, we presented the results of a study at reconstruction-level where we find similar results. The boosted Higgs channel therefore is a worthwhile albeit challenging alternative to the likewise difficult $t\bar{t}h$ channel.

The second strategy is devoted to the search for third generation squarks that are predicted by the MSSM. As our setup we chose a natural SUSY model where all SUSY particles but the stops, the light sbottom and the higgsinos are heavy. The event shape of the squark pair production can range from unboosted to very boosted top quarks and depends crucially on the mass spectrum of the light particles that is a priori not known. To circumvent this restriction in the analysis design, we combined several reconstruction methods for hadron-

ically decaying top quarks that work efficiently at different top transverse momenta. We then used this input for an analysis that is scale invariant and based on the two top quarks plus missing energy final state. We found that this analysis can exclude light stops and sbottoms up to masses of more than 1 100 GeV at 95% CL for an integrated luminosity of $100\,\mathrm{fb}^{-1}$. This analysis could therefore be used to put stringent bounds on the masses of the third generation squarks already within the next years. Moreover, the idea of combining several top taggers for a boost independent reconstruction could be used in other scenarios where top quarks with very different boosts are expected.

8. Acknowledgments

First of all I would like to thank Andreas Weiler for his supervision. Thanks to him, I could work on very distinct and interesting projects that not only deepened my understanding of particle physics but also extended my set of methods to tackle future problems. In addition, I thus had the chance to collaborate with several other physicists and could get to know their way of thinking and working. Moreover, Andreas always supported me beyond the pure physics in many different ways during the past three years. From enabling me to spend a long period of my PhD at CERN to supporting me in fellowship, conference, summer school and postdoc applications. Finally, I thank him for encouraging me to write the postdoc applications which led to very interesting and exciting perspectives for the next years.

Next I would like to thank Christian Sander for being the second referee of this thesis, Jan Louis for being the head of the thesis committee and Caren Hagner and Jürgen Reuter for agreeing on being my referees for the defense.

From Christophe Grojean I received support in various ways. Not only was it very great to work with him, but he also enabled me to participate in the Cargese Summer School, brought me forward by inviting me to give talks at interesting conferences, and supported me during my postdoc applications.

I am grateful to Michael Spannowsky for the fruitful collaboration in two very interesting projects, for inviting me to a visit at the IPPP in Durham and for his support in the application phase.

In addition, I thank Gerhard Buchalla for his support during both my master studies in Munich and the postdoc applications.

During the past three years I could work with many people and thank all of them for the great collaborations. In particular I would like to emphasize the helpful discussions with Ennio Salvioni and Rakhi Mahbubani during which I learned and understood a lot.

Two people contributed to and influenced my career in a relatively early stage. First, my secondary school physics teacher Mr. Allgeier who prepared me in the best possible way for my studies and second Georg Weiglein who suggested me to come to DESY for my PhD. I thank both of them.

I had the chance to participate in two summer schools during my PhD, in TASI 2013 and the Cargese Summer School in 2014. They gave me an unique opportunity to get to know

areas of physics beyond my specialization and meet other PhD students of my field. I thank the participants for the great time, the speakers for the excellent lectures and interesting discussions but especially the organizers for their effort.

I am grateful for the generous funding of the Joachim Herz Stiftung that allowed me to focus on my PhD and to make the experience of organizing a workshop. Besides Mrs. Herz, I would like to thank in particular Eva Ackermann and Mr. Maxton-Küchenmeister for setting up interesting and helpful meetings and their support that went far beyond mere financial aspects.

I also would like to thank the members of the theory groups at DESY and at CERN for their hospitality and the inspiring atmosphere I could experience in both places. Moreover I thank Maren Arnold-Vargen, Mirko Siemssen and Stefanie Tepass of the PIER Helmholtz Graduate School for their support and the organization of interesting workshops.

For their support during the writing phase, valuable comments to the draft, finding plenty of the missing commas, and pointing out questionable grammatical constructions, I am deeply grateful to Sarah Andreas, Mikael Chala, Bijan Chokoufe, Elina Fuchs, and Özgür Sahin who in addition patiently answered my questions about statistics.

Besides professional contacts I met many more people in the past years who contributed to a pleasant atmosphere in the institute but also beyond. Among all these people I would like to thank in particular Sarah Andreas and Valerie Domcke for the warm welcome in the office when I first arrived in Hamburg and for the many activities outside of the office, Bijan Chokoufe and Joules Schweizer for the computer questions I could ask and the great atmosphere in the office, Karen De Causmaecker, Frédéric Dreyer and Ben Page for the many lunches, coffee brakes and interesting (physics) discussions that made my time at CERN so much more valuable, and finally Nele Müller, Özgür Sahin and Clemens Wieck for the experience of organizing a workshop together, the dinners and for being more than just the other JHS fellows.

I would also like to emphasize my thank to my family, foremost my parents, for their support, the great and many things they enabled me to experience and for the supportive letters and parcels that reached me wherever I was living.

Last but most of all I am deeply grateful to Elina for all the support and for encouraging me when my results seemed to fall apart.

A. Amplitudes for $pp \to h + jet$ with CP-violating couplings

In this appendix we collect the analytical expressions of the amplitudes contributing to $pp \to h + \text{jet}$ for CP-violating Higgs couplings. We consider first the one-loop amplitudes mediated by the coupling $\tilde{\kappa}_t$ in Eq. (5.0.7).

The $gg \to hg$ amplitude can be expressed in terms of helicity amplitudes $\mathcal{M}_{\lambda_1\,\lambda_2\,\lambda_3}$, where the λ_i denote the helicities of the incoming ($i = 1, 2$) and outgoing ($i = 3$) gluons. Out of the eight possible helicity combinations only four are independent and related to the remaining four amplitudes through $\mathcal{M}_{\lambda_1\,\lambda_2\,\lambda_3} = \mathcal{M}_{-\lambda_1\,-\lambda_2\,-\lambda_3}$. The amplitudes are given by[1]

$$\mathcal{M}_{+++}(s,t,u) = \mathcal{N}\, F_1(s,t,u)\,, \tag{A.0.1}$$

$$\mathcal{M}_{++-}(s,t,u) = \mathcal{N}\, F_1(s,u,t)\,, \tag{A.0.2}$$

$$\mathcal{M}_{-+-}(s,t,u) = \mathcal{N}\, F_2(s,t,u)\,, \tag{A.0.3}$$

$$\mathcal{M}_{-++}(s,t,u) = \mathcal{N}\, F_3(s,t,u)\,, \tag{A.0.4}$$

where the form factors F_i are defined as

$$F_1(s,t,u) = \sqrt{\frac{t}{s\,u}}\;\left[G(s,t) - G(s,u) + G(t,u)\right]\,, \tag{A.0.5}$$

$$F_2(s,t,u) = -\frac{m_h^2}{\sqrt{s\,t\,u}}\left[G(s,t) + G(s,u) + G(t,u)\right]\,, \tag{A.0.6}$$

$$F_3(s,t,u) = \sqrt{\frac{s}{t\,u}}\;\left[G(s,t) + G(s,u) - G(t,u)\right]\,, \tag{A.0.7}$$

$$G(x,y) = x\,y\,D_0(x,y) + 2x\,C_0(y) + 2y\,C_0(x)\,, \tag{A.0.8}$$

with $C_0(x) \equiv C_0(0, x, m_h^2, m_t^2, m_t^2, m_t^2)$ and $D_0(x,y) \equiv D_0(0,0,0,m_h^2,x,y,m_t^2,m_t^2,m_t^2,m_t^2)$, where the scalar integrals are given in the conventions of Ref. [169]. The common factor $\mathcal{N}$ reads

$$\mathcal{N} = \frac{\sqrt{3}\,\alpha_s^{3/2} m_t^2 \tilde{\kappa}_t}{\sqrt{\pi}\,v}\,. \tag{A.0.9}$$

[1] We define $s = (p_1 + p_2)^2$, $t = (p_1 - p_3)^2$ and $u = (p_1 - p_4)^2$, where $p_{1,2}$ are the momenta of the ingoing gluons, p_3 is the momentum of the outgoing gluon and p_4 the momentum of the Higgs. Conservation of momentum is expressed as $p_1 + p_2 = p_3 + p_4$.

The unaveraged cross section is then given by

$$\sum_{\text{pol.}} |\mathcal{M}(gg \to hg)|^2 = \sum_{\lambda_1\,\lambda_2\,\lambda_3} |\mathcal{M}_{\lambda_1\,\lambda_2\,\lambda_3}|^2 \,. \tag{A.0.10}$$

Similarly, the squared matrix element for $q\bar{q} \to hg$ can be expressed in helicity amplitudes $\mathcal{M}^{q\bar{q}}_{\lambda_1\,\lambda_2\,\lambda_3}$ where $\lambda_{1,2}$ now denote the polarization of the incoming quark and anti-quark, respectively, and λ_3 the helicity of the outgoing gluon. The four non-zero combinations are related via

$$\mathcal{M}^{q\bar{q}}_{R\,L\,+}(s,t,u) = -\mathcal{M}^{q\bar{q}}_{L\,R\,-}(s,t,u) = -M^{q\bar{q}}_{R\,L\,-}(s,u,t) = \mathcal{M}^{q\bar{q}}_{L\,R\,+}(s,u,t) \tag{A.0.11}$$

and given by

$$\mathcal{M}^{q\bar{q}}_{R\,L\,+}(s,t,u) = -\frac{2\sqrt{2}}{\sqrt{3}\,s}\mathcal{N}\,t\,C_0(s)\,. \tag{A.0.12}$$

The unaveraged squared matrix element for the unpolarized cross section is then given by

$$\sum_{\text{pol.}} |\mathcal{M}_{q\bar{q}}(s,t,u)|^2 = \sum_{\lambda_1\,\lambda_2\,\lambda_3} \left|\mathcal{M}^{q\bar{q}}_{\lambda_1\,\lambda_2\,\lambda_3}(s,t,u)\right|^2 = \frac{16}{3}\mathcal{N}^2\frac{t^2+u^2}{s}\,|C_0(s)|^2\,. \tag{A.0.13}$$

Finally, the squared matrix elements for the processes $qg \to qh$ and $\bar{q}g \to \bar{q}h$ are obtained via the permutations

$$\sum_{\text{pol.}} |\mathcal{M}_{qg}(s,t,u)|^2 = -\sum_{\text{pol.}} |\mathcal{M}_{q\bar{q}}(u,t,s)|^2\,, \qquad \sum_{\text{pol.}} |\mathcal{M}_{\bar{q}g}(s,t,u)|^2 = -\sum_{\text{pol.}} |\mathcal{M}_{q\bar{q}}(t,s,u)|^2\,, \tag{A.0.14}$$

respectively.

For a large mass of the fermion running in the loops, $m_t^2 \gg s, -t, -u, m_h^2$, we can expand the scalar functions $C_0(x)$ and $D_0(x,y)$ in powers of $1/m_t^2$. Keeping only the leading terms we have

$$C_0(x) \to -\frac{1}{2\,m_t^2}\,, \qquad D_0(x,y) \to \frac{1}{6\,m_t^4}\,. \tag{A.0.15}$$

In this limit the amplitudes $\mathcal{M}_{gg,q\bar{q}}$ simplify greatly: they are independent of m_t, and equal to the tree-level amplitudes computed using the effective coupling proportional to $\tilde{\kappa}_g$ in Eq. (5.0.7) (the equality holds for $\tilde{\kappa}_t = \tilde{\kappa}_g$). The amplitudes squared and summed over polarizations take the simple form

$$\sum_{\text{pol.}} |\mathcal{M}_{gg}|^2 \to \frac{3g_s^6\tilde{\kappa}_t^2}{8\pi^4 v^2}\,\frac{s^4+t^4+u^4+m_h^8}{stu}\,, \qquad \sum_{\text{pol.}} |\mathcal{M}_{q\bar{q}}|^2 \to \frac{g_s^6\tilde{\kappa}_t^2}{16\pi^4 v^2}\,\frac{t^2+u^2}{s}\,. \tag{A.0.16}$$

B. The CL_s method

When setting up an analysis, one eventually want to determine which points of the parameter space of a given theory it is expected to exclude with how much luminosity. Or alternatively, given a measurement, one wants to be able to say whether it excludes a given signal hypothesis or not. A commonly used method for this is the CL_s method [11–13], which is a conservative approximation to the actual exclusion limit.

Given a measured distribution of an observable consisting of N independent bins, one obtains the likelihood

$$L(H, \boldsymbol{d}) = \prod_{i=1}^{N} \frac{e^{-h_i} h_i^{d_i}}{d_i!}\,, \tag{B.0.1}$$

where it is assumed that the number of events in each bin is Poisson distributed, H is the hypothesis that one expects to measure h_i events in the i-th bin, d_i is the number of events that are actually measured in this bin, and $\boldsymbol{d} = \{d_1, ..., d_N\}$ is the collection of the d_i. As a test statistic to discriminate the background hypothesis b from the signal + background hypothesis $s + b$ one uses the likelihood ratio

$$Q(\boldsymbol{d}) = \frac{L(s + b, \boldsymbol{d})}{L(b, \boldsymbol{d})}\,, \tag{B.0.2}$$

which is an ideal choice since it minimizes the misclassification probability due to the Neyman-Pearson Lemma [253]. Next, the probability distribution functions (pdf) $f(\boldsymbol{d})$ of $Q(\boldsymbol{d})$ or equivalently of $-2 \ln Q(\boldsymbol{d})$ are needed for the two $\boldsymbol{d}$ that are expected by the background and the signal + background hypothesis, respectively. Whether one chooses $Q(\boldsymbol{d})$ or $-2 \ln Q(\boldsymbol{d})$ does not change the final result, but for conventional and computational reasons mostly the latter is chosen. In principle, the pdf can be calculated explicitly from the likelihoods, however, this can become difficult if too many bins are involved. Therefore they are usually obtained by generating toy models with Monte Carlo methods. Once the pdf are known, one can define

$$CL_b = \int_{-2 \ln Q_{\text{obs}}}^{\infty} f(b)\, \mathrm{d}(-2 \ln Q) \qquad \text{and} \qquad CL_{s+b} = \int_{-2 \ln Q_{\text{obs}}}^{\infty} f(s + b)\, \mathrm{d}(-2 \ln Q)\,, \tag{B.0.3}$$

where Q_{obs} is the observed value for Q, and CL_b and CL_{s+b} are the confidences in the background and signal + background hypothesis, respectively.

When the two pdf for the two hypothesis are very similar, good confidences in both hypotheses are possible. One therefore needs to normalize the value for the signal + background hypothesis to the background-only hypothesis and thus defines

$$CL_s = \frac{CL_{s+b}}{CL_b}\,. \tag{B.0.4}$$

Now, a small value for CL_s means that the outcome of the measurement favors the background-only hypothesis and the signal is said to be excluded at $1 - CL_s$ confidence level.

When estimating the power of an analysis, one obtains toy models of the signal and background hypotheses from Monte Carlo event generators and then calculates CL_s, assuming that no signal is present. The result then shows up to which confidence level a certain signal can be excluded with the analysis in question.

Bibliography

[1] C. Grojean, E. Salvioni, M. Schlaffer, and A. Weiler, "*Very boosted Higgs in gluon fusion*," *JHEP* **1405** (2014) 022, arXiv:1312.3317 [hep-ph].

[2] M. Schlaffer, M. Spannowsky, M. Takeuchi, A. Weiler, and C. Wymant, "*Boosted Higgs Shapes*," *Eur.Phys.J.* **C74** no. 10, (2014) 3120, arXiv:1405.4295 [hep-ph].

[3] R. Mahbubani, M. Schlaffer, M. Spannowsky, and A. Weiler, "*Scale invariant SUSY searches*." In preparation.

[4] M. E. Peskin and D. V. Schroeder, *An Introduction to quantum field theory*. Addison-Wesley, Reading, USA, 1995.

[5] M. Bohm, A. Denner, and H. Joos, *Gauge theories of the strong and electroweak interaction*. Teubner, Stuttgart, Germany, 2001.

[6] S. P. Martin, "*A Supersymmetry primer*," *Adv.Ser.Direct.High Energy Phys.* **21** (2010) 1–153, arXiv:hep-ph/9709356 [hep-ph].

[7] J. Wess and J. Bagger, *Supersymmetry and supergravity*. Univ. Pr., Princeton, USA, 1992.

[8] J. Santiago, "*The Physics of Electroweak Symmetry Breaking*," June, 2009. http://www.ugr.es/~jsantiago/PoEWSBLectures.pdf.

[9] R. Contino, "*The Higgs as a Composite Nambu-Goldstone Boson*," arXiv:1005.4269 [hep-ph].

[10] C. Csaki and P. Tanedo, "*Beyond the Standard Model*,". http://www.physics.uci.edu/~tanedo/files/notes/ESHEP_Csaki.pdf.

[11] T. Junk, "*Confidence level computation for combining searches with small statistics*," *Nucl.Instrum.Meth.* **A434** (1999) 435–443, arXiv:hep-ex/9902006 [hep-ex].

[12] A. L. Read, "*Modified frequentist analysis of search results (the CL_s method)*,". http://cds.cern.ch/record/451614.

[13] A. L. Read, "*Presentation of search results: The CL(s) technique*," *J.Phys.* **G28** (2002) 2693–2704.

[14] **ATLAS** Collaboration, G. Aad *et al.*, "*Observation of a new particle in the search for the Standard Model Higgs boson with the ATLAS detector at the LHC*," *Phys.Lett.* **B716** (2012) 1–29, arXiv:1207.7214 [hep-ex].

[15] **CMS** Collaboration, S. Chatrchyan *et al.*, "*Observation of a new boson at a mass of 125 GeV with the CMS experiment at the LHC*," *Phys.Lett.* **B716** (2012) 30–61, arXiv:1207.7235 [hep-ex].

[16] G. 't Hooft, "*Naturalness, chiral symmetry, and spontaneous chiral symmetry breaking*," *NATO Sci.Ser.B* **59** (1980) 135.

[17] E. Noether, "*Invariant Variation Problems*," *Gott.Nachr.* **1918** (1918) 235–257, arXiv:physics/0503066 [physics].

[18] D. Hanneke, S. Fogwell, and G. Gabrielse, "*New Measurement of the Electron Magnetic Moment and the Fine Structure Constant*," *Phys.Rev.Lett.* **100** (2008) 120801, arXiv:0801.1134 [physics.atom-ph].

[19] D. Hanneke, S. F. Hoogerheide, and G. Gabrielse, "*Cavity Control of a Single-Electron Quantum Cyclotron: Measuring the Electron Magnetic Moment*," arXiv:1009.4831 [physics.atom-ph].

[20] T. Aoyama, M. Hayakawa, T. Kinoshita, and M. Nio, "*Tenth-Order QED Contribution to the Electron g-2 and an Improved Value of the Fine Structure Constant*," *Phys.Rev.Lett.* **109** (2012) 111807, arXiv:1205.5368 [hep-ph].

[21] Y. Nambu, "*Quasiparticles and Gauge Invariance in the Theory of Superconductivity*," *Phys.Rev.* **117** (1960) 648–663.

[22] Y. Nambu and G. Jona-Lasinio, "*Dynamical Model of Elementary Particles Based on an Analogy with Superconductivity. 1.*," *Phys.Rev.* **122** (1961) 345–358.

[23] Y. Nambu and G. Jona-Lasinio, "*DYNAMICAL MODEL OF ELEMENTARY PARTICLES BASED ON AN ANALOGY WITH SUPERCONDUCTIVITY. II*," *Phys.Rev.* **124** (1961) 246–254.

[24] J. Goldstone, "*Field Theories with Superconductor Solutions*," *Nuovo Cim.* **19** (1961) 154–164.

[25] J. Goldstone, A. Salam, and S. Weinberg, "*Broken Symmetries*," *Phys.Rev.* **127** (1962) 965–970.

[26] P. W. Anderson, "*Plasmons, Gauge Invariance, and Mass*," *Phys. Rev.* **130** (Apr, 1963) 439–442.

[27] F. Englert and R. Brout, "*Broken Symmetry and the Mass of Gauge Vector Mesons*," *Phys.Rev.Lett.* **13** (1964) 321–323.

[28] G. Guralnik, C. Hagen, and T. Kibble, "*Global Conservation Laws and Massless Particles*," *Phys.Rev.Lett.* **13** (1964) 585–587.

[29] P. W. Higgs, "*Broken symmetries, massless particles and gauge fields*," *Phys.Lett.* **12** (1964) 132–133.

[30] P. W. Higgs, "*Broken Symmetries and the Masses of Gauge Bosons*," *Phys.Rev.Lett.* **13** (1964) 508–509.

[31] P. W. Higgs, "*Spontaneous Symmetry Breakdown without Massless Bosons*," *Phys.Rev.* **145** (1966) 1156–1163.

[32] G. 't Hooft, "*Renormalizable Lagrangians for Massive Yang-Mills Fields*," *Nucl.Phys.* **B35** (1971) 167–188.

[33] R. Peccei, "*The Strong CP problem and axions*," *Lect.Notes Phys.* **741** (2008) 3–17, arXiv:hep-ph/0607268 [hep-ph].

[34] S. Weinberg, "*Implications of Dynamical Symmetry Breaking*," *Phys.Rev.* **D13** (1976) 974–996.

[35] E. Gildener, "*Gauge Symmetry Hierarchies*," *Phys.Rev.* **D14** (1976) 1667.

[36] L. Susskind, "*Dynamics of Spontaneous Symmetry Breaking in the Weinberg-Salam Theory*," *Phys.Rev.* **D20** (1979) 2619–2625.

[37] G. 't Hooft, C. Itzykson, A. Jaffe, H. Lehmann, P. Mitter, *et al.*, "*Recent Developments in Gauge Theories. Proceedings, Nato Advanced Study Institute, Cargese, France, August 26 - September 8, 1979*," *NATO Sci.Ser.B* **59** (1980) pp.1–438.

[38] P. Fayet, "*Supersymmetry and Weak, Electromagnetic and Strong Interactions*," *Phys.Lett.* **B64** (1976) 159.

[39] P. Fayet, "*Spontaneously Broken Supersymmetric Theories of Weak, Electromagnetic and Strong Interactions*," *Phys.Lett.* **B69** (1977) 489.

[40] P. Fayet, "*Relations Between the Masses of the Superpartners of Leptons and Quarks, the Goldstino Couplings and the Neutral Currents*," *Phys.Lett.* **B84** (1979) 416.

[41] G. R. Farrar and P. Fayet, "*Phenomenology of the Production, Decay, and Detection of New Hadronic States Associated with Supersymmetry*," *Phys.Lett.* **B76** (1978) 575–579.

[42] S. Dimopoulos, S. Raby, and F. Wilczek, "*Supersymmetry and the Scale of Unification*," *Phys.Rev.* **D24** (1981) 1681–1683.

[43] L. E. Ibanez and G. G. Ross, "*Low-Energy Predictions in Supersymmetric Grand Unified Theories*," *Phys.Lett.* **B105** (1981) 439.

[44] W. J. Marciano and G. Senjanovic, "*Predictions of Supersymmetric Grand Unified Theories*," *Phys.Rev.* **D25** (1982) 3092.

[45] S. R. Coleman and J. Mandula, "*All Possible Symmetries of the S Matrix*," *Phys.Rev.* **159** (1967) 1251–1256.

[46] R. Haag, J. T. Łopuszański, and M. Sohnius, "*All Possible Generators of Supersymmetries of the s Matrix*," *Nucl.Phys.* **B88** (1975) 257.

[47] S. Dimopoulos and H. Georgi, "*Softly Broken Supersymmetry and SU(5)*," *Nucl.Phys.* **B193** (1981) 150.

[48] U. Ellwanger, C. Hugonie, and A. M. Teixeira, "*The Next-to-Minimal Supersymmetric Standard Model*," *Phys.Rept.* **496** (2010) 1–77, `arXiv:0910.1785 [hep-ph]`.

[49] F. Gliozzi, J. Scherk, and D. I. Olive, "*Supersymmetry, Supergravity Theories and the Dual Spinor Model*," *Nucl.Phys.* **B122** (1977) 253–290.

[50] O. Aharony, S. S. Gubser, J. M. Maldacena, H. Ooguri, and Y. Oz, "*Large N field theories, string theory and gravity*," *Phys.Rept.* **323** (2000) 183–386, `arXiv:hep-th/9905111 [hep-th]`.

[51] J. Wess and B. Zumino, "*Supergauge Transformations in Four-Dimensions*," *Nucl.Phys.* **B70** (1974) 39–50.

[52] L. Girardello and M. T. Grisaru, "*Soft Breaking of Supersymmetry*," *Nucl.Phys.* **B194** (1982) 65.

[53] S. Dimopoulos and D. W. Sutter, "*The Supersymmetric flavor problem*," *Nucl.Phys.* **B452** (1995) 496–512, arXiv:hep-ph/9504415 [hep-ph].

[54] D. Chung, L. Everett, G. Kane, S. King, J. D. Lykken, *et al.*, "*The Soft supersymmetry breaking Lagrangian: Theory and applications*," *Phys.Rept.* **407** (2005) 1–203, arXiv:hep-ph/0312378 [hep-ph].

[55] **MSSM Working Group**, Djouadi, A. *et al.*, "*The Minimal supersymmetric standard model: Group summary report*," arXiv:hep-ph/9901246 [hep-ph].

[56] S. Heinemeyer, W. Hollik, and G. Weiglein, "*The Masses of the neutral CP - even Higgs bosons in the MSSM: Accurate analysis at the two loop level*," *Eur.Phys.J.* **C9** (1999) 343–366, arXiv:hep-ph/9812472 [hep-ph].

[57] S. Heinemeyer, W. Hollik, and G. Weiglein, "*QCD corrections to the masses of the neutral CP - even Higgs bosons in the MSSM*," *Phys.Rev.* **D58** (1998) 091701, arXiv:hep-ph/9803277 [hep-ph].

[58] S. Heinemeyer, W. Hollik, and G. Weiglein, "*Precise prediction for the mass of the lightest Higgs boson in the MSSM*," *Phys.Lett.* **B440** (1998) 296–304, arXiv:hep-ph/9807423 [hep-ph].

[59] E. Hardy, "*Is Natural SUSY Natural?*," *JHEP* **1310** (2013) 133, arXiv:1306.1534 [hep-ph].

[60] R. Jackiw and K. Johnson, "*Dynamical Model of Spontaneously Broken Gauge Symmetries*," *Phys.Rev.* **D8** (1973) 2386–2398.

[61] J. Cornwall and R. Norton, "*Spontaneous Symmetry Breaking Without Scalar Mesons*," *Phys.Rev.* **D8** (1973) 3338–3346.

[62] M. Weinstein, "*Conserved currents, their commutators and the symmetry structure of renormalizable theories of electromagnetic, weak and strong interactions*," *Phys.Rev.* **D8** (1973) 2511.

[63] S. Weinberg, "*Implications of Dynamical Symmetry Breaking: An Addendum*," *Phys.Rev.* **D19** (1979) 1277–1280.

[64] E. Eichten and K. D. Lane, "*Dynamical Breaking of Weak Interaction Symmetries*," *Phys.Lett.* **B90** (1980) 125–130.

[65] R. F. Dashen, "*Chiral SU(3) x SU(3) as a symmetry of the strong interactions*," *Phys.Rev.* **183** (1969) 1245–1260.

[66] R. F. Dashen, "*Some features of chiral symmetry breaking*," *Phys.Rev.* **D3** (1971) 1879–1889.

[67] M. E. Peskin and T. Takeuchi, "*Estimation of oblique electroweak corrections*," *Phys.Rev.* **D46** (1992) 381–409.

[68] S. Dimopoulos and L. Susskind, "*Mass Without Scalars*," *Nucl.Phys.* **B155** (1979) 237–252.

[69] D. B. Kaplan and H. Georgi, "*SU(2) x U(1) Breaking by Vacuum Misalignment*," *Phys.Lett.* **B136** (1984) 183.

[70] D. B. Kaplan, H. Georgi, and S. Dimopoulos, "*Composite Higgs Scalars*," *Phys.Lett.* **B136** (1984) 187.

[71] M. J. Dugan, H. Georgi, and D. B. Kaplan, "*Anatomy of a Composite Higgs Model*," *Nucl.Phys.* **B254** (1985) 299.

[72] K. Agashe, R. Contino, and A. Pomarol, "*The Minimal composite Higgs model*," *Nucl.Phys.* **B719** (2005) 165–187, arXiv:hep-ph/0412089 [hep-ph].

[73] R. Contino, D. Marzocca, D. Pappadopulo, and R. Rattazzi, "*On the effect of resonances in composite Higgs phenomenology*," *JHEP* **1110** (2011) 081, arXiv:1109.1570 [hep-ph].

[74] B. Bellazzini, C. Csáki, and J. Serra, "*Composite Higgses*," *Eur.Phys.J.* **C74** no. 5, (2014) 2766, arXiv:1401.2457 [hep-ph].

[75] B. Gripaios, A. Pomarol, F. Riva, and J. Serra, "*Beyond the Minimal Composite Higgs Model*," *JHEP* **0904** (2009) 070, arXiv:0902.1483 [hep-ph].

[76] M. Frigerio, A. Pomarol, F. Riva, and A. Urbano, "*Composite Scalar Dark Matter*," *JHEP* **1207** (2012) 015, arXiv:1204.2808 [hep-ph].

[77] M. Chala, "$h \to \gamma\gamma$ *excess and Dark Matter from Composite Higgs Models*," *JHEP* **1301** (2013) 122, arXiv:1210.6208 [hep-ph].

[78] J. Callan, Curtis G., S. R. Coleman, J. Wess, and B. Zumino, "*Structure of phenomenological Lagrangians. 2.*," *Phys.Rev.* **177** (1969) 2247–2250.

[79] S. R. Coleman, J. Wess, and B. Zumino, "*Structure of phenomenological Lagrangians. 1.*," *Phys.Rev.* **177** (1969) 2239–2247.

[80] S. R. Coleman and E. J. Weinberg, "*Radiative Corrections as the Origin of Spontaneous Symmetry Breaking*," *Phys.Rev.* **D7** (1973) 1888–1910.

[81] A. Pomarol and F. Riva, "*The Composite Higgs and Light Resonance Connection*," *JHEP* **1208** (2012) 135, arXiv:1205.6434 [hep-ph].

[82] D. B. Kaplan, "*Flavor at SSC energies: A New mechanism for dynamically generated fermion masses*," *Nucl.Phys.* **B365** (1991) 259–278.

[83] G. Panico and A. Wulzer, "*The Discrete Composite Higgs Model*," *JHEP* **1109** (2011) 135, arXiv:1106.2719 [hep-ph].

[84] O. Matsedonskyi, G. Panico, and A. Wulzer, "*Light Top Partners for a Light Composite Higgs*," *JHEP* **1301** (2013) 164, arXiv:1204.6333 [hep-ph].

[85] R. Contino and A. Pomarol, "*The holographic composite Higgs*," *Comptes Rendus Physique* **8** (2007) 1058–1067.

[86] F. Caracciolo, A. Parolini, and M. Serone, "*UV Completions of Composite Higgs Models with Partial Compositeness*," *JHEP* **1302** (2013) 066, arXiv:1211.7290 [hep-ph].

[87] J. Barnard, T. Gherghetta, and T. S. Ray, "*UV descriptions of composite Higgs models without elementary scalars*," *JHEP* **1402** (2014) 002, arXiv:1311.6562 [hep-ph].

[88] G. Ferretti and D. Karateev, "*Fermionic UV completions of Composite Higgs models*," *JHEP* **1403** (2014) 077, arXiv:1312.5330 [hep-ph].

[89] G. Ferretti, "*UV Completions of Partial Compositeness: The Case for a SU(4) Gauge Group*," *JHEP* **1406** (2014) 142, arXiv:1404.7137 [hep-ph].

[90] L. Reina and S. Dawson, "*Next-to-leading order results for t anti-t h production at the Tevatron*," *Phys.Rev.Lett.* **87** (2001) 201804, arXiv:hep-ph/0107101 [hep-ph].

[91] W. Beenakker, S. Dittmaier, M. Kramer, B. Plumper, M. Spira, *et al.*, "*Higgs radiation off top quarks at the Tevatron and the LHC*," *Phys.Rev.Lett.* **87** (2001) 201805, arXiv:hep-ph/0107081 [hep-ph].

[92] W. Beenakker, S. Dittmaier, M. Kramer, B. Plumper, M. Spira, *et al.*, "*NLO QCD corrections to t anti-t H production in hadron collisions*," *Nucl.Phys.* **B653** (2003) 151–203, arXiv:hep-ph/0211352 [hep-ph].

[93] LHC Higgs Cross Section Working Group, 2014. https://twiki.cern.ch/twiki/bin/view/LHCPhysics/CERNYellowReportPageAt1314TeV.

[94] **ATLAS** Collaboration, "*Search for the Standard Model Higgs boson produced in association with top quarks and decaying to $b\bar{b}$ in pp collisions at $\sqrt{s} = 8$ TeV with the ATLAS detector at the LHC*," Tech. Rep. ATLAS-CONF-2014-011, CERN, Geneva, Mar, 2014.

[95] **CMS** Collaboration, V. Khachatryan *et al.*, "*Precise determination of the mass of the Higgs boson and tests of compatibility of its couplings with the standard model predictions using proton collisions at 7 and 8 TeV*," arXiv:1412.8662 [hep-ex].

[96] **ATLAS** Collaboration, "*Physics at a High-Luminosity LHC with ATLAS*," arXiv:1307.7292 [hep-ex].

[97] **CMS** Collaboration, "*Projected Performance of an Upgraded CMS Detector at the LHC and HL-LHC: Contribution to the Snowmass Process*," arXiv:1307.7135 [hep-ex].

[98] W. Buchmuller and D. Wyler, "*Effective Lagrangian Analysis of New Interactions and Flavor Conservation*," *Nucl.Phys.* **B268** (1986) 621–653.

[99] B. Grzadkowski, M. Iskrzynski, M. Misiak, and J. Rosiek, "*Dimension-Six Terms in the Standard Model Lagrangian*," *JHEP* **1010** (2010) 085, arXiv:1008.4884 [hep-ph].

[100] G. Giudice, C. Grojean, A. Pomarol, and R. Rattazzi, "*The Strongly-Interacting Light Higgs*," *JHEP* **0706** (2007) 045, arXiv:hep-ph/0703164 [hep-ph].

[101] R. Contino, M. Ghezzi, C. Grojean, M. Muhlleitner, and M. Spira, "*Effective Lagrangian for a light Higgs-like scalar*," *JHEP* **1307** (2013) 035, arXiv:1303.3876 [hep-ph].

[102] J. Elias-Miro, J. Espinosa, E. Masso, and A. Pomarol, "*Higgs windows to new physics through d=6 operators: constraints and one-loop anomalous dimensions*," *JHEP* **1311** (2013) 066, arXiv:1308.1879 [hep-ph].

[103] J. R. Ellis, M. K. Gaillard, and D. V. Nanopoulos, "*A Phenomenological Profile of the Higgs Boson*," *Nucl.Phys.* **B106** (1976) 292.

[104] M. A. Shifman, A. Vainshtein, M. Voloshin, and V. I. Zakharov, "*Low-Energy Theorems for Higgs Boson Couplings to Photons*," *Sov.J.Nucl.Phys.* **30** (1979) 711–716.

[105] A. Vainshtein, V. I. Zakharov, and M. A. Shifman, "*Higgs Particles*," *Sov.Phys.Usp.* **23** (1980) 429–449.

[106] J. F. Gunion, H. E. Haber, G. L. Kane, and S. Dawson, "*The Higgs Hunter's Guide*," *Front.Phys.* **80** (2000) 1–448.

[107] F. Wilczek, "*Decays of Heavy Vector Mesons Into Higgs Particles*," *Phys.Rev.Lett.* **39** (1977) 1304.

[108] J. R. Ellis, M. Gaillard, D. V. Nanopoulos, and C. T. Sachrajda, "*Is the Mass of the Higgs Boson About 10-GeV?*," *Phys.Lett.* **B83** (1979) 339.

[109] T. G. Rizzo, "*Gluon Final States in Higgs Boson Decay*," *Phys.Rev.* **D22** (1980) 178.

[110] H. Georgi, S. Glashow, M. Machacek, and D. V. Nanopoulos, "*Higgs Bosons from Two Gluon Annihilation in Proton Proton Collisions*," *Phys.Rev.Lett.* **40** (1978) 692.

[111] M. Gillioz, R. Grober, C. Grojean, M. Muhlleitner, and E. Salvioni, "*Higgs Low-Energy Theorem (and its corrections) in Composite Models*," *JHEP* **1210** (2012) 004, arXiv:1206.7120 [hep-ph].

[112] U. Langenegger, M. Spira, A. Starodumov, and P. Trueb, "*SM and MSSM Higgs Boson Production: Spectra at large transverse Momentum*," *JHEP* **0606** (2006) 035, arXiv:hep-ph/0604156 [hep-ph].

[113] C. Arnesen, I. Z. Rothstein, and J. Zupan, "*Smoking Guns for On-Shell New Physics at the LHC*," *Phys.Rev.Lett.* **103** (2009) 151801, arXiv:0809.1429 [hep-ph].

[114] E. Bagnaschi, G. Degrassi, P. Slavich, and A. Vicini, "*Higgs production via gluon fusion in the POWHEG approach in the SM and in the MSSM*," *JHEP* **1202** (2012) 088, arXiv:1111.2854 [hep-ph].

[115] W. Furry, "*A Symmetry Theorem in the Positron Theory*," *Phys.Rev.* **51** (1937) 125–129.

[116] R. V. Harlander, S. Liebler, and T. Zirke, "*Higgs Strahlung at the Large Hadron Collider in the 2-Higgs-Doublet Model*," *JHEP* **1402** (2014) 023, arXiv:1307.8122 [hep-ph].

[117] C. Englert, M. McCullough, and M. Spannowsky, "*Gluon-initiated associated production boosts Higgs physics*," *Phys.Rev.* **D89** no. 1, (2014) 013013, arXiv:1310.4828 [hep-ph].

[118] A. Falkowski, "*Pseudo-goldstone Higgs production via gluon fusion*," *Phys.Rev.* **D77** (2008) 055018, arXiv:0711.0828 [hep-ph].

[119] I. Low and A. Vichi, "*On the production of a composite Higgs boson*," *Phys.Rev.* **D84** (2011) 045019, arXiv:1010.2753 [hep-ph].

[120] A. Azatov and J. Galloway, "*Light Custodians and Higgs Physics in Composite Models*," *Phys.Rev.* **D85** (2012) 055013, arXiv:1110.5646 [hep-ph].

[121] C. Delaunay, C. Grojean, and G. Perez, "*Modified Higgs Physics from Composite Light Flavors*," *JHEP* **1309** (2013) 090, arXiv:1303.5701 [hep-ph].

[122] M. Montull, F. Riva, E. Salvioni, and R. Torre, "*Higgs Couplings in Composite Models*," *Phys.Rev.* **D88** (2013) 095006, arXiv:1308.0559 [hep-ph].

[123] R. V. Harlander, T. Neumann, K. J. Ozeren, and M. Wiesemann, "*Top-mass effects in differential Higgs production through gluon fusion at order* α_s^4," *JHEP* **1208** (2012) 139, arXiv:1206.0157 [hep-ph].

[124] **CMS** Collaboration, S. Chatrchyan *et al.*, "*Inclusive search for a vector-like T quark with charge* $\frac{2}{3}$ *in pp collisions at* $\sqrt{s} = 8$ *TeV*," *Phys.Lett.* **B729** (2014) 149–171, arXiv:1311.7667 [hep-ex].

[125] **ATLAS** Collaboration, **ATLAS** Collaboration, "*Search for heavy top-like quarks decaying to a Higgs boson and a top quark in the lepton plus jets final state in pp collisions at* $\sqrt{s} = 8$ *TeV with the ATLAS detector*," Tech. Rep. ATLAS-CONF-2013-018, CERN, Geneva, Mar, 2013.

[126] **ATLAS** Collaboration, **ATLAS** Collaboration, "*Search for pair production of new heavy quarks that decay to a* **Z** *boson and a third generation quark in* **pp** *collisions at* $\sqrt{\mathbf{s}} = \mathbf{8}$ *TeV with the ATLAS detector*," Tech. Rep. ATLAS-CONF-2013-056, CERN, Geneva, Jun, 2013.

[127] **ATLAS** Collaboration, **ATLAS** Collaboration, "*Search for anomalous production of events with same-sign dileptons and b jets in 14.3* fb^{-1} *of pp collisions at* $\sqrt{s} = 8$ *TeV with the ATLAS detector*," Tech. Rep. ATLAS-CONF-2013-051, CERN, Geneva, May, 2013. Not published in the proceedings.

[128] **ATLAS** Collaboration, **ATLAS** Collaboration, "*Search for pair production of heavy top-like quarks decaying to a high-*p_{T} *W boson and a b quark in the lepton plus jets final state in pp collisions at* $\sqrt{s} = 8$ *TeV with the ATLAS detector*," Tech. Rep. ATLAS-CONF-2013-060, CERN, Geneva, Jun, 2013.

[129] **ATLAS** Collaboration, **ATLAS** Collaboration, "*Search for production of vector-like quark pairs and of four top quarks in the lepton plus jets final state in pp collisions at* $\sqrt{s} = 8$ *TeV with the ATLAS detector*," Tech. Rep. ATLAS-CONF-2015-012, CERN, Geneva, Mar, 2015.

[130] A. De Simone, O. Matsedonskyi, R. Rattazzi, and A. Wulzer, "*A First Top Partner Hunter's Guide*," *JHEP* **1304** (2013) 004, arXiv:1211.5663 [hep-ph].

[131] J. Aguilar-Saavedra, R. Benbrik, S. Heinemeyer, and M. Pérez-Victoria, "*Handbook of vectorlike quarks: Mixing and single production*," *Phys.Rev.* **D88** no. 9, (2013) 094010, arXiv:1306.0572 [hep-ph].

[132] M. Buchkremer, G. Cacciapaglia, A. Deandrea, and L. Panizzi, "*Model Independent Framework for Searches of Top Partners*," *Nucl.Phys.* **B876** (2013) 376–417, arXiv:1305.4172 [hep-ph].

[133] A. Azatov, M. Salvarezza, M. Son, and M. Spannowsky, "*Boosting Top Partner Searches in Composite Higgs Models*," *Phys.Rev.* **D89** no. 7, (2014) 075001, arXiv:1308.6601 [hep-ph].

[134] J. Kearney, A. Pierce, and J. Thaler, "*Top Partner Probes of Extended Higgs Sectors*," *JHEP* **1308** (2013) 130, arXiv:1304.4233.

[135] C. Delaunay, T. Flacke, J. Gonzalez-Fraile, S. J. Lee, G. Panico, *et al.*, "*Light Non-degenerate Composite Partners at the LHC*," *JHEP* **1402** (2014) 055, arXiv:1311.2072 [hep-ph].

[136] Z. Kunszt and F. Zwirner, "*Testing the Higgs sector of the minimal supersymmetric standard model at large hadron colliders*," *Nucl.Phys.* **B385** (1992) 3–75, arXiv:hep-ph/9203223 [hep-ph].

[137] V. D. Barger, M. Berger, A. Stange, and R. Phillips, "*Supersymmetric Higgs boson hadroproduction and decays including radiative corrections*," *Phys.Rev.* **D45** (1992) 4128–4147.

[138] H. Baer, M. Bisset, C. Kao, and X. Tata, "*Observability of gamma gamma decays of Higgs bosons from supersymmetry at hadron supercolliders*," *Phys.Rev.* **D46** (1992) 1067–1075.

[139] J. F. Gunion and L. H. Orr, "*Detecting the Higgs bosons of the minimal supersymmetric model*," *Phys.Rev.* **D46** (1992) 2052–2067.

[140] J. F. Gunion, H. E. Haber, and C. Kao, "*Searching for the CP odd Higgs boson of the minimal supersymmetric model at hadron supercolliders*," *Phys.Rev.* **D46** (1992) 2907–2917.

[141] A. Djouadi, M. Spira, and P. Zerwas, "*Production of Higgs bosons in proton colliders: QCD corrections*," *Phys.Lett.* **B264** (1991) 440–446.

[142] M. Spira, A. Djouadi, D. Graudenz, and P. Zerwas, "*Higgs boson production at the LHC*," *Nucl.Phys.* **B453** (1995) 17–82, arXiv:hep-ph/9504378 [hep-ph].

[143] S. Dawson, "*Radiative corrections to Higgs boson production*," *Nucl.Phys.* **B359** (1991) 283–300.

[144] D. Graudenz, M. Spira, and P. Zerwas, "*QCD corrections to Higgs boson production at proton proton colliders*," *Phys.Rev.Lett.* **70** (1993) 1372–1375.

[145] H. E. Haber and G. L. Kane, "*Implications of a Higgs Interpretation of the Zeta (8.3)*," *Nucl.Phys.* **B250** (1985) 716.

[146] A. Djouadi, "*Squark effects on Higgs boson production and decay at the LHC*," *Phys.Lett.* **B435** (1998) 101–108, arXiv:hep-ph/9806315 [hep-ph].

[147] J. R. Espinosa, C. Grojean, V. Sanz, and M. Trott, "*NSUSY fits*," *JHEP* **1212** (2012) 077, arXiv:1207.7355 [hep-ph].

[148] A. Delgado, G. F. Giudice, G. Isidori, M. Pierini, and A. Strumia, "*The light stop window*," *Eur.Phys.J.* **C73** no. 3, (2013) 2370, arXiv:1212.6847 [hep-ph].

[149] J. Casas, A. Lleyda, and C. Munoz, "*Strong constraints on the parameter space of the MSSM from charge and color breaking minima*," *Nucl.Phys.* **B471** (1996) 3–58, arXiv:hep-ph/9507294 [hep-ph].

[150] A. Kusenko, P. Langacker, and G. Segre, "*Phase transitions and vacuum tunneling into charge and color breaking minima in the MSSM*," *Phys.Rev.* **D54** (1996) 5824–5834, arXiv:hep-ph/9602414 [hep-ph].

[151] **ATLAS** Collaboration, G. Aad *et al.*, "*Search for a supersymmetric partner to the top quark in final states with jets and missing transverse momentum at* $\sqrt{s} = 7$ *TeV with the ATLAS detector*," *Phys.Rev.Lett.* **109** (2012) 211802, arXiv:1208.1447 [hep-ex].

[152] **ATLAS** Collaboration, G. Aad *et al.*, "*Search for direct top squark pair production in final states with one isolated lepton, jets, and missing transverse momentum in*

$\sqrt{s} = 7$ *TeV pp collisions using 4.7* fb^{-1} *of ATLAS data*," *Phys.Rev.Lett.* **109** (2012) 211803, arXiv:1208.2590 [hep-ex].

[153] **ATLAS** Collaboration, G. Aad *et al.*, "*Search for a heavy top-quark partner in final states with two leptons with the ATLAS detector at the LHC*," *JHEP* **1211** (2012) 094, arXiv:1209.4186 [hep-ex].

[154] **ATLAS** Collaboration, G. Aad *et al.*, "*Search for top squark pair production in final states with one isolated lepton, jets, and missing transverse momentum in* $\sqrt{s}$ *=8 TeV pp collisions with the ATLAS detector*," *JHEP* **1411** (2014) 118, arXiv:1407.0583 [hep-ex].

[155] **ATLAS** Collaboration, G. Aad *et al.*, "*Search for direct pair production of the top squark in all-hadronic final states in proton-proton collisions at* $\sqrt{s} = 8$ *TeV with the ATLAS detector*," *JHEP* **1409** (2014) 015, arXiv:1406.1122 [hep-ex].

[156] **ATLAS** Collaboration, G. Aad *et al.*, "*Search for direct top-squark pair production in final states with two leptons in pp collisions at* $\sqrt{s} = 8$*TeV with the ATLAS detector*," *JHEP* **1406** (2014) 124, arXiv:1403.4853 [hep-ex].

[157] **ATLAS** Collaboration, G. Aad *et al.*, "*Measurement of Spin Correlation in Top-Antitop Quark Events and Search for Top Squark Pair Production in pp Collisions at* $\sqrt{s} = 8$ *TeV Using the ATLAS Detector*," arXiv:1412.4742 [hep-ex].

[158] **ATLAS** Collaboration, G. Aad *et al.*, "*Search for pair-produced third-generation squarks decaying via charm quarks or in compressed supersymmetric scenarios in pp collisions at* $\sqrt{s} = 8$ *TeV with the ATLAS detector*," *Phys.Rev.* **D90** no. 5, (2014) 052008, arXiv:1407.0608 [hep-ex].

[159] **CMS**. Collaboration, "*Search for top squarks decaying to a charm quark and a neutralino in events with a jet and missing transverse momentum*," Tech. Rep. CMS-PAS-SUS-13-009, CERN, Geneva, 2014.

[160] **CMS** Collaboration, S. Chatrchyan *et al.*, "*Search for top-squark pair production in the single-lepton final state in pp collisions at* $\sqrt{s}$ *= 8 TeV*," *Eur.Phys.J.* **C73** no. 12, (2013) 2677, arXiv:1308.1586 [hep-ex].

[161] **CMS**. Collaboration, "*Search for top squarks in multijet events with large missing momentum in proton-proton collisions at 8 TeV*," Tech. Rep. CMS-PAS-SUS-13-015, CERN, Geneva, 2013.

[162] **CMS**. Collaboration, "*Exclusion limits on gluino and top-squark pair production in natural SUSY scenarios with inclusive razor and exclusive single-lepton searches at 8 TeV.*," Tech. Rep. CMS-PAS-SUS-14-011, CERN, Geneva, 2014.

[163] Y. Kats and D. Shih, "*Light Stop NLSPs at the Tevatron and LHC*," *JHEP* **1108** (2011) 049, arXiv:1106.0030 [hep-ph].

[164] J. Fan, M. Reece, and J. T. Ruderman, "*Stealth Supersymmetry*," *JHEP* **1111** (2011) 012, arXiv:1105.5135 [hep-ph].

[165] J. Fan, M. Reece, and J. T. Ruderman, "*A Stealth Supersymmetry Sampler*," *JHEP* **1207** (2012) 196, arXiv:1201.4875 [hep-ph].

[166] Y. Bai, A. Katz, and B. Tweedie, "*Pulling Out All the Stops: Searching for RPV SUSY with Stop-Jets*," *JHEP* **1401** (2014) 040, arXiv:1309.6631 [hep-ph].

[167] T. Hahn, "*Generating Feynman diagrams and amplitudes with FeynArts 3*," *Comput.Phys.Commun.* **140** (2001) 418–431, arXiv:hep-ph/0012260 [hep-ph].

[168] T. Hahn and C. Schappacher, "*The Implementation of the minimal supersymmetric standard model in FeynArts and FormCalc*," *Comput.Phys.Commun.* **143** (2002) 54–68, arXiv:hep-ph/0105349 [hep-ph].

[169] T. Hahn and M. Perez-Victoria, "*Automatized one loop calculations in four-dimensions and D-dimensions*," *Comput.Phys.Commun.* **118** (1999) 153–165, arXiv:hep-ph/9807565 [hep-ph].

[170] A. Martin, W. Stirling, R. Thorne, and G. Watt, "*Parton distributions for the LHC*," *Eur.Phys.J.* **C63** (2009) 189–285, arXiv:0901.0002 [hep-ph].

[171] M. Whalley, D. Bourilkov, and R. Group, "*The Les Houches accord PDFs (LHAPDF) and LHAGLUE*," arXiv:hep-ph/0508110 [hep-ph].

[172] M. Spira, "*HIGLU: A program for the calculation of the total Higgs production cross-section at hadron colliders via gluon fusion including QCD corrections*," arXiv:hep-ph/9510347 [hep-ph].

[173] R. K. Ellis, I. Hinchliffe, M. Soldate, and J. van der Bij, "*Higgs Decay to tau+ tau-: A Possible Signature of Intermediate Mass Higgs Bosons at the SSC*," *Nucl.Phys.* **B297** (1988) 221.

[174] U. Baur and E. N. Glover, "*Higgs Boson Production at Large Transverse Momentum in Hadronic Collisions*," *Nucl.Phys.* **B339** (1990) 38–66.

[175] R. Boughezal, F. Caola, K. Melnikov, F. Petriello, and M. Schulze, "*Higgs boson production in association with a jet at next-to-next-to-leading order in perturbative QCD*," *JHEP* **1306** (2013) 072, arXiv:1302.6216 [hep-ph].

[176] S. Hoeche, F. Krauss, and M. Schonherr, "*Uncertainties in MEPS@NLO calculations of h+jets*," *Phys.Rev.* **D90** no. 1, (2014) 014012, arXiv:1401.7971 [hep-ph].

[177] T. Neumann and M. Wiesemann, "*Finite top-mass effects in gluon-induced Higgs production with a jet-veto at NNLO*," *JHEP* **1411** (2014) 150, arXiv:1408.6836 [hep-ph].

[178] H. Mantler and M. Wiesemann, "*Top- and bottom-mass effects in hadronic Higgs production at small transverse momenta through LO+NLL*," *Eur.Phys.J.* **C73** no. 6, (2013) 2467, arXiv:1210.8263 [hep-ph].

[179] M. Grazzini and H. Sargsyan, "*Heavy-quark mass effects in Higgs boson production at the LHC*," *JHEP* **1309** (2013) 129, arXiv:1306.4581 [hep-ph].

[180] J. Campbell, K. Ellis, and C. Williams, "*MCFM - Monte Carlo for FeMtobarn processes*," April, 2013. http://mcfm.fnal.gov.

[181] **Particle Data Group**, J. Beringer *et al.*, "*Review of Particle Physics (RPP)*," *Phys.Rev.* **D86** (2012) 010001.

[182] A. Katz, M. Son, and B. Tweedie, "*Ditau-Jet Tagging and Boosted Higgses from a Multi-TeV Resonance*," *Phys.Rev.* **D83** (2011) 114033, arXiv:1011.4523 [hep-ph].

[183] **LHC Higgs Cross Section Working Group**, S. Heinemeyer *et al.*, "*Handbook of LHC Higgs Cross Sections: 3. Higgs Properties*," arXiv:1307.1347 [hep-ph].

[184] J. Alwall, M. Herquet, F. Maltoni, O. Mattelaer, and T. Stelzer, "*MadGraph 5 : Going Beyond*," *JHEP* **1106** (2011) 128, arXiv:1106.0522 [hep-ph].

[185] M. Bahr, S. Gieseke, M. Gigg, D. Grellscheid, K. Hamilton, *et al.*, "*Herwig++ Physics and Manual*," *Eur.Phys.J.* **C58** (2008) 639–707, arXiv:0803.0883 [hep-ph].

[186] K. Arnold, L. d'Errico, S. Gieseke, D. Grellscheid, K. Hamilton, *et al.*, "*Herwig++ 2.6 Release Note*," arXiv:1205.4902 [hep-ph].

[187] J. Bellm, S. Gieseke, D. Grellscheid, A. Papaefstathiou, S. Platzer, *et al.*, "*Herwig++ 2.7 Release Note*," arXiv:1310.6877 [hep-ph].

[188] C. Anastasiou, R. Boughezal, and F. Petriello, "*Mixed QCD-electroweak corrections to Higgs boson production in gluon fusion*," *JHEP* **0904** (2009) 003, arXiv:0811.3458 [hep-ph].

[189] D. de Florian and M. Grazzini, "*Higgs production through gluon fusion: Updated cross sections at the Tevatron and the LHC*," *Phys.Lett.* **B674** (2009) 291–294, arXiv:0901.2427 [hep-ph].

[190] **LHC Higgs Cross Section Working Group**, S. Dittmaier *et al.*, "*Handbook of LHC Higgs Cross Sections: 1. Inclusive Observables*," arXiv:1101.0593 [hep-ph].

[191] M. Bonvini and S. Marzani, "*Resummed Higgs cross section at N^3LL*," *JHEP* **1409** (2014) 007, arXiv:1405.3654 [hep-ph].

[192] M. L. Mangano, M. Moretti, F. Piccinini, R. Pittau, and A. D. Polosa, "*ALPGEN, a generator for hard multiparton processes in hadronic collisions*," *JHEP* **0307** (2003) 001, arXiv:hep-ph/0206293 [hep-ph].

[193] T. Sjostrand, S. Mrenna, and P. Z. Skands, "*PYTHIA 6.4 Physics and Manual*," *JHEP* **0605** (2006) 026, arXiv:hep-ph/0603175 [hep-ph].

[194] M. L. Mangano, M. Moretti, and R. Pittau, "*Multijet matrix elements and shower evolution in hadronic collisions: $Wb\bar{b}$ + n jets as a case study*," *Nucl.Phys.* **B632** (2002) 343–362, arXiv:hep-ph/0108069 [hep-ph].

[195] S. Hoeche, F. Krauss, N. Lavesson, L. Lonnblad, M. Mangano, *et al.*, "*Matching parton showers and matrix elements*," arXiv:hep-ph/0602031 [hep-ph].

[196] P. Nason, S. Dawson, and R. K. Ellis, "*The Total Cross-Section for the Production of Heavy Quarks in Hadronic Collisions*," *Nucl.Phys.* **B303** (1988) 607.

[197] W. Beenakker, H. Kuijf, W. van Neerven, and J. Smith, "*QCD Corrections to Heavy Quark Production in p anti-p Collisions*," *Phys.Rev.* **D40** (1989) 54–82.

[198] S. Moch and P. Uwer, "*Theoretical status and prospects for top-quark pair production at hadron colliders*," *Phys.Rev.* **D78** (2008) 034003, arXiv:0804.1476 [hep-ph].

[199] Y. L. Dokshitzer, G. Leder, S. Moretti, and B. Webber, "*Better jet clustering algorithms*," *JHEP* **9708** (1997) 001, arXiv:hep-ph/9707323 [hep-ph].

[200] M. Wobisch and T. Wengler, "*Hadronization corrections to jet cross-sections in deep inelastic scattering*," arXiv:hep-ph/9907280 [hep-ph].

[201] M. Cacciari, G. P. Salam, and G. Soyez, "*FastJet User Manual*," *Eur.Phys.J.* **C72** (2012) 1896, arXiv:1111.6097 [hep-ph].

[202] A. J. Barr, B. Gripaios, and C. G. Lester, "*Measuring the Higgs boson mass in dileptonic W-boson decays at hadron colliders*," *JHEP* **0907** (2009) 072, arXiv:0902.4864 [hep-ph].

[203] B. Gripaios, K. Nagao, M. Nojiri, K. Sakurai, and B. Webber, "*Reconstruction of Higgs bosons in the di-tau channel via 3-prong decay*," *JHEP* **1303** (2013) 106, arXiv:1210.1938 [hep-ph].

[204] **CMS** Collaboration, V. Khachatryan *et al.*, "*Search for top-squark pairs decaying into Higgs or Z bosons in pp collisions at* $\sqrt{s}$*=8 TeV*," *Phys.Lett.* **B736** (2014) 371–397, arXiv:1405.3886 [hep-ex].

[205] **CMS** Collaboration, S. Chatrchyan *et al.*, "*Search for anomalous production of events with three or more leptons in pp collisions at* $\sqrt{(s)} = 8$ *TeV*," *Phys.Rev.* **D90** no. 3, (2014) 032006, arXiv:1404.5801 [hep-ex].

[206] **CMS** Collaboration, "*Search for supersymmetry in pp collisions at sqrt(s) = 8 TeV in events with three leptons and at least one b-tagged jet*," Tech. Rep. CMS-PAS-SUS-13-008, CERN, Geneva, 2013.

[207] **CMS** Collaboration, S. Chatrchyan *et al.*, "*Search for new physics in events with same-sign dileptons and jets in pp collisions at* $\sqrt{s}$ *= 8 TeV*," *JHEP* **1401** (2014) 163, arXiv:1311.6736.

[208] M. Papucci, J. T. Ruderman, and A. Weiler, "*Natural SUSY Endures*," *JHEP* **1209** (2012) 035, arXiv:1110.6926 [hep-ph].

[209] M. Czakon, A. Mitov, M. Papucci, J. T. Ruderman, and A. Weiler, "*Closing the stop gap*," *Phys.Rev.Lett.* **113** no. 20, (2014) 201803, arXiv:1407.1043 [hep-ph].

[210] T. Plehn, G. P. Salam, and M. Spannowsky, "*Fat Jets for a Light Higgs*," *Phys.Rev.Lett.* **104** (2010) 111801, arXiv:0910.5472 [hep-ph].

[211] T. Plehn, M. Spannowsky, M. Takeuchi, and D. Zerwas, "*Stop Reconstruction with Tagged Tops*," *JHEP* **1010** (2010) 078, arXiv:1006.2833 [hep-ph].

[212] J. M. Butterworth, A. R. Davison, M. Rubin, and G. P. Salam, "*Jet substructure as a new Higgs search channel at the LHC*," *Phys.Rev.Lett.* **100** (2008) 242001, arXiv:0802.2470 [hep-ph].

[213] L. G. Almeida, S. J. Lee, G. Perez, G. Sterman, and I. Sung, "*Template Overlap Method for Massive Jets*," *Phys.Rev.* **D82** (2010) 054034, arXiv:1006.2035 [hep-ph].

[214] K. Rehermann and B. Tweedie, "*Efficient Identification of Boosted Semileptonic Top Quarks at the LHC*," *JHEP* **1103** (2011) 059, arXiv:1007.2221 [hep-ph].

[215] J. Thaler and L.-T. Wang, "*Strategies to Identify Boosted Tops*," *JHEP* **0807** (2008) 092, arXiv:0806.0023 [hep-ph].

[216] D. E. Kaplan, K. Rehermann, M. D. Schwartz, and B. Tweedie, "*Top Tagging: A Method for Identifying Boosted Hadronically Decaying Top Quarks*," *Phys.Rev.Lett.* **101** (2008) 142001, arXiv:0806.0848 [hep-ph].

[217] L. G. Almeida, S. J. Lee, G. Perez, I. Sung, and J. Virzi, "*Top Jets at the LHC*," *Phys.Rev.* **D79** (2009) 074012, arXiv:0810.0934 [hep-ph].

[218] **CMS** Collaboration, "*A Cambridge-Aachen (C-A) based Jet Algorithm for boosted top-jet tagging*," Tech. Rep. CMS-PAS-JME-09-001, CERN, 2009. Geneva, Jul, 2009.

[219] J. Thaler and K. Van Tilburg, "*Identifying Boosted Objects with N-subjettiness*," *JHEP* **1103** (2011) 015, arXiv:1011.2268 [hep-ph].

[220] T. Plehn, M. Spannowsky, and M. Takeuchi, "*Boosted Semileptonic Tops in Stop Decays*," *JHEP* **1105** (2011) 135, arXiv:1102.0557 [hep-ph].

[221] M. Jankowiak and A. J. Larkoski, "*Jet Substructure Without Trees*," *JHEP* **1106** (2011) 057, arXiv:1104.1646 [hep-ph].

[222] J. Thaler and K. Van Tilburg, "*Maximizing Boosted Top Identification by Minimizing N-subjettiness*," *JHEP* **1202** (2012) 093, arXiv:1108.2701 [hep-ph].

[223] T. Plehn, M. Spannowsky, and M. Takeuchi, "*How to Improve Top Tagging*," *Phys.Rev.* **D85** (2012) 034029, arXiv:1111.5034 [hep-ph].

[224] T. Plehn and M. Spannowsky, "*Top Tagging*," *J.Phys.* **G39** (2012) 083001, arXiv:1112.4441 [hep-ph].

[225] T. Plehn, M. Spannowsky, and M. Takeuchi, "*Stop searches in 2012*," *JHEP* **1208** (2012) 091, arXiv:1205.2696 [hep-ph].

[226] D. E. Kaplan, K. Rehermann, and D. Stolarski, "*Searching for Direct Stop Production in Hadronic Top Data at the LHC*," *JHEP* **1207** (2012) 119, arXiv:1205.5816 [hep-ph].

[227] B. Dutta, T. Kamon, N. Kolev, K. Sinha, and K. Wang, "*Searching for Top Squarks at the LHC in Fully Hadronic Final State*," *Phys.Rev.* **D86** (2012) 075004, arXiv:1207.1873 [hep-ph].

[228] M. R. Buckley, T. Plehn, and M. Takeuchi, "*Buckets of Tops*," *JHEP* **1308** (2013) 086, arXiv:1302.6238 [hep-ph].

[229] A. Djouadi, M. Muhlleitner, and M. Spira, "*Decays of supersymmetric particles: The Program SUSY-HIT (SUspect-SdecaY-Hdecay-InTerface)*," *Acta Phys.Polon.* **B38** (2007) 635–644, arXiv:hep-ph/0609292 [hep-ph].

[230] M. Papucci, K. Sakurai, A. Weiler, and L. Zeune, "*Fastlim: a fast LHC limit calculator*," arXiv:1402.0492 [hep-ph].

[231] J. Alwall, R. Frederix, S. Frixione, V. Hirschi, F. Maltoni, *et al.*, "*The automated computation of tree-level and next-to-leading order differential cross sections, and their matching to parton shower simulations*," arXiv:1405.0301 [hep-ph].

[232] P. Lenzi and J. Butterworth, "*A Study on Matrix Element corrections in inclusive Z/ gamma* production at LHC as implemented in PYTHIA, HERWIG, ALPGEN and SHERPA*," arXiv:0903.3918 [hep-ph].

[233] W. Beenakker, M. Kramer, T. Plehn, M. Spira, and P. Zerwas, "*Stop production at hadron colliders*," *Nucl.Phys.* **B515** (1998) 3–14, arXiv:hep-ph/9710451 [hep-ph].

[234] W. Beenakker, S. Brensing, M. Kramer, A. Kulesza, E. Laenen, *et al.*, "*Supersymmetric top and bottom squark production at hadron colliders*," *JHEP* **1008** (2010) 098, arXiv:1006.4771 [hep-ph].

[235] W. Beenakker, S. Brensing, M. Kramer, A. Kulesza, E. Laenen, *et al.*, "*Squark and Gluino Hadroproduction*," *Int.J.Mod.Phys.* **A26** (2011) 2637–2664, arXiv:1105.1110 [hep-ph].

[236] S. Catani, L. Cieri, G. Ferrera, D. de Florian, and M. Grazzini, "*Vector boson production at hadron colliders: a fully exclusive QCD calculation at NNLO*," *Phys.Rev.Lett.* **103** (2009) 082001, arXiv:0903.2120 [hep-ph].

[237] A. Kardos, Z. Trocsanyi, and C. Papadopoulos, "*Top quark pair production in association with a Z-boson at NLO accuracy*," *Phys.Rev.* **D85** (2012) 054015, arXiv:1111.0610 [hep-ph].

[238] M. Czakon, P. Fiedler, and A. Mitov, "*Total Top-Quark Pair-Production Cross Section at Hadron Colliders Through $O(\alpha_S^4)$*," *Phys.Rev.Lett.* **110** (2013) 252004, arXiv:1303.6254 [hep-ph].

[239] I.-W. Kim, M. Papucci, K. Sakurai, and A. Weiler, "*ATOM: Automated Testing Of Models*." In preparation.

[240] A. Buckley, J. Butterworth, L. Lonnblad, D. Grellscheid, H. Hoeth, *et al.*, "*Rivet user manual*," *Comput.Phys.Commun.* **184** (2013) 2803–2819, arXiv:1003.0694 [hep-ph].

[241] M. Cacciari, G. P. Salam, and G. Soyez, "*The Anti-k_t jet clustering algorithm*," *JHEP* **0804** (2008) 063, arXiv:0802.1189 [hep-ph].

[242] **ATLAS** Collaboration, "*Search for direct top squark pair production in final states with one isolated lepton, jets, and missing transverse momentum in sqrts = 8,TeV pp collisions using 21 fb^{-1} of ATLAS data*," Tech. Rep. ATLAS-CONF-2013-037, CERN, Geneva, Mar, 2013.

[243] **CMS** Collaboration, S. Chatrchyan *et al.*, "*Identification of b-quark jets with the CMS experiment*," *JINST* **8** (2013) P04013, arXiv:1211.4462 [hep-ex].

[244] **ATLAS** Collaboration, "*ATLAS Sensitivity to the Standard Model Higgs in the HW and HZ Channels at High Transverse Momenta*," Tech. Rep. ATL-PHYS-PUB-2009-088, CERN, Geneva, Aug, 2009.

[245] R. Bartoldus *et al.*, "*Technical Design Report for the Phase-I Upgrade of the ATLAS TDAQ System*," Tech. Rep. CERN-LHCC-2013-018. ATLAS-TDR-023, CERN, Geneva, Sep, 2013. Final version presented to December 2013 LHCC.

[246] C. Lester and D. Summers, "*Measuring masses of semiinvisibly decaying particles pair produced at hadron colliders*," *Phys.Lett.* **B463** (1999) 99–103, arXiv:hep-ph/9906349 [hep-ph].

[247] A. Barr, C. Lester, and P. Stephens, "*m(T2): The Truth behind the glamour*," *J.Phys.* **G29** (2003) 2343–2363, arXiv:hep-ph/0304226 [hep-ph].

[248] H.-C. Cheng and Z. Han, "*Minimal Kinematic Constraints and m(T2)*," *JHEP* **0812** (2008) 063, arXiv:0810.5178 [hep-ph].

[249] T. Junk, "*Sensitivity, Exclusion and Discovery with Small Signals, Large Backgrounds, and Large Systematic Uncertainties*," 2007. https://plone4.fnal.gov:4430/P0/phystat/packages/0711001.

[250] H.-C. Cheng and I. Low, "*TeV symmetry and the little hierarchy problem*," *JHEP* **0309** (2003) 051, arXiv:hep-ph/0308199 [hep-ph].

[251] H.-C. Cheng and I. Low, "*Little hierarchy, little Higgses, and a little symmetry*," *JHEP* **0408** (2004) 061, arXiv:hep-ph/0405243 [hep-ph].

[252] H.-C. Cheng, I. Low, and L.-T. Wang, "*Top partners in little Higgs theories with T-parity*," *Phys.Rev.* **D74** (2006) 055001, arXiv:hep-ph/0510225 [hep-ph].

[253] J. Neyman and E. S. Pearson, "*On the Problem of the Most Efficient Tests of Statistical Hypotheses*," *Philosophical Transactions of the Royal Society of London A: Mathematical, Physical and Engineering Sciences* **231** no. 694-706, (1933) 289–337.